DEVELOPING A METHODOLOGY FOR REDUCING DIAMOND BREAKAGE WITHIN PROCESSING PLANT

Motsi John Chele

Supervisors: Prof. Aubrey N Mainza, Prof. Carl M Evertsson & Dr. Sherry Bremner

A dissertation submitted to the Faculty of Engineering and the Built Environment, University of Cape Town in fulfilment of the requirements for the degree of Master of Science in Chemical Engineering.

July 2020

ABSTRACT

Diamond breakage has been a problem experienced by diamond operations. Material breakage characterisation methods has been used to determine the hardness or resistance to breakage of diamond host rock, ceramic diamond simulants and simulants embedded in the concrete blocks. This establishes a relationship between specific input energy and degree of breakage that can be used for size reduction to minimise diamond breakage.

Ceramic diamond simulants have been used in the process to identify areas that are more prevalent to diamond breakage. It was found that sections of high impact such as the cone crushers and drop height in the surge bins had the highest risk of diamond breakage.

Kimberlite ore and ceramic diamond simulants were subjected to compressive breakage in drop weight test. The progeny particle size distribution and degree of breakage were compared. Standard breakage characterisation models were fitted to the breakage data of tested material and relative hardness parameters determined to establish the energy threshold.

The breakage tests results showed that the ceramic diamond simulants were very hard while the kimberlite ore and concrete blocks were medium to soft. The material hardness parameters were determined from fitting the breakage data to the standard impact breakage characterisation models (t_{10}-E_{cs} breakage model and Size dependent breakage model). Concrete blocks and Kimberlite ore showed less resistance to compressive breakage as demonstrated by higher A values compared to the ceramic diamond simulants. Applying material hardness categories presented by Napier-Munn et al (1999), Kimberlite ore was soft, concrete blocks ranged medium to soft and ceramic diamond simulants very hard.

The remedial measures implemented in the process were to rubber line the concentrate bins in the recovery to minimise the impact forces, as well the surge bins in the process plant were controlled in such a way that reduces the drop height. Finally, the cone crushers and pan feeders operating philosophy has been improved to start at high speed to achieve choke feed conditions faster and to promote interparticle crushing. The close side settings were also optimized to reduce liner to liner interaction rather enhance particle-to-particle interaction.

Through the optimised process, it had been observed that the diamond breakage had dropped below 5% level of the total stones recovered at +5cts. The methodology developed proved to be working after being tested in the chosen flowsheet.

PLAGIARISM DECLARATION

I know the meaning of plagiarism and declare that all the work in the document, save for that which is properly acknowledged, is my own. This thesis/dissertation has been submitted to the Turnitin module (or equivalent similarity and originality checking software) and I confirm that my supervisor has seen my report and any concerns revealed by such have been resolved with my supervisor.

Signed by candidate

Signature: _____

Date: 14 July 2020

Table of Contents

ACKNOWLEDGEMENTS

First and foremost, I would like to thank God for being my guide and protector through every step of the way during this journey of my research study.

I would like to take this opportunity to acknowledge the people who immensely took part to make sure success is achieved in this thesis.

I would like to thank my supervisors Prof. Aubrey Mainza for his guidance, patience and assistance during the period of my MSc studies. I would also like to thank my co-supervisor Prof. Magnus Evertsson for making time to review the work undertaken in this project. Dr. Sherry Bremner for review the experimental work and mostly for continuous review of the thesis write-up. To, Dr. Paul Bepswa and Mr Aton Bolander, a special appreciation of taking part in the plant survey campaigns. I would also like to thank my colleagues, Ntate Thabo Khoboko, Mme Motena Takalimane and the rest of the production team for their unfailing support during the test work undertaken in this project.

Profuse appreciation to my beloved wife Mme Machabeli Chele for her continuous encouragement and support throughout the journey of my studies. A special thank you, to my sons, Chabeli Chele, Khotso Chele and Motsi Jnr Chele, for understanding that *Daddy* will not always be with them all the time because of his studies.

I would also like to express my gratitude to my sponsor and the external consultants whom they were engaged to assess the outcomes of this work.

Finally, I would like to thank my brother and his wife (Uncle Lekoapa and Aunty Matsebo) for their endless support during the difficult times for dispatching hope and emotional support.

LIST OF FIGURES

LIST OF TABLES

LIST OF ABBREVIATIONS

DWT	Drop weight tester
CDM	Consolidated De-Beers Mines
DEM	Discrete element method
CSS	Close side setting
OSS	Open side setting
JKRBT	Julius Kruttschnitt rotary breakage tester
UCS	Uniaxial compressive strength
SHPB	Split Hopkinson pressure bar
JKMRC	Julius Kruttschnitt mineral research centre
ROM	Run of mine
DMS	Dense medium separation
SG	Specific gravity
UCT	University of Cape Town
DebTech	De-Beers technologies
RPM	Revolutions per minute

SYMBOLS AND NOMENCLATURE

E_{cs}	Specific comminution energy (kWh/t)
M_r	Mass of the rebound pendulum
M_i	Mass of input pendulum
E_{is}	Specific input energy (kWh/t)
E_t	Energy transmitted to the rebound pendulum
e	Coefficient of restitution
θ	Angle of displacement of rebound pendulum
h_i	Initial drop height (cm)
$\bar{m}$	Mean mass (Kg)
M_d	Mass of drop weight (Kg)
E_k	Kinetic energy
m	Mass of the particle
Xg	geometric mean size of feed particle (m)
N	Rotor speed (rpm)
V_i	Velocity of the particle prior to impact
V_r	Radial velocity
V_t	Tangential velocity
$v_{(\alpha)}$	Velocity distribution as a function of eccentricity angle
ω_n	Eccentric speed
Ri(α)	Radius from which a particle with speed v(α) originates
ηv	Volumetric filling ratio
ρ u	Uncompressed bulk density
δN	Size distribution width
SN	Compression ratio
ξ_{IP}	Amount of interparticle breakage
A_{ip}	Crushing zone, which is cut by, choke level
A_{tot}	Total area of crushing zone
Ab	Ore specific impact breakage parameter
t_{10}	Product size distribution '' fineness'' index
M	maximum t10 for a material subject to breakage (%)

X	initial particle size(m)
k	successive number of with the single impact
E_{min}	energy threshold
Li	Luminescence intensity
mV	millivolts
C (x;y, h)	The single particle breakage function for self-breakage of a particle of size y in free fall from height h
P(y,h)	The probability that a particle of size y will shatter when falling a vertical height h
P(h)	The distribution density for effective drop heights in the mill (drum scrubber) or surge bins

CHAPTER 1

1. INTRODUCTION

The purpose of this research is to develop a methodology for minimising diamond breakage in the processing plant. The research was carried out by performing material characterisation using kimberlite ore, ceramic diamond simulants as received from the manufacturer and embedded in concrete of different strengths. Kimberlites inherently have different properties such as hardness; the simulants were embedded in concrete of different strengths to mimic the kimberlite host rock. A plant survey was also conducted to determine the flow of material in the circuit and the requisite size reduction on different comminution stages. The data from the plant surveys was used to generate a model for the circuit; which was subsequently used to perform simulations for different scenarios to identify optimal operating conditions to minimise diamond breakage.

1.1 Background

Diamond breakage remains a key concern for diamond mine producers due to its significant impact on revenue. The design of the newly constructed diamond extraction plant is believed to incorporate best principles in terms of reducing diamond breakage potential. Despite this, there are still areas within the process where breakage of diamonds occur, that cause damage, especially to stones with a well-developed cleavage or those with hollows vacated by inclusions and sometimes because of stresses caused by differential expansion between host and inclusion (Robinson,1979).

The zones within the diamond production cycle where breakage might occur in a conventional circuit includes:

- Comminution (scrubbing and crushing),
- Material transport (gravel pumping and drop heights within storage bins and transfer chutes), and
- transfer points for sorted diamonds.

There is some data in literature to corroborate diamond breakage during transfer impact zones, and for diamond-on-diamond dynamic forces (C.D.M, 1977) and Rider & Roodt. (2003). However, there is limited literature on diamond breakage during the comminution stages of the diamond-winning cycle available in the public domain. This includes the multiple crushing stages to liberate locked diamonds from kimberlite ore.

1.2 Scope of work and limitations

The current work focuses on identifying areas in the comminution circuit where diamond breakage occurs. An operating process plant was used for this study so that intricacies peculiar to diamond processing can be accounted for in this project. The specific process units in the chosen flowsheet were examined and studies were performed to identify conditions under which diamond breakage occurs. This will involve performing a plant survey to calibrate the performance of the circuit and parametric studies on individual comminution units in the circuit where there is the highest risk of diamond breakage.

Ceramic diamond simulants, both “As-Is” and “embedded in concrete of different strengths”, were used to mimic diamonds in their liberated and unliberated form respectively. The experimental results were fitted with models in JKSimMet to extract a set of operating parameters that were used to analyse the comminution survey data.

Plant survey and drop weight tests were undertaken for Ore characterisation. The tests were performed on Kimberlite ore to gain a better understanding of particle breakage in diamond processing plants. Earlier work undertaken by (Herbst et al., 2008) showed that kimberlitic ores have very low concentrations of diamonds therefore experimental assessments are not possible with diamonds themselves. Discrete element method (DEM) simulation were used in their studies to predict breakage of diamonds. It is worth noting that DEM will not be considered in the current study as it goes beyond the scope defined for this body of work.

1.3 Hypotheses

1) Seeding of ceramic diamond simulants at different points of the diamond processing plant can be used to identify equipment involved in the breakage of liberated diamonds because the forces that could cause breakage in simulants will be similar to those that would break diamonds.

2) Breakage of the ceramic diamond simulants embedded in concrete of predetermined strength can be used to indicate the breakage of unliberated diamonds.

3) Larger close side setting (CSS) of cone crushers minimises contact forces between the crusher liners and simulants surfaces, thus reduces breakage.

1.4 Key Questions

1) Where does most diamond breakage occur in the processing plant?

2) Does changing the close side settings in crushers lead to changes in simulant breakage behaviour?

3) What are the energy thresholds for simulants to break if they are liberated or embedded in concrete?

1.5 Objectives

The objectives for this thesis are:

1) To investigate and identify the key process areas that contribute to diamond breakage as measured by seeding ceramic diamond simulants at different points in the processing plant.

2) To perform crusher tests at different close side setting (CSS) and seed simulants for selected crusher tests to assess the impact of CSS on simulants breakage. The diamond breakage is evaluated using the ceramic diamond simulants with similar properties.

3) To perform particle characterisation tests using JK Rotary Breakage Tester (JKRBT) and Drop weight test devices to determine the energy that may lead to breakage for liberated and unliberated diamonds.

4) To conduct plant surveys to obtain mass balance to assess the relative flow of material in the circuit, and to evaluate progressive breakage of material in different stages of the process. Develop circuit model that can be used to optimize and establish a set of operating parameters where diamond breakage should be minimized.

1.6 Thesis Outline

Chapter 1- Introduction

The background to the study, along the scope of work and objectives are presented in this chapter.

Chapter 2- Literature review

Chapter 2 gives the review of the literature relevant to the study as well as the description of the chosen flowsheet. This chapter covers the discussion around particle breakage fundamentals, breakage devices in comminution studies and the unit operations installed on the chosen flowsheet.

Chapter 3- Methodology development

This chapter outlines the proposed framework for identifying and minimising diamond breakage in the processing plant.

Chapter 4- Experimental programme

This chapter provides the details of the procedure undertaken to perform the tests both in the processing plant and in the metallurgical laboratory. The plant sampling and sample preparation done on the material used, the experimental setup and procedures used for breakage tests.

Chapter 5- Results and Discussion

Both the results obtained in the processing plant and metallurgical laboratory were presented in this chapter.

Chapter 6- Modelling and Simulation

This chapter provide models used to calibrate the unit processes and validate the optimal operational parameters.

Chapter 7- Evaluating methodology and proposed remedial measures

Chapter 7 provides remedial measure implemented in minimising diamond breakage and testing the methodology developed for the study.

Chapter 8- Conclusions and Recommendations

This chapter summarises the key findings on the research work undertaken as well as recommendations made for future work.

CHAPTER 2

2. LITERATURE REVIEW

This chapter provides background to the literature aligned with particle breakage and comminution circuit operations pertaining to this study. Particle breakage characterisation units and techniques are reviewed and discussed. The literature survey in this thesis is focused on particle breakage characterisation, comminution energy requirement for particle breakage and comminution devices within the kimberlitic ore processing operation. Diamond breakage has been a problem for many years in the extraction processes of this mineral. Unfortunately, breakage leads to value loss hence the literature was reviewed to fill the gap of breakage by developing a methodology to reduce diamond breakage.

Since most of the comminution aspects of diamond extraction involve breaking the rock to liberate the diamonds, papers on diamond extraction are rare so the principles of comminution are considered in the general sense as applied to any other ore.

This study is in two parts, the first part deals with understanding the particle breakage characterization and the second part deals with the circuit studies, whereby an assessment is done on equipment deemed susceptible to diamond breakage.

2.1 Background to comminution studies

Comminution is the size reduction of pieces of large particle size to a smaller average particle size (Napier-Munn et al., 1996; Henk et al., 2016 & Yahyaei et al., 2016). The particle breakage in comminution processes take place in different forms depending on the material properties such as chemical or mineral composition, ore texture, particle size and the breakage mechanism within the particle size reduction unit (Resabal., 2016; Wills & Napier-Munn., 2006).

The particle fractures due to the imposition of compressive stress applied rapidly by impact and the secondary fracture is created by high shearing stress particularly at the surface of the particle (King., 2001). The particles follow certain fracture patterns when subjected to load with different modes (King., 2001 & Andersen., 2005). Particle fracture is mainly influenced by factors such as the particle shape, size and other material properties like elasticity, homogeneity, flaws of the particle and ultimately the type of stress applied (Bernotat & Schönert., 1988).

2.2 Fracture pattern for rock particles

Diamonds are normally encapsulated in their host rock (Kimberlite), so it is therefore important for them to be liberated in any form for economic recovery. Comminution principles are used universally for liberation purposes. There are different mechanisms applied to liberate the diamonds. The following section will discuss the fracture patterns.

2.2.1 Shatter

This fracture mechanism of shattering is induced by rapid application of compressive stress. A continuum of product size is produced, and this process is unselective (King., 2001). The shattering process involves a series of stages whereby the parent particle is fractured and subsequently followed by fracturing of the progeny particles until all the energy available for fracture is expended (King., 2001 & Tavares., 2007). Shattering is mostly common in industrial autogenous mills and ball mills. Figure 1, demonstrates the two-point compression of a single particle that results in an internal stress pattern.

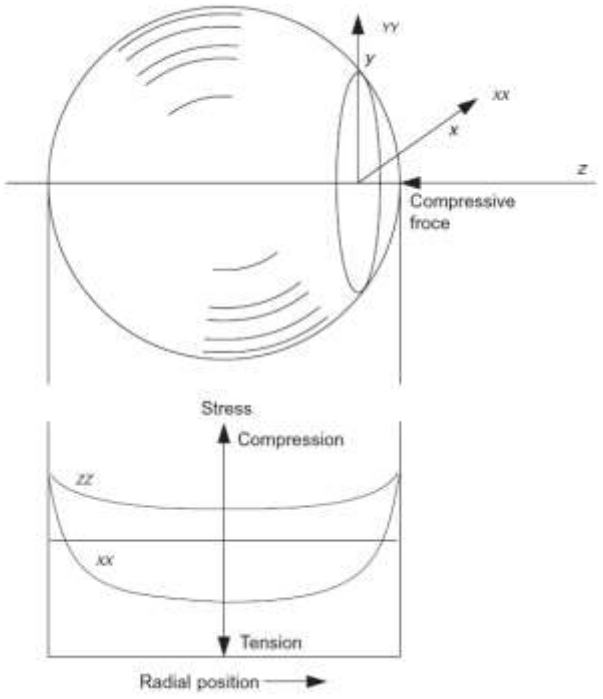

Figure 1: Two-point compression of a single particle with the resultant internal stress (King., 2001)

2.2.2 Cleavage

Cleavage is the tendency of a mineral to break along smooth planes parallel to zones of weak bonding. When the parent rock has some preferred surfaces along which fracture is likely to take place, cleavage yields. If multiple fractures of the progeny fragments does not occur, this

mechanism of fracture tends to produce numerous comparatively large fragments together that reflect the grain size of the original material with much finer particles that originate at the points of application of the stress (Kelly & Spottiswood., 1989; King., 2001). The size distribution of the product particles is relatively narrow but will often be bimodal shown in Figure 2. This distribution could be because of not enough energy is applied onto the surface of the particle and this can also produce progeny particles of similar size.

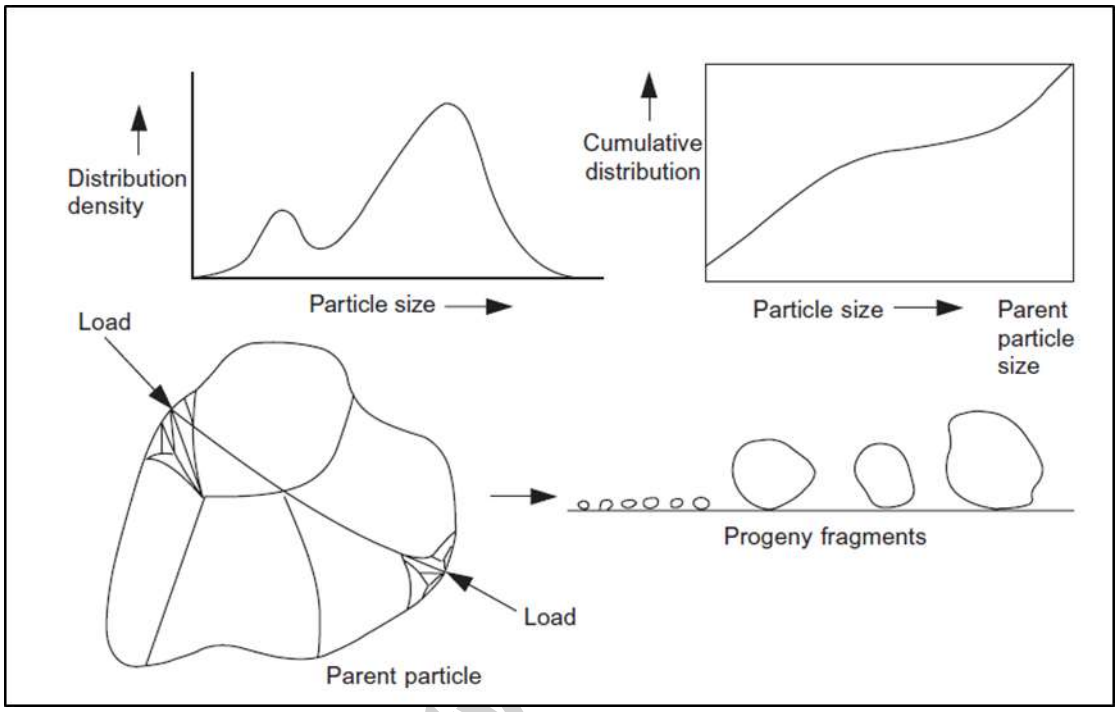

Figure 2: Cleavage fracture without successive fracture of progeny fragments (King., 2001).

2.2.3 Attrition

Attrition is the process of size reduction by rubbing away or wearing down the particle size by friction. Shear Strain between two or more particle surfaces moving in parallel results in finer product because of shearing action (Davis & Dawson.,1989, Kalman.,2000;Chen.,2014 &Resabal.,2016). In this process the parent particle hardly alters the size, but more daughter particles are produced with smaller size than the parent size, because of initial stresses not being enough to cause fracture cited by (King,2001). In diamond extraction process, this mechanism of size reduction is preferred as there is minimal impact of particle which could increase the chances of diamond breakage. Figure 3, illustrates the results of attritioning process. Which can be inferred that the probability of diamond breakage is very low.

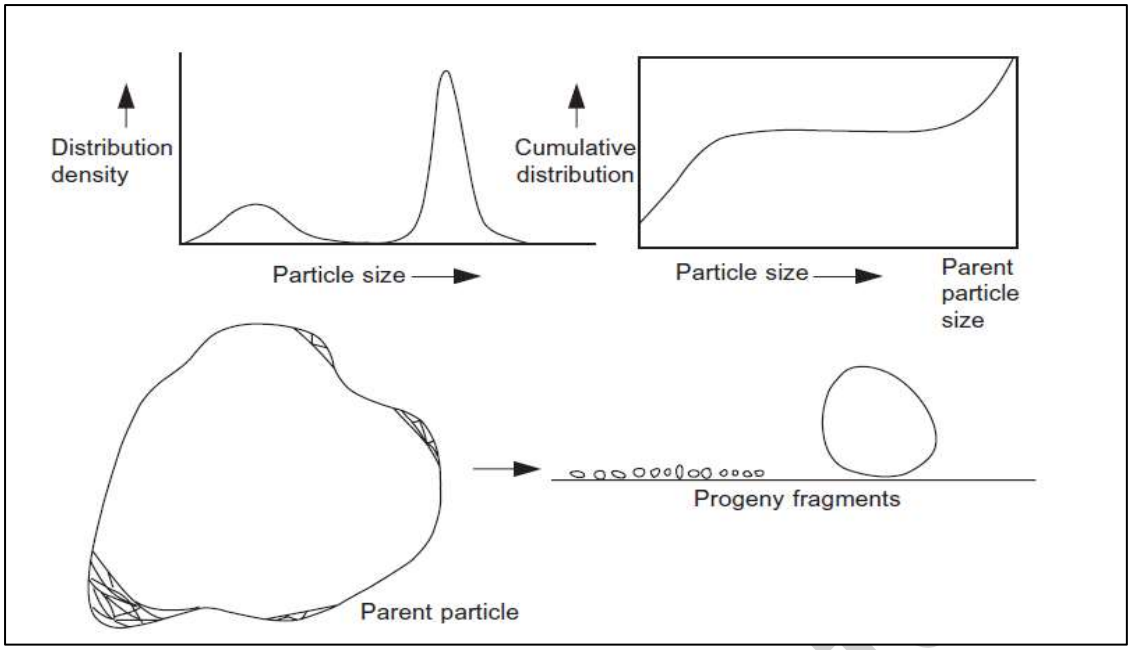

Figure 3:Attrition and chipping produce products with a narrow size spectrum at the parent size and another hump at small sizes (King.,2001)

2.3 Particle breakage mechanisms

Many research studies have shown that the particle breaks when the applied stress exceeds the tensile strength of the rock (Anderson., 2005; Potapov & Campbell.,2001; Yahyaei et al.,2016). Particle size reduction can be achieved through different comminution principles and the most predominant principles are compression, impact, and shear (Attrition and Abrasion).

2.3.1 Compression

One form of load application during a comminution process is compression in which the rock particles are compressed slowly, and the particle fails when the uniaxial compressive strength (UCS) has been exceeded (Henk et al., 2015; Salman et al., 2007). The process mostly take place in the application of high-pressure grinding rolls.

2.3.2 Impact

Particle breakage takes place through impacting the ore with a stiff object, fracturing the ore particle. This mechanism of particle breakage occurs mainly through two modes. In the first mode, the ore is placed on a rigid anvil and is impacted by a rigid object, compressing the ore and leading to breakage. In the second case, the ore is launched at a rigid target, resulting in

breakage (Austin., 2002). The application of the breakage method is applicable to both the JK rotary breakage test and Drop weight test.

2.3.3 Shear (Abrasion/Attrition)

Abrasion occurs because of comparably sized particles rubbing against each other, resulting in more rounded particles. The applied stresses are not large enough to break the particle, thus it remains intact but undergoes gradual wearing of its surface (Hogg.,1999).

2.4 Particle breakage characterisation

In a diamond processing plant, the comminution process follows; primary crushing, scrubbing and finally the secondary and tertiary crushing sequences.

During ore size reduction a lot of energy is being consumed. However, Tavares & King. (1998) have indicated that industrial comminution processes are inefficient in the use of energy; thus, a significant amount of this energy is used in operating the equipment rather than breaking the particles.

In any particle fracture or particle breakage, energy is expended to some extent for mineral liberation. Numerous researchers have undertaken to study the particle breakage to have a greater understanding of fracture modes to enhance energy efficiency in comminution operations (Narayanan & Whiten., 1988; Pauw & Mar'e., 1988; King & Bourgeois., 1993; Tavares & King., 2004).

The mechanism of the particle fracture process is mostly understood from single particle breakage and there is a general agreement in the literature on the basic model description (Tavares & King., 1998). Single particle impact breakage testing is a valued technique for characterizing ore competency and establishing ore parameters that are used in breakage modelling and simulation in comminution research (Napier-Munn et al., 1996). Ore characterization tests are useful for measuring the ore-specific energy/size-reduction behaviour. Several devices have been developed for the controlled breakage of single particles under impact loading to determine comminution parameters. These devices include the twin pendulum device, drop weight tester, Split Hopkinson Pressure Bar (SHPB), Rotary Breakage Tester, and the Short Impact Load Cell (Napier-Munn et al., 1996). The devices are discussed in the following section.

The twin pendulum device, Split Hopkinson pressure bar and Short impact load cell will be briefly discussed while Drop weight test and the Rotary breakage tester will be discussed in detail for the purpose of this study.

2.4.1 Twin Pendulum Test

This device was developed by JKMRC for single particle breakage tests. The conditions require that the energy used to break a particle can be determined together with the product size distribution (Napier-Munn et al.,1996). The results obtained from the twin pendulum test are used to generate ore-specific breakage functions for each of the related comminution models.

The unit is made up of an input and rebound pendulum fixed on a firm structure demonstrated in Figure 4.

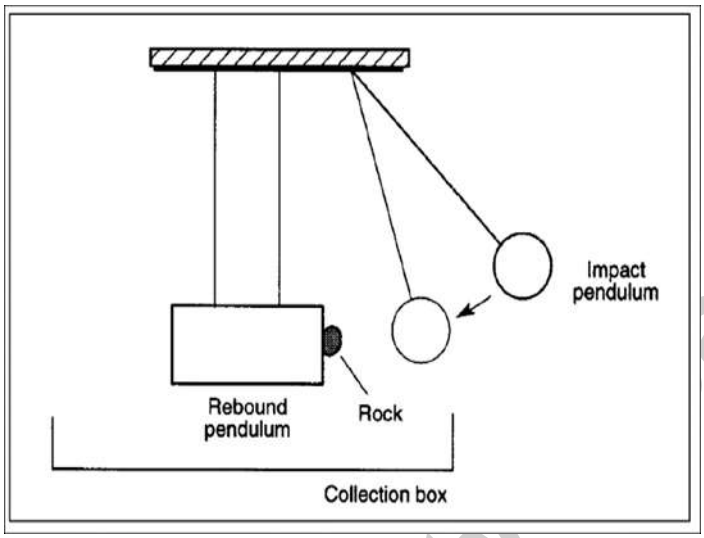

Figure 4:Diagram of a twin pendulum demonstrating the impact and rebound pendulus and the positioning of the rock sample when the breakage test is undertaken (Napier-Munn et al.,1996).

The impact pendulum is released from different known heights conditional to the required input energy and collides with the rock particle attached to the rebound pendulum. The rebound pendulum swings on impact and its motion is monitored by laser and computer. The specific comminution energy can then be determined using (1), (Napier-Munn et al.,1996).

$$Ecs = \frac{Mr}{Mi + Mr} * (1 - e^2)Eis \quad (1)$$

Where, M_r is the mass of the rebound pendulum, M_i is the mass of the input pendulum, e is the coefficient of restitution, E is the specific input energy (kWh/t) and m is the mass of the

particle. The specific comminution energy E_{cs} (kWh/t) is then defined as the amount of energy used to break a particle per unit mass.

The twin pendulum is advantageous due to its simplicity for estimating the specific energy utilized for impact breakage. On the other hand, its operation and the results attained have weaknesses. Its design restricts the range of input energies and particle sizes that can be tested. In addition, it is time consuming in its operation as large numbers of particles need to be tested for the results to be statistically significant. The breakage energy calculations are inaccurate due to the secondary motion of the rebound pendulum (Napier-Munn et al.,1996).

Upon completion of the breakage test, a particle of the known mass is attached to the rebound pendulum and the impact pendulum is pulled backward to a known height and released to collide with and break the particle. After the impact, the rebound pendulum swings and passes through a laser beam and time taken to complete oscillation is measured and recorded on a computer to determine the period (Weedon & Wilson.,2000).

After the breakage test is completed, the energy transmitted to the rebound pendulum is determined by using (2)(Napier-Munn et al.,1996).

$$Et = Mr(L - Lcos\theta) \tag{2}$$

Where, E_t is the energy transmitted to the rebound pendulum(J), M_r is the mass of the rebound pendulum(kg), L is the length of the pendulum and θ is the angle of displacement of the rebound pendulum from its equilibrium position(rad).

Because of the encountered limitations of the twin pendulum, the drop weight tester was developed as an option for the single impact particle breakage (Napier-Munn et al.,1996).

2.4.2 Split Hopkinson Pressure Bar

Kolsky originally developed the split Hopkinson pressure bar technique. (1949 & 1963). This technique has been used by many researchers to obtain dynamic compression properties of solid material (Frew et al., 2001). The apparatus is utilized to determine the stress -strain response (Huang et al., 2014).

To date there have been many modifications made of the original SHPB or Kolsky Bar, however the various devices essentially operate in a similar manner (Gary & Blumenthal.,2000). The SHPB is useful for determining the failure properties of ductile materials such as metals (Frew et al., 2001).

A conventional SHPB device consists of striker, incident and transmission bars. A sample of the material whose compression properties are being investigated is placed between the incident and transmission bars. The striker bar is launched at the incident bar using a launching mechanism (such as a gas gun, coiled spring or rail gun), causing the transmission of an elastic compression wave from the incident bar to the sample upon impact. An elastic tensile wave is reflected into the incident bar and an elastic compression wave is transmitted into the transmission bar when the impedance of the sample is less than that of the bars. The incident and transmission bars are equipped with strain gauges which measure the strain and the generated data can be used to determine the response of the sample upon impact (Song & Chen.,2005). A diagram of a conventional SHPB is shown in Figure 5.

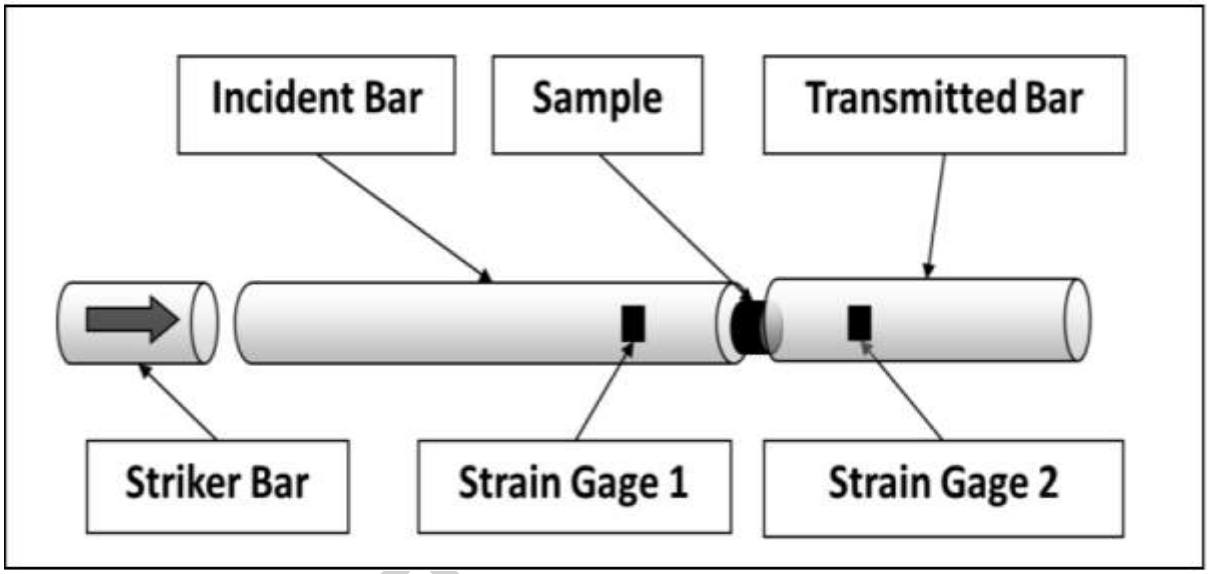

Figure 5:Diagram of the split Hopkinson bar indicating the incident and the transmitter bar,strain gauges and sample positioning in the device (adapted from Song & Chen.,2005)

If the pressures in the bars remain within their elastic limits, the force vs time histories recorded from the impact can be used to determine fracture properties of the specimen. The stress on the particle sample is evaluated according to (3) (Nicholas,1982):

$$\delta 1 = EA/As(\varepsilon i + \varepsilon r) \tag{3}$$

$$\delta 2 = EA/As(\varepsilon t) \tag{4}$$

If $\delta_1=\delta_2$, the stress on both ends of the sample are equal, the sample is in dynamic stress equilibrium and the stress strain rate and strain are given by;

$$\delta s = EA/As(\varepsilon t) \tag{5}$$

$$\frac{d\varepsilon s}{dt} = -2c/Lo(\varepsilon t) \tag{6}$$

$$\varepsilon s = -2c/Lo \int_0^1 \varepsilon t(\tau) d\tau \tag{7}$$

As discussed by (Ravichandran & Subhash,1994; Gray & Blumenthal,1999 ; Gray,1999), equations 5, 6 and 7 assume that the sample is in dynamic stress equilibrium. It is therefore decided that equilibrium should be examined by comparing δ1 and δ2 at the ends of the samples given by 3 and 4. If δ1 and δ2 are in reasonable agreement, only then it is reasonable to use equations 5,6 and 7 to calculate sample stress, strain rate and strain. The use of the original SHPB has been found to be limited in comminution research (Tavares,2007). The SHPB is tedious in nature of the experiments and presents great variability encountered in the fragmentation behaviour of geological material (Salman et al.,2007). A more effective and suitable alternative to the SHPB is the impact load cell which will be discussed in the next section.

2.4.3 Impact Load Cell

The impact load cell is a combination of the drop weight and split Hopkinson pressure bar (Salman.,2007). This technique was originally developed by Weichert (ultra-fast load cell) in 1986 to calculate both the load and deformation, a particle encounters during impact (Bourgeois & Banini,2002;Tavares,2007). The device can also be utilised to measure compressive force and energy absorbed by the particle (Bourgeois & Banini,2002).

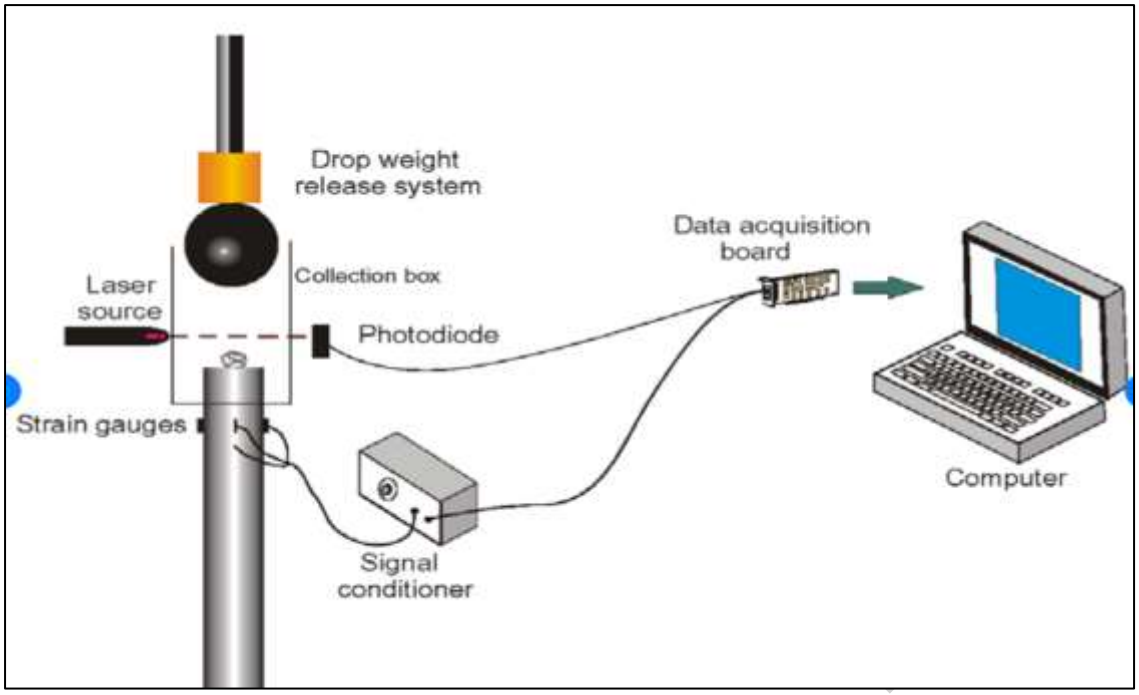

Figure 6:An illustration of the impact load cell (Adapted from Tavares.,2007)

The advantages of the load cell are that it offers exact time measurement, can be used for bed and single particle breakage and has a wide range of energies and sizes. This energy absorption is measured directly as a function of time by combining the dynamic measurements of force and particle compression (Bourgeois & Banini.,2002).

This is the minimum energy absorbed by a mineral particle subjected to impact loading prior to fracture. It is normally reported as a frequency distribution for a sample of particles of a given type and size and has been found to obey the log-normal probability distribution (King and Bourgeois.,1993). Measurements of distribution of energy-at-first fracture have been shown to be extremely sensitive to small variations in ore breakage propensity (Tavares and King.,1998). Robust methods have been tested for comparison of such distributions (Milin and King.,1994).

Despite the significant advantages over impact drop weight tester, impact load cell is not commercially available or used in-situ (Bourgeois & Banini.,2002). The choice of using the drop weight test and JK rotary breakage tester was mainly due to availability of resources while the rest of the devices were not used because they were not readily available.

2.4.4 Drop weight test

The twin pendulum was phased out by introducing the drop weight tester for analysing characteristics of different ores for single particle impact breakage (Napier-Munn.,1996; Genc et al.,2004; Tavares.,2007; Thenjiwe.,2017). Particle breakage distribution of a material can be described as the appearance of the fragments after the breakage of a single particle of varied sizes.

The drop weight test device consists of a steel drop weight confined in Perspex mounted on two guide rails as shown in Figure 7 (Napier-Munn et al.,1996).

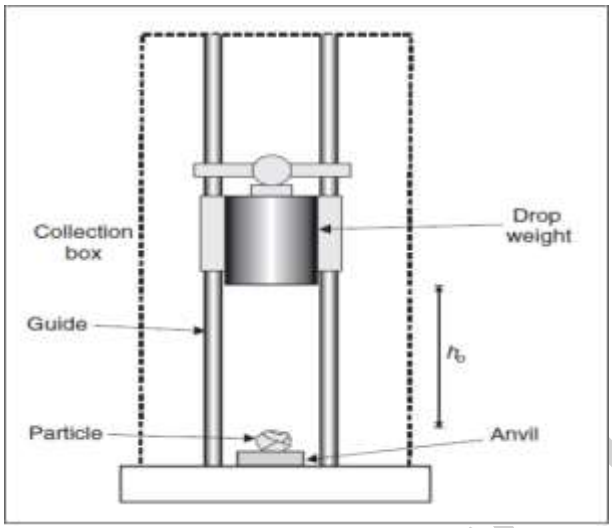

Figure 7:An illustration of the drop weight testing device demonstrating the drop weight at its initial height h_o and particle sample before breakage test in undertaken (Napier-Munn etal.,1996; Tavares.,2007 and Salman et al.,2007)

The particle, placed on a steel anvil, gets crushed as the weight falls under gravity after its release by a pneumatic switch. The device is built on a rigid steel frame which is bolted to a concrete base. A continuum of input energy can be produced by varying the release height and the mass of the drop weight.

When the sample is screened into narrow size fractions, the mean mass of each set of particles to be broken is calculated. The relationship between the required specific input energy for each test and the height at which the weight is released is established by Equation (8).

$$h_{i_1} = \frac{\bar{m}E_{is}}{0.0272M_d} \tag{8}$$

where h_i is the initial drop height (cm), $\bar{m}$ is the mean mass (kg) and M_d is the mass of the drop weight (kg).

According to Napier-Munn et al (1996), the specific comminution energy E_{cs} (kWh/t) equals to the specific input energy E_{is} (kWh/t), as long as the drop weight does not rebound after impact.

An additional 10 cm is usually added to the calculated drop height to allow for the fact that the drop weight rests at some height above the anvil because of the crushed particle after a breakage test is conducted. The height added to the calculated drop height ensures that the final specific comminution energy obtained is correct.

The offset in height (h_f) can be measured for each breakage test and is used to compute the actual input energy with respect to Equation (9).

$$E_{is} = \frac{0.0272 M_d (h_i - h_f)}{\bar{m}} \tag{9}$$

The drop weight test is used to investigate the relationship between input energy and the product size distribution. Salman et al.(2007), has cited that the results of the drop weight tester are useful for validating breakage models.

However, the DWT does not give information about the actual energy used by the rock particles during breakage (Bourgeois & Banini.,2002). Also testing of repetitive impacts at small energies using the DWT is time-consuming (Shi et al.,2009). The frictional losses from the guide rails and rebounding velocities from weights at greater heights lower the energy that is transferred to the particle (Radziszewski & Laplante.,2006).

2.4.5 JK Rotatory Breakage tester

The rotatory breakage device was developed in 2006 due to the limitation discovered in another single particle breakage device particularly the drop weight tester. Recent developments in DEM of milling have shown that small energy impacts occur much more frequently than high energy impacts (Djordjevic et al.,2004). Due to this observation the requirement in breakage testing will be the characterization for the incremental breakage at lower impact energies. However, testing of repetitive impacts at small energies using the DW tester is very time- consuming and hence impractical (Kojovic & Shi,2008; Yahyaei et al.,2015).

The JKRBT was developed for rapid particle breakage characterisation tests. This unit uses a rotor-stator impacting system in which particles gain a regulated kinetic energy while they are

spun in the rotor and are then ejected and impacted against the stator causing the particle breakage (Kojovic & Shi,2009).Figure 8 shows the JKRBT unit with the direction indicator in which the particles are guided.

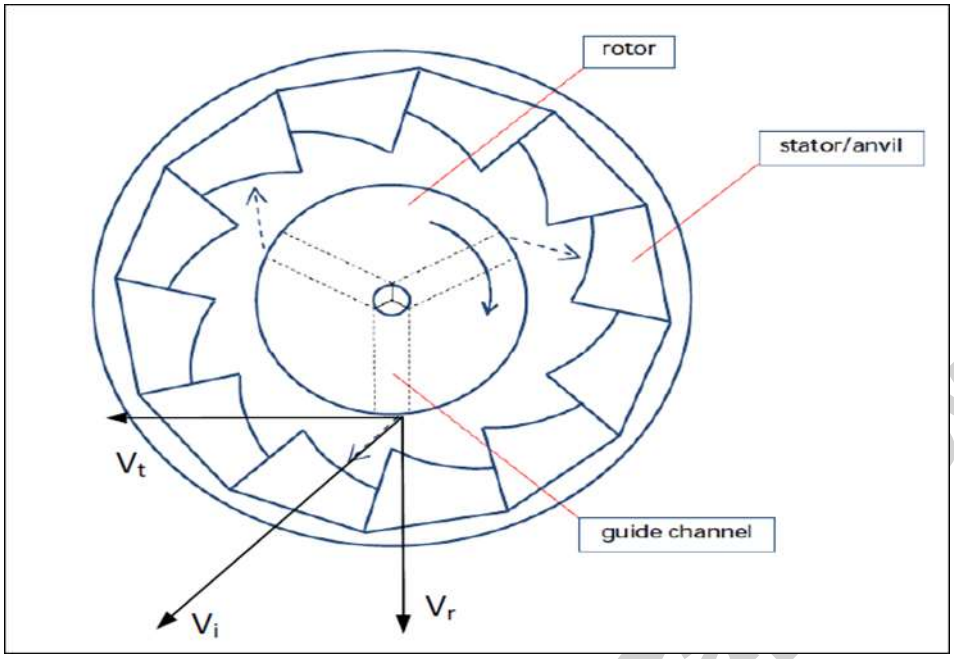

Figure 8:Sketch of the velocity component of a particle being ejected from the rotor (Adapted from Shi & Kojovic.,2001)

JKRBT possesses features that include rapid characterisation of particle breakage properties; ability to test large number of particles to offer statistically more valid results; controlled specific energy due to its independency of the particle mass; achieving higher specific energy levels than the DWT for coarser particles and has a good repeatability in product size distribution (Henk et al.,2015). The JKRBT has a wide range of specific impact energies from 0.001 to 3.8 kWh/t as cited by (Yahyaei et al.,2015).

The specific energy E_{cs} in JKRBT test is determined by equation (10);

$$E_{CS} = \frac{E_k}{m} = \frac{0.5mV_i^2}{m} \tag{10}$$

$$= 3.04 \times 10^{-6} C^2 N^2 \left(r + \frac{xg}{2}\right)^2$$

Where E_{cs} is the specific input energy(kWh/t), E_k is the kinetic energy, m is the mass of the particle (kg), r is the rotor radius(m), X_g is the geometric mean size of feed particle(m), N is the rotor speed(rpm),C is the velocity constant and V_i is the velocity of the particle prior to impact(Shi et al.,2009).

The specific comminution energy of the JKRBT is mostly dependent on the impact velocity of the feed particle, thus the rotor speed and particle size play a role (Shi et al., 2009). The impact velocity is the resultant of the rotor tangential velocity (V_t) and the radial velocity (V_r) as shown on Figure 8. The particle 's velocity ejected from the rotor is determined by the equation(11);

$$V_i^2 = V_r^2 + V_t^2 \tag{11}$$

The assumption has been made that the particle's velocity being ejected is like the impact velocity at the stator (Bbosa,2007; Chikochi,2017). Then the velocity components (V_r and V_t) are assumed to be equal therefore V_i is determined by equation (12).

$$V_i = \sqrt{2V_t} \tag{12}$$

The JKRBT can be used for both single impact and incremental breakage as demonstrated in work done by Bbosa.(2007) as well as Bonfils & Powell(2013).

2.5 Elements influencing breakage behaviour of particles

There are few elements that influences particle breakage, these are energy available to create a crack or cause breakage, particle size and shape, competency or resistance of material to breakage. There are conditions either single particle or bed breakage and confined or unconfined conditions in which the particles are broken (Stamboliadis.,2002; Shi & Kojovic, 2007; Tavares.,2007; Lee & Evertsson.,2013).

The following factors influencing particle breakage will be discussed for the purpose of this study, input energy, particle size and the conditions (confined and unconfined).

2.5.1 Influence of input energy on particle breakage

The specific input energy in size reduction processes has been demonstrated as the most important parameter regulating progeny size distribution from single particle breakage (Tavares & King.,2002; Tavares.,2007).

It was discovered that input energy was proportional to the volume of material broken by Kick (1885) and he proposed another energy-size reduction relationship. He formulated a "law of comminution" based on the assumption that energy supplied to a body increases the level of strain within the body to propagate its internal micro-cracks and that the strain energy of the body is proportional to its volume. Tavares (2007) also pointed out that increasing the input

energy, increases the stressing intensity which in turn intensifies the propagation of cracks in a material.

Due to the increase of input energy, the degree of breakage generally increases (Narayanan., 1985; Kapur et al.,1997; Banini.,2000; Shi & Kojovic.,2007). Bonfils & Powell.(2013) highlighted that a particle that survives an impact becomes increasingly weaker with repeated impact cycles and eventually breaks if the energy applied is above energy threshold the particle can resist.

It was also substantiated by Napier-Munn(1996), that particles of infinite fineness are not the resultant of a single loading event by increasing stressing energy indefinitely. In the work done by Tavares (2007), the maximum product size distribution is dependent on the orientation of distribution of the daughter particles from the first few fracture events, loading geometry, loading rate and on the materials pliability to agglomerate. In addition, Tavares and King (2002) showed that particle weakening from repeated impacts is the result of the growth of crack-like damage.

2.5.2 Influence of particle size on particle breakage

The impact of the particle size on the particle breakage has been investigated broadly in Studies undertaken by Tavares & King.(1998), Banini. (2000), Shi & Kojovic (2007). Tavares & King(1998) observed that the ability of a particle to resist a force without fracturing (particle strength) increases with a decrease in particle size. By contrast, bigger particles tend to offer less resistance to breakage (weaker) and therefore are easier to break than smaller particles. These findings were also confirmed by Banini.(2000) as well as Shi & Kojovic (2007). This trend is because the crack density of larger particles is much greater than that for smaller particles (Tavares & King.,1998). As pointed out by Anderson.(2005), the presence of internal cracks and flaws plays an important role in the fracture of the material.

2.5.3 Influence of particle breakage under confined and unconfined conditions

Confined conditions are required if interparticle breakage is to occur when a bed of particles is compressed. The particle bed could either be fully or partly confined. If no confinement at all is achieved, then only single particle breakage can occur. For choke-fed conditions particularly in the cone crusher, the inlet zone together with the zones down to and including the choke zone will be choke fed and therefore be confined. This implies that interparticle breakage occurs. Single particle breakage will also occur for particles with a particle size larger than the local closed size setting. For the crushing zones below the choke zone the volume

increase makes the forming of confined particle beds unlikely. Therefore, it is assumed that only single particle breakage will occur in these zones (Evertsson.,2000).

When the material enters the crusher chamber, it follows three material flow mechanics;

1. Sliding
2. Free fall
3. Squeezing (Compression)

There are three factors identified to describe interaction flow size reduction; number of crushing zones(capacity), breakage modes and compression ratio. The diagram demonstrates the material flow in the cone crusher chamber with respect to the capacity (Evertsson.,2000) as demonstrated in Figure 9.

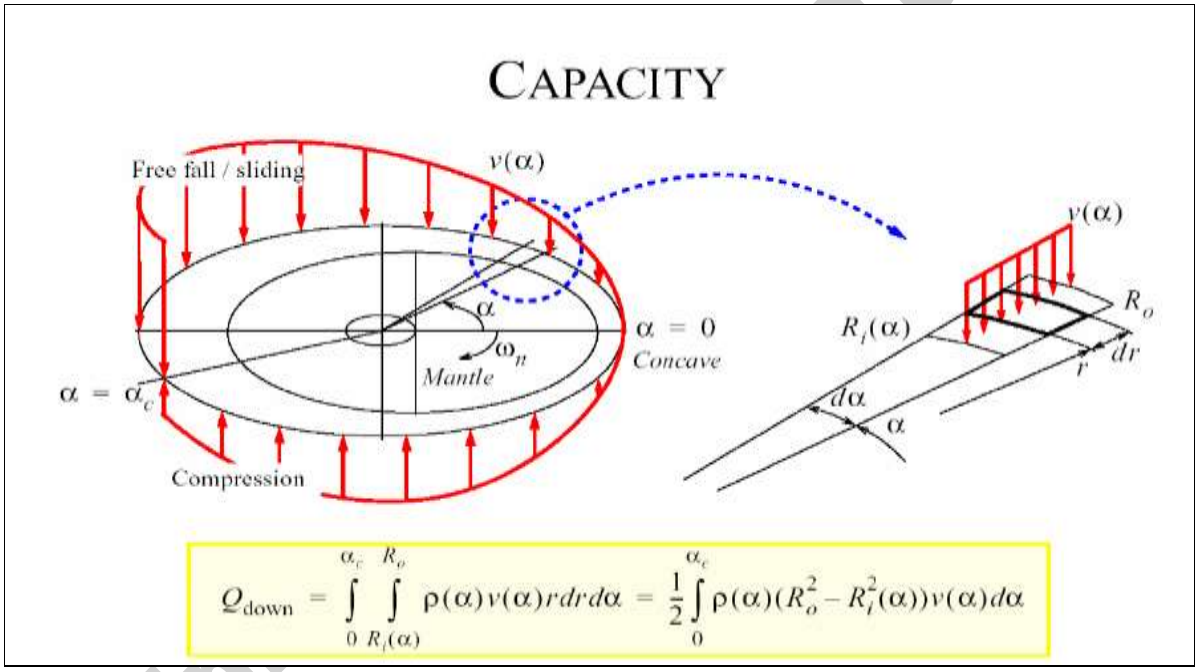

Figure 9:Material flow model in a cone crusher (Evertsson.,2000 & Quarry academy.,2005)

The crushing process can be described with two functions thus selection (S) and Breakage (B) which is referred to rock breakage behaviour.

Dependencies_ compression ratio, Figure 10, illustrates the direction of the inter dependency of size reduction cycle.

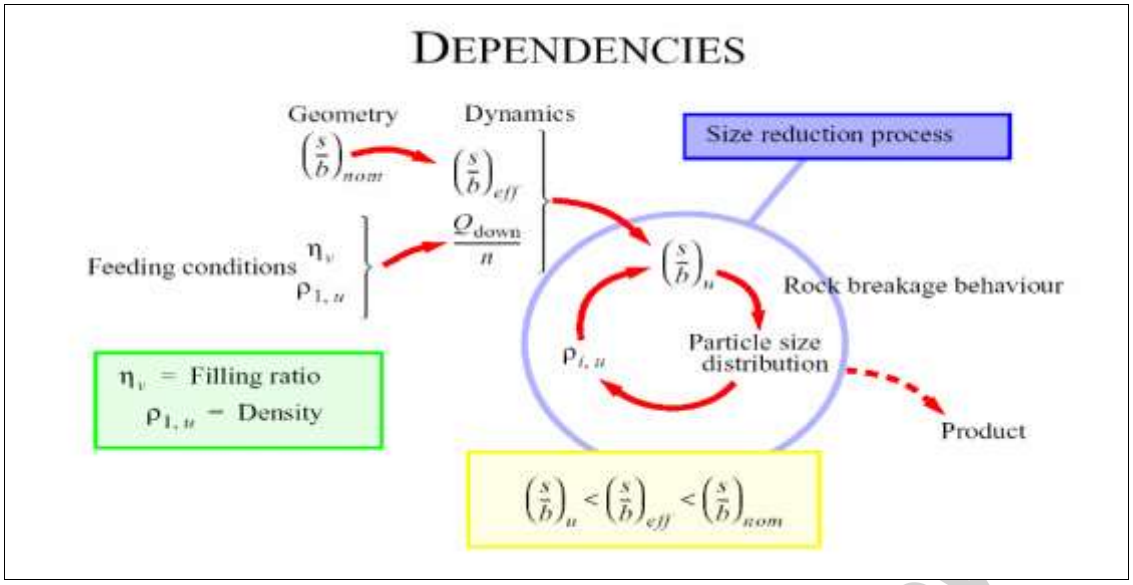

Figure 10:Direction of interdependence for a size reduction cycle(Evertsson.,2000)

$\left(\frac{s}{b}\right)_{u,i}$ = Compression ratio

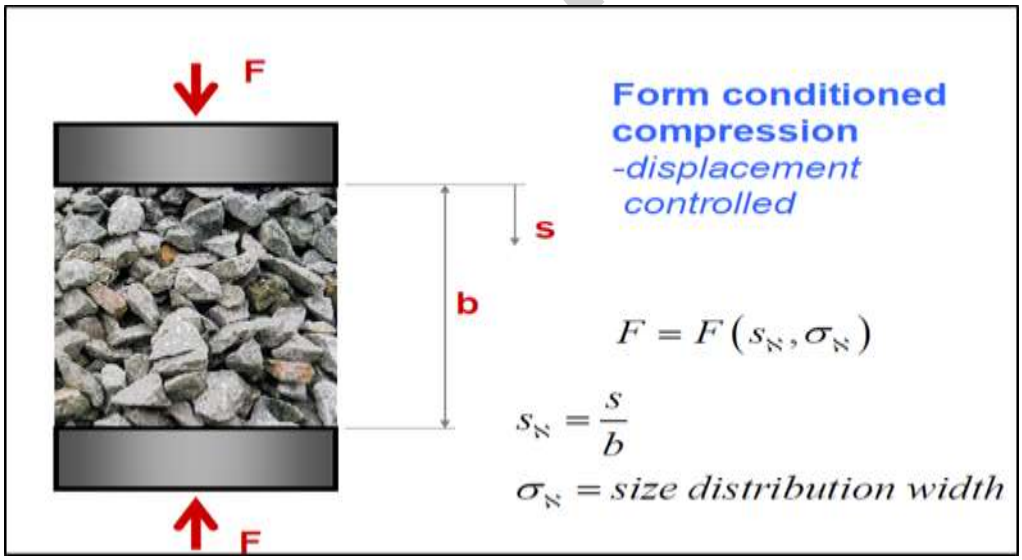

Figure 11:Form conditioned compression-displacement controlled (Evertsson.,2000)

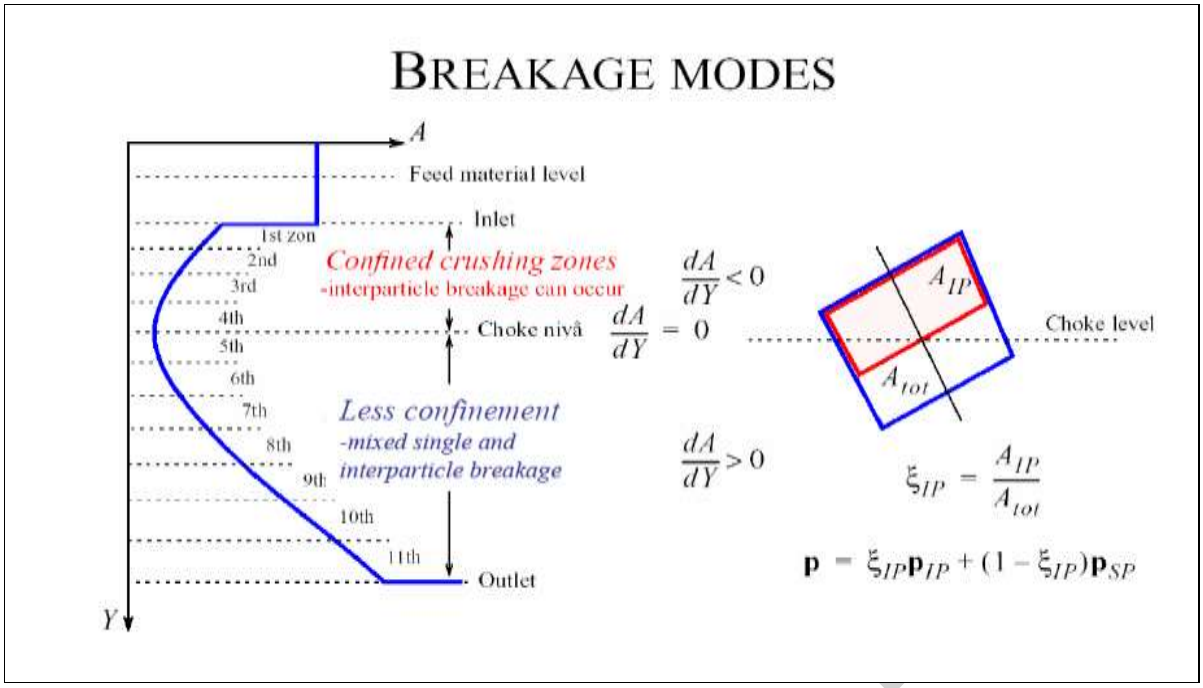

Figure 12:Sketch demonstrating confined and unconfined conditions for single and interparticle breakage (Evertsson.,2000 & Bengtsson et al.,2006)

While Figure 11 shows the form conditioned compression for the controlled displacement, Figure 12, illustrates the breakage modes as the particle movement in different zone within the crusher chamber. A bed of particles can be stressed in confined or unconfined conditions. Confinement refers to any surfaces which affect the lateral movement of particles when stress is applied to the bed. Wall friction affects the stress distribution in the bed; particles in contact with the confining surface are stressed differently to internal ones. The non-uniform stress distribution leads to a complex stress field in the bed (Schönert.,1996).

In confined conditions, typically those found in devices such as high-pressure grinding rolls and cone crushers, the movement of particles contained in the bed is restricted. Therefore, most of the particles undergo stressing when an impact force is applied as very few particles escape from the bed. Fully confined particle beds, defined as ideal particle beds, have been widely used to investigate inter-particle breakage within the bed (Tang et al.,2001). An ideal particle bed is characterized as possessing: a homogeneous structure, homogeneous compaction, a known volume or mass of the stressed particles and negligible wall effects in respect to the overall size reduction effect (Nguyen et al.,2002).

In fine grinding devices such as roller, tumbling and scrubbing mills, some of the particles stressed between the grinding media can escape and be re-positioned within the bed (King.,2000;Clermont.,2010&Weber.,2010). In these devices' particles are stressed in unconfined conditions, in which no lateral restriction of particles occurs. Unconfined conditions

are useful for investigating the breakage behaviour of particles stressed in a similar manner to that occurring in industrial grinding machines.

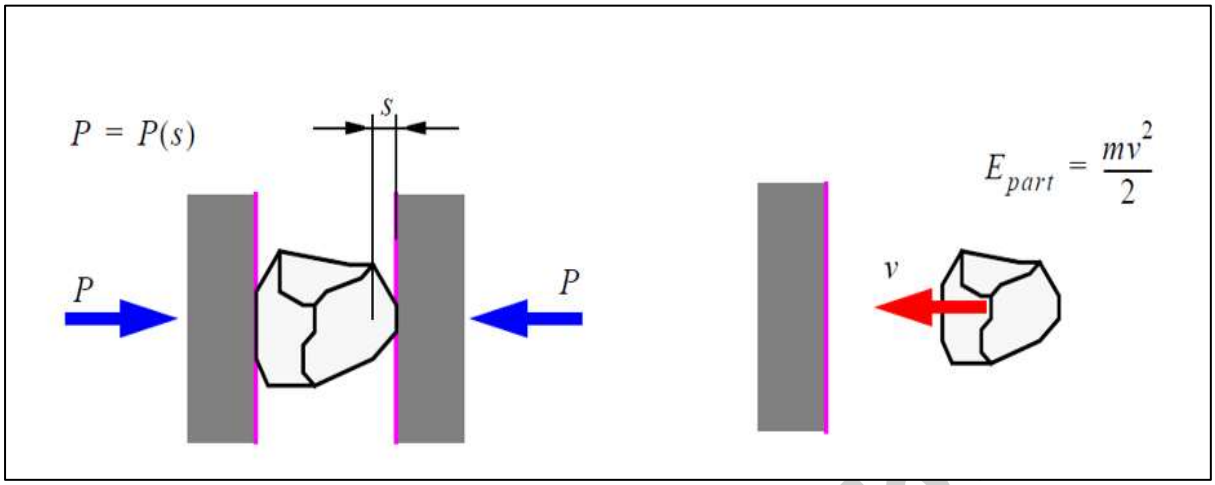

Figure 13:The main difference between form conditioned (left) and energy conditioned (right) breakage in the principle for energy input (Evertsson.,2000)

Figure *13* demonstrates another form of fragmentation principle during particle breakage. This type of breakage is an energy controlled form of breakage. The energy can be induced to the particles by the rotor which in turn accelerates the particle 's velocity close to the peripheral speed on the rotor. The particles are then impacted on the walls of other particles where fragmentation takes place (Evertsson.,2000).

In work done by Barrios et al. (2013) very thin sheets of paper were used to prevent the particles from falling off the bed. It was assumed that the thin paper did not offer significant resistance to the movement of particles when impacted; hence the bed could be classified as unconfined. Since material is not constrained within unconfined beds, a part of it gets ejected when stresses are applied to the bed (Schonert.,1991).

2.6 Standard impact breakage characterization models

Breakage or hardness characterisation models involve an application of numerical methods relations to represent the relationship between the specific energy input and the resultant product size distribution (Napier-Munn et al.,1996; Kojovic &Shi.,2007). A master curve comprising the breakage performance of various materials can be used to describe the breakage probability function of different materials (Vogel & Peukert.,2004; Ballantyne et al.,2013). This information is useful in predicting the performance in comminution devices (Morrell et al.,1996; Bueno et al.,2013).

2.6.1 Ore parameters in modelling (t_{10} breakage model)

The results from the impact breakage tests are used to relate the energy input to the size distribution of the product. The method employed by the JKMRC is the characteristic t_{10} marker. t_n is defined as the cumulative mass % of product passing an aperture of 1/n of the original mean particle size. Therefore, t_2 is the mass percentage of product passing half of the original particle size, t_4 the percentage passing 25% of the original particle size and t_{10} is the percentage passing one tenth of the parent particle size (Whiten.,1972).

An ore-specific family of t-curves can be generated by plotting the t_{10} value against t_2, t_4, t_{25}, t_{50} and t_{75} at different input energies as shown in Figure 15. This graph is useful as it generates the complete product size distribution, expressed as cumulative mass percent passing, for any t_{10} value.

After extensive experiments it was found that the same family of t-curves describes the breakage behaviour of a wide range of ore types.

This relationship can be represented by equation (13):

$$t_{10} = A(1 - e^{-bE}cs) \tag{13}$$

Where E_{cs} is the specific comminution energy (kWh/t) and Axb are ore-specific impact breakage parameters characterising the ore's breakage behaviour.

The impact breakage parameters, A and b, characterize the material's fragmentation behaviour and can be determined through interpretation of typical t_{10}-E_{cs} curve shown in Figure14 (Tavares., 2007).

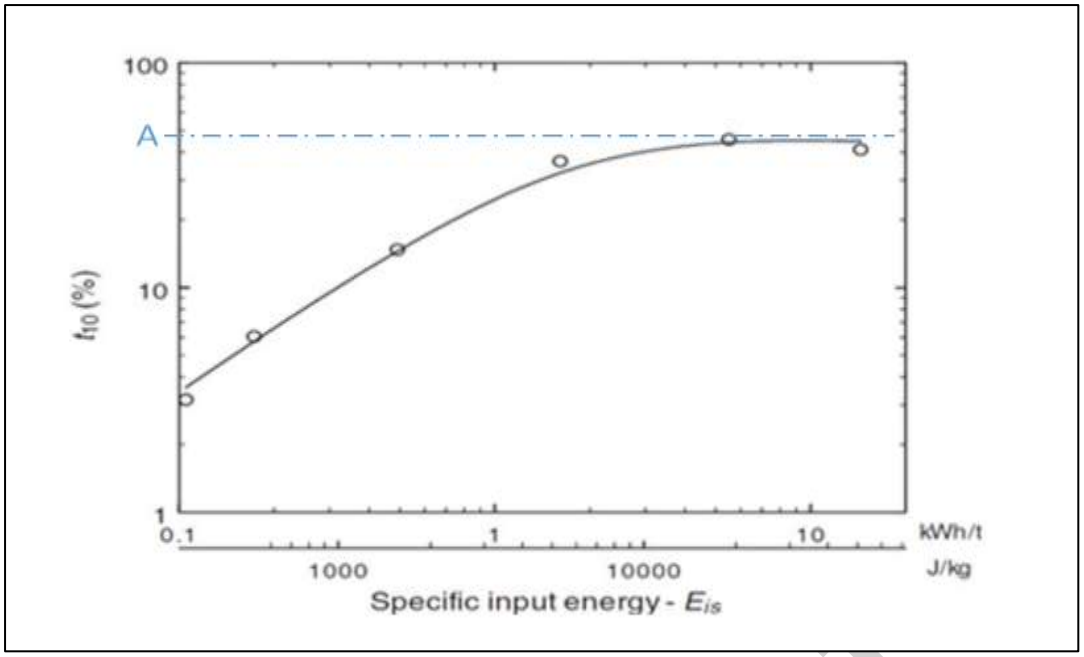

Figure14:Relationship between the parameter t_{10} and specific input energy(E_{cs} or E_{is})(Adapted from Tavares.,2007)

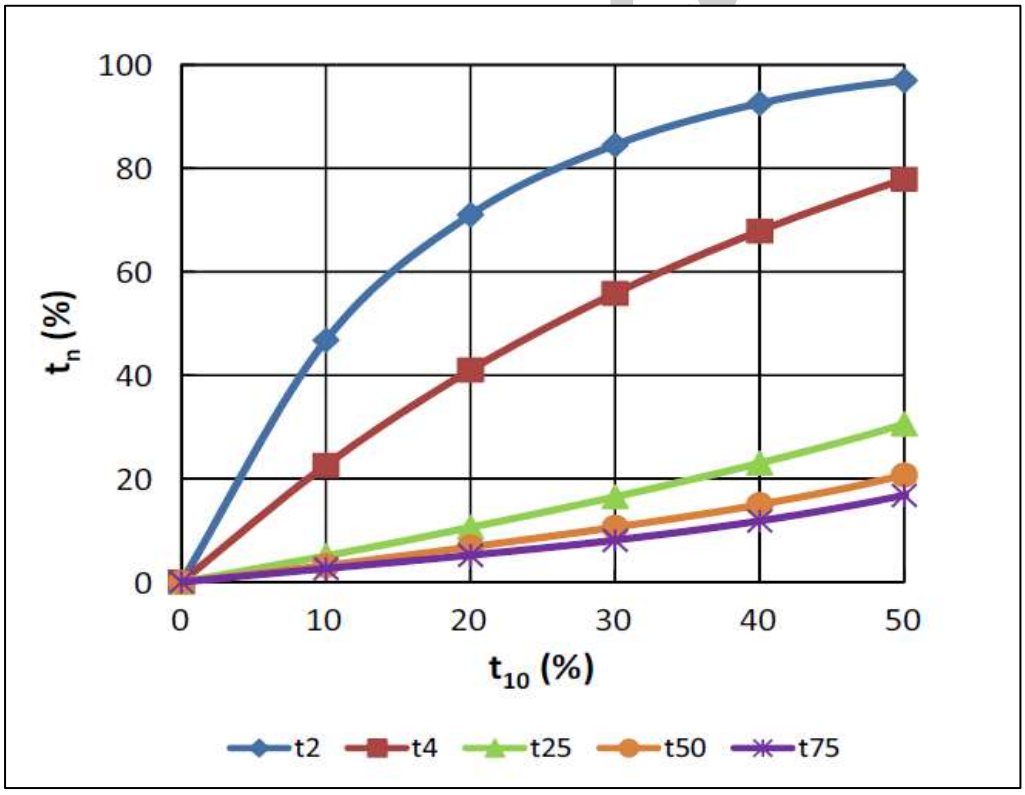

Figure 15:t_n-family of curves of ore breakage (Zuo & Shi.,2016)

Since particle (x) incorporated in the Vogel-Peukert breakage probability model, it was anticipated that the particle size effect on the breakage can be accommodated using the fundamental breakage model structure. The Vogel-Peukert probability model was therefore revised to describe the breakage index t_{10} by Shi & Kojovic (2007). Figure 15, shows the determination of size distribution parameter t_n from the breakage index t_{10}(Zuo & Shi.,2016).

Figure 15 show the tn family of curves of ore breakage tested by Zuo &Shi (2016). t_{10} can be interpreted as a 'fineness index' implying that ore types with larger t_{10} values are more amenable to breakage resulting in a finer product size distribution. A is a limiting value, usually around 50 for hard ores, indicating at higher energies less additional breakage occurs as the size reduction process becomes less efficient. The product A×b has commonly been used as an index for rating the ore's resistance to breakage (Shi et al., 2013). It is equal to the gradient of the curve at "zero" energy.

A larger 'A×b' value implies a 'softer' ore more amenable to breakage. The data reduction procedure adopted by the JKMRC has a weakness: it does not take particle size into account. It was found (Shi & Kojovic.,2007; Banini.,2000) that larger particles exhibit a larger crack density than smaller particles – larger particles tend to be weaker and therefore easier to break than smaller particles.

Since the previous procedure only uses one set of average A and b parameters, it is assumed that all rocks will behave the same when subjected to identical specific energies. This simplification leads to questionable model outputs (Masuret.,2015).

Shi & Kojovic (2007) proposed a modified t_{10}-energy relationship, taking account of particle size, specific impact energy as well as the number of collisions applied. The size-dependent model will be discussed in the next section.

2.6.2 Ore parameters in modelling (size-dependent breakage model)

Shi and Kojovic (2007) reported a size-dependent model to describe the degree of breakage index, which is modified from a breakage probability model published by Vogel and Peukert (2004), in relation to material property, particle size and net cumulative impact energy.

The size dependent model, as shown in Equation (14);

$$t_{10} = M(\{1 - e^{-fmat\ x\ k\ (Ecs\ -Emin)}\}) \quad (14)$$

where M is the maximum t_{10} for a material subject to breakage (in %), fmat (kg/J/m) is the material breakage property, x (m) is the initial particle size, k is the successive number of impacts with the single impact energy and E_{min} is the threshold energy. These last two parameters are set to 1 and 0 respectively.

The modified model directly correlates to the t_{10} breakage model (equation 14) such that the value of A would be replaced by M, while b replaced by $f_{mat}.x$, and E_{cs} replaced by $k(E_{cs}-E_{min})$. The model was validated through several test with various types of ore and quarry material (Banini.,2000; Shi & Kojovic., 2007).

2.7 Typical Diamond processing plant flowsheet

Separating diamonds from kimberlite or lamproite ore requires a primarily mechanical, multi-step liberation process. The ore must be broken down into progressively smaller pieces, until the diamond crystals can be physically recovered with little or no damage. The various operations such as Letseng diamond mine (Bornman.,2010), Mothae diamond mine(Lynn & Ferriera.,2013), Jawaneng Diamond mine(du Plessis & Sewana.,2003), Gahcho Kue mine(Johnson & Pilotto.,2018), and Argyle Diamond mine(Shigley,Chapman & Elison.,2001) use these five basic operations:

1. Crushing the ore (in several stages)

2. Scrubbing the broken rock fragments with water to remove dust and clay

3. Screening the ore into specific size fractions

4. Starting from a particular size fraction of the ore, concentrating the diamonds using a heavy medium separation

5. Separating the diamonds from the other heavy minerals by means of X-ray luminescence technology

In the final step, X-rays are used to make the diamonds luminesce. An optical sensor triggers a blast of air to remove each diamond from the concentrate.

These X-ray sorters, which were developed specifically for use of diamond recovery can detect diamonds during sorting.

Table 1 demonstrates the similar units in a typical plant flow sheet of diamond processing plant.

Table 1: Review of the similar processing units in a typical diamond processing plant

Mine	**Letseng Diamond Mine**	**Mothae Diamond Mine**	**Mountain Province Diamond**	**Argyle Diamond Mine**
Reference	Bornman,2010	Lynn & Ferriera,2013	Johnson & Pilotto,2018	Shigley, Chapman& Elison,2001
Primary crushing	X	X	X	X
Scrubber	X	X	X	X
Secondary crushing	X	X	X	X
Tertiary crushing	X	X	X	X
Screening and classification	X	X	X	X
Dense medium separation modules	X	X	X	X
X-ray sorting machines (Flowsort)	X	X	X	X
VE single sorter		X		
XRT sorter		X		

A review of diamond processing plant showed that the process flowsheets shows that there is a conventionally acknowledged flowsheet with similar arrangement of equipment and stages. The differences in the flowsheet are related mainly to capacity, size and number of process units for each stage. The design for the processing plant where the current study was performed follows the conventional diamond processing approached which contains many of the aspects captured in Table 1. The process description and material flow are outlined in detail in section 2.8. The equipment where diamond breakage is likely to occur has been given prominence in the process equipment description.

2.8 Process description and material flow

The run-of-mine (ROM) ore is processed through the plant which comprises of a conventional diamond processing circuit with a combination of jaw and cone crushers, coarse and fines dense medium separation circuits, and continuous X-ray fluorescence technology.These relevant unit processes are described in more detail in this document. Figure 16 shows plant flow diagram

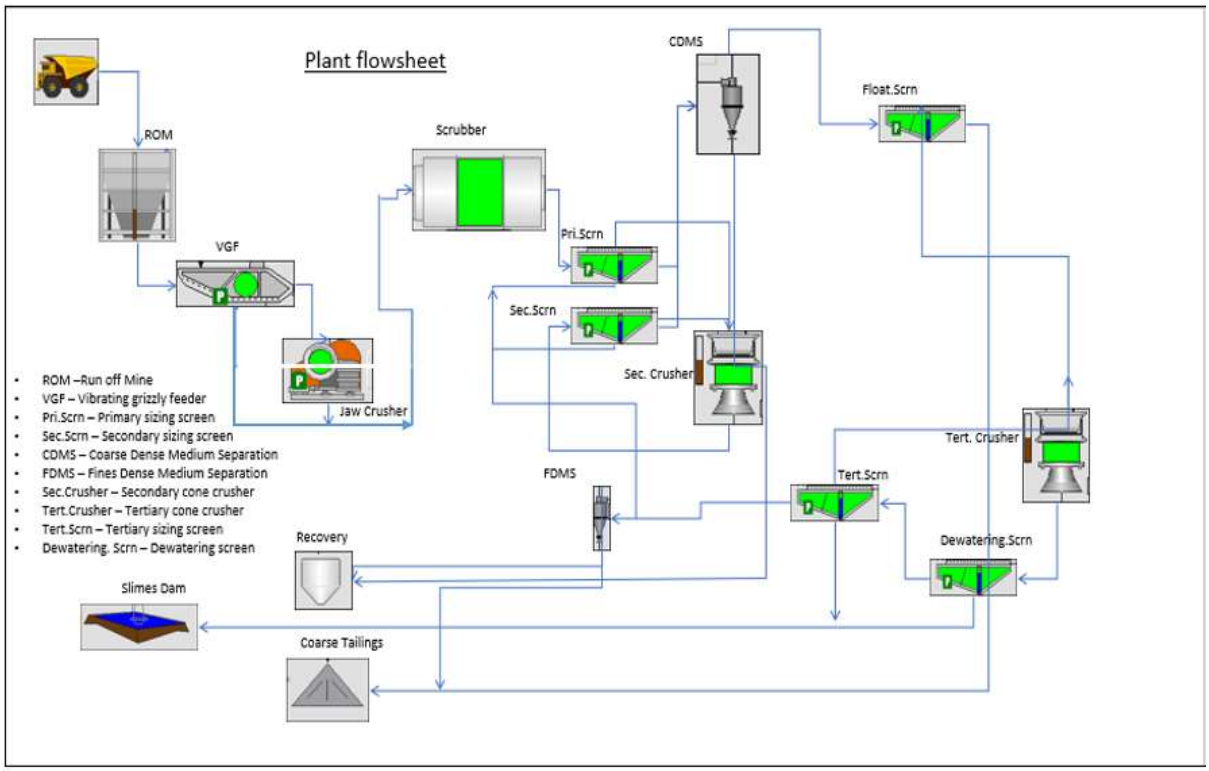

Figure 16: Plant flow diagram

2.8.1 Ore Receiving, Primary Crushing, Scrubbing and Screening

ROM material is fed directly into the plant feed bin via articulated dump trucks. The bin is fitted with a Static Grizzly to protect downstream processes from oversize material. The oversize ROM material is broken down by means of a hydraulic Rock Breaker on top of the static grizzly and reports to the feed bin.

Ore is withdrawn at a controlled rate from the feed bin by an Apron Feeder and discharged onto a Vibrating Grizzly Feeder. The +120 mm grizzly oversize reports to the Primary Jaw Crusher, where the material is crushed to minus 120 mm. The product is combined with the grizzly undersize and conveyed to a splitter chute arrangement to feed two Scrubbers. The scrubbers de-agglomerate fines/clay material from the feed and each discharge onto two

double deck Scrubber Sizing Screens. Spray water is added to the top and bottom decks of the screens to facilitate the screening process. The sizing screens' top deck oversize (+40 mm) is conveyed to the secondary crusher feed bins. The sizing screens' bottom deck oversize (+4-40 mm) is conveyed to the Coarse Dense Medium Separation feed bins. The screens effluent (-4 mm) is pumped to a set of De-Sliming Screens.

2.8.2 Secondary Crushing

Material in the +40mm size fraction is withdrawn at a controlled feed rate from the Secondary Crusher feed bins to ensure choke feed conditions to two Secondary Cone Crushers. The crushed product is conveyed to a double deck Secondary Crusher Sizing Screen. The top deck oversize (+40mm) is kept in closed-circuit to the crusher feed bins. The bottom deck oversize (+4-40mm) is conveyed to the Coarse Dense Medium Separation (DMS) feed bins. The sizing screen effluent (-4mm) is pumped to the De-Sliming screens.

2.8.3 Dense Medium Separation Feed Preparation

The 1.25 mm to 4 mm fraction from the de-sliming section, together with 1.25 mm to 4 mm material from the tertiary crushing circuit described in section 2.8.5 makes up the feed to the Fines DMS feed bins. Material gravitates from the DMS feed bins onto vibrating feeders discharging onto the DMS feed conveyors at a controlled rate (the conveyors are equipped with weightometers).

2.8.4 Coarse Dense Medium Separation

Coarse DMS circuit consists of two identical DMS modules as described further in this section. Coarse DMS feed is conveyed to the feed preparation screens from where the clean 4 – 40 mm oversize fraction is discharged into the DMS mixing box where the ore is mixed with ferrosilicon medium at the correct density before it is pumped to the Dense Medium Cyclone where separation takes place.

The higher density particles (product) move outwards and down the wall of the cyclone and are discharged through the spigot. The less dense particles (discard) move towards the central axis of the cyclone, are caught in the vortex, and discharged through the overflow.

The discard (cyclone floats) are discharged from the Dense Medium cyclones onto the Floats drain and rinse screens. It is first drained and then washed to remove adhering medium. The screen top deck oversize (nominally +10 mm) is conveyed to the tertiary crushing circuit and the bottom deck oversize (-10 mm) is conveyed to the tailings system.

The product (cyclone sinks) is discharged onto the double deck Sinks drain and rinse and sizing screens where it is first drained and then washed to remove adhering medium. The remainder of the screen is used to size the DMS concentrate into three size fractions, namely: middles (+4-8 mm), coarse (+8-16 mm) and extra coarse (+16-40 mm) for processing through the coarse Final Recovery modules.

2.8.5 Tertiary Crushing

Coarse DMS floats material in the 10-40 mm size fraction is conveyed to three Cone Crushers. Material is withdrawn from the feed bins by vibrating pan feeders at a controlled feed rate to ensure choke feed conditions in the tertiary crushers. The cone crushers are water flushed.

Each crusher's product is discharged onto separate Dewatering screens and is then conveyed to a Tertiary Crusher sizing screen. The +10 mm top deck oversize remains in closed circuit and is recycled back to the crushers. The 1.25 to 10 mm fraction is conveyed to the Fines DMS feed bins.

2.8.6 Fines Dense Medium Separation

The Fines DMS circuit also consists of two identical DMS modules which operate in a similar manner as the Coarse DMS modules. The only processing difference between the modules is the sizing of DMS concentrate into three different size fractions, namely: fines (+1.25 -3 mm), coarse (+3-6 mm) and extra coarse (+6-12 mm) for processing through the fines Final Recovery module.

2.8.7 Coarse and Fines Final Recovery Circuit

Each DMS module has an integrated Final Recovery circuit. Collected concentrates are processed through X-Ray fluorescence machines for final concentration. The final concentrate is dried before discharging into the Sorthouse glovebox hoppers for the different size fractions. Final recovery tailings are stored for potential future re-treatment with alternative technologies.

2.9 Unit operation and applications

The units that have an impact on the diamond breakage has been reviewed in detail in the next section.

2.9.1 Scrubber

The scrubber operation is likened to a tumbling mill operation, particularly an autogenous mill where the charge is only the ore material. The particle breakage mechanism in the scrubber follows three methods; impact, attrition and abrasion where there is particle to particle interaction. The main function of the scrubber is to wash the dirt and clay from the feed and it further de-agglomerates clays and the ore to potentially expose any locked diamonds. According to Wills & Napier-Munn.,(2006) a combination of compressive or tensile stresses can break the particles with weak crystalline structure.

The three modes of particle breakage in tumbling mills (abrasion, attrition and impact) are illustrated below (Napier-Munn et al.,1996).

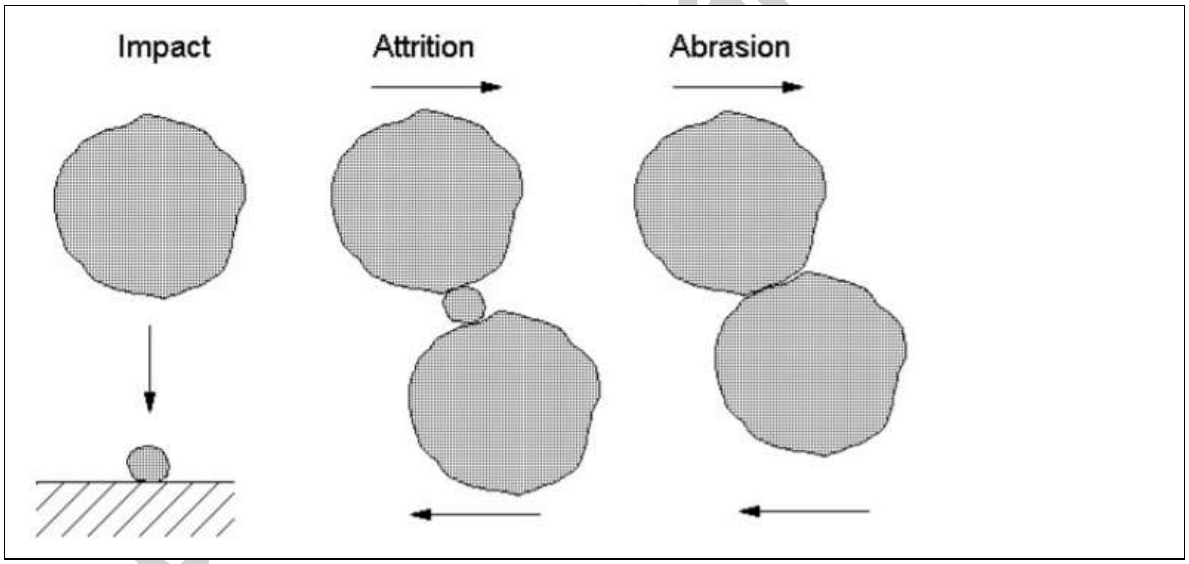

Figure 17: Principal breakage mechanism (Napier-Munn.,1996)

In particle breakage through abrasion, there is a surface contact between the particles and they rub against one another in a parallel motion. Kelly & Spottiswood(1982), described abrasion as the process that takes place when insufficient energy is subjected to the particle to create a fracture and small pieces are broken off leaving the parent particle mostly intact. Abrasion occurs when two or more particles moves along their planes of contact and small pieces of the surface are worn off, leaving the

core of the particle largely intact. Abrasion is the main mechanism of comminution in autogenous grinding, Wills(2005).

During impact particle breakage, the impacting particle travels in a perpendicular direction to the plane of contact (Napier-Munn et al.,1996). The energy imparted to the particle is more than what is required to generate a fracture. Kelly & Spottiswood (1982) described this condition as the particle being overloaded in several areas producing progeny particles of a wide range of size distribution. It is also stated by Napier-Munn et al. (1996) that the magnitude of breakage is directly linked to the energy per unit mass that the targeted particle receives.

The attrition particle breakage mechanism takes place preferentially on conditions of particle on particle interaction (Wills & Napier-Munn.,2006). Smaller particles are fragmented before larger ones; thus, the contacting particles increases the extent of compressive stress resulting in shear failure (Napier-Munn et al.,1996; Wills & Napier-Munn.,2006; Kelly & Spottiswood.,1982; Hayes.,2003). The energy exerted on the particle is just enough to propagate the existing crack (Kelly & Spottiswood.,1982).

The different breakage mechanisms that occur within the tumbling mills(scrubber) are allocated mainly to two positions in the mill. The first position is the toe region where impact breakage occurs, and the second is within the body of the charge as it is lifted by the rotation of the mill. The frequency with which the charge turns, and the energy of impact determines the amount of breakage that occurs. Abrasion and attrition mainly influence the breakage of finer particles and occur within the body of the charge, as it is lifted by the rotation of the mill. The body of the charge comprises a series of layers that slip over each other, and the frequency of breakage depends on the relative velocity of the layers, which is dependent on the internal friction angel of the material and the rotational speed of the mill. The impact energy is dependent of the height of the fall and the weight of the lumps.

The rotational speed of the mill is important since it governs the nature of the product, grain size distribution, throughput and the amount of wear on the mill linings. If the speed is too low the grinding medium tends to roll down to the toe and essentially abrasion grinding occurs. If the rotational speed is too high the grinding media hits the mill linings instead of the toe of the charge and the linings wears rapidly. If the speed is even higher, above “critical speed” the whole mill charge starts to centrifuge. Motion

of the charge in the mill is demonstrated in Figure 18. An increase in speed up to 40-50% of the critical speed increases the capacity, e.g. throughput, of the mill. In practice mills are driven at 50-90% of critical speed, Wills.(2005).

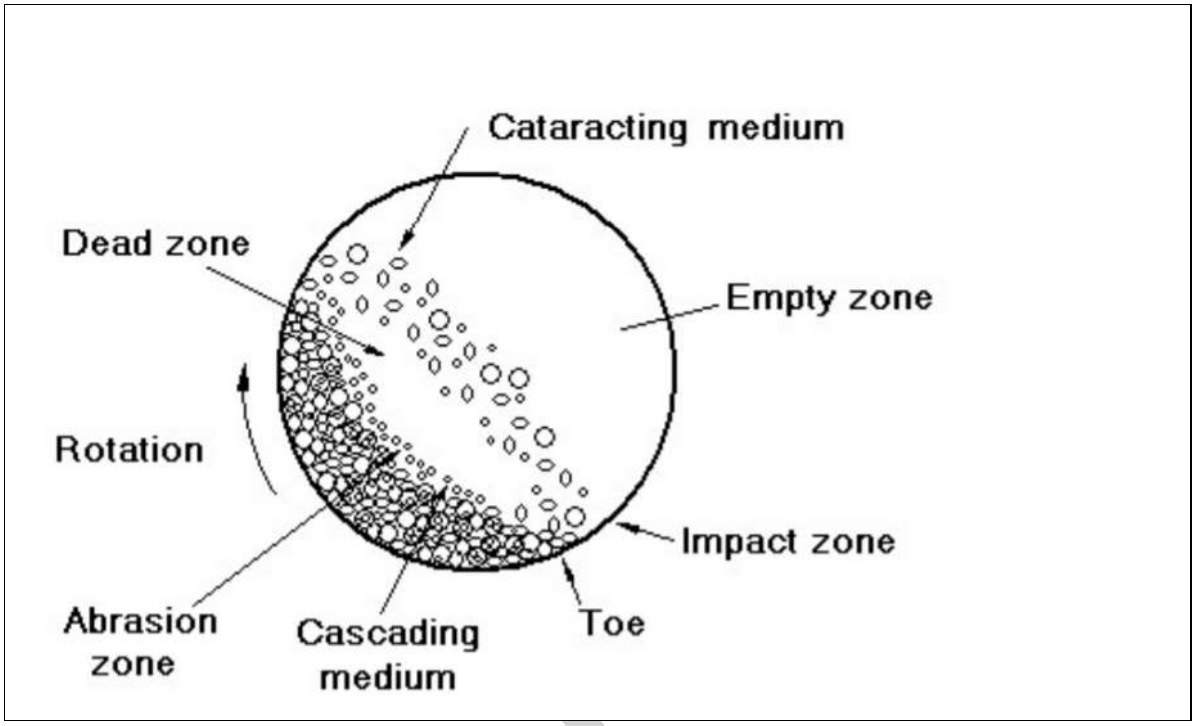

Figure 18: Motion of charge in tumbling mills (Scrubber) (Adapted from Wills.,2005)

The geometry of the grinding mills affects the size of the final product. A small diameter to length ratio gives a finer product than a large diameter mill does, and more of the breakage is caused by abrasion, Wills (2005).

The tumbling mills have been developed to a high degree of mechanical efficiency and reliability, however they are very wasteful in terms of energy expended, since the ore is mostly broken as a result of repeated, random impacts which break liberated and unliberated particles (Wills & Atkinson.,1993).

The influence of feed size on scrubber performance naturally is derived from feed ore. Any changes in the feed size distribution therefore results in a change in product size distribution, this in turn affects the breakage characteristics of the scrubber (Napier-Munn.,1996).

2.9.2 Crushing

Crushing operation is the initial mechanical stage of size reduction and it is mainly to liberate minerals of interest (Wills & Napier-Munn.,2006). The ore is crushed and delivered to subsequent ore processing unit operations. According to Napier-Munn et al.(1996), the most important machine dimensions are;

- Throat dimension, the largest rock that can be crushed
- Open side setting (OSS), largest gap aperture the material can fall
- Close side setting (CSS)
- Stroke or Throw and
- Liner dimensions

The capacity of the crusher is dependent on the feed size of the material, strength of the feed and the filling of the crusher chamber. The crushing of the material is not affecting the shape of the grain size distribution curve that much, in fact mainly the coarsest material is being crushed, the finer material is originated by blasting, Shimkus et al.(1998). By choke feeding crushers more fines material can be produced, by inter particle breakage, Napier-Munn (1996). The blasting affects the crushing performance in several ways, besides that the rock mass is liberated and it is weakened by increasing the number of cracks/micro- cracks, Nielsen and Kristiansen.(1996) and Eloranta.(2001).

Comminution take place in every unit that reduces particulate size material such as bulk commodities or ore. Large feed particles are fractured yielding the material in an increasingly fine product. Breakage of larger size material is typical referred to crushing whilst breakage of smaller material is referred as grinding (Cleary.,2017). In an earlier work done by (Napier-Munn et al.,1996) it was shown that a cone crusher is a device that breaks the rocks by squeezing them between an eccentrically gyrating cone and concave.

A concept of a crusher model that gives the product size after the crusher is described by Valery et al.(2001). In this model the feed material undergoes a series of breakage and classification stages as it passes down the crusher chamber reducing in size referred to Figure 19. Each breakage event is assumed to produce the same geometric size reduction.

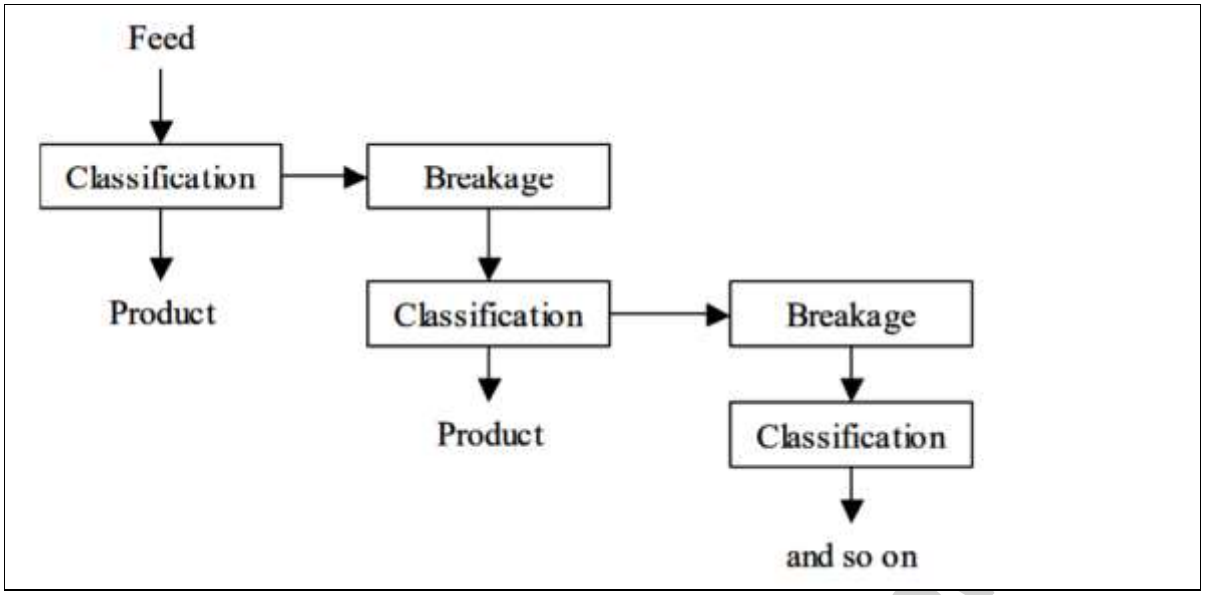

Figure 19: Concept of a crusher model (Napier-Munn et al.,1996 & Valery et al.,2001)

Classification in the chamber of the crusher is controlled by the open and closed side setting (Valery.,2001). If the rock is larger than the open side setting (OSS) then it will remain in the chamber and be broken. On the contrary if the rock is smaller than the closed side setting (CSS) it will fall through the chamber and not be crushed. For rocks which are in between the CSS and OSS in size a probability exists from them to either remain or pass out of the crusher. This probability (classification) function has a shape like that shown in Figure 20. It is described by 3 parameters - K1, K2, K3, where K1 and K2 ideally should equal the CSS and OSS respectively and K3 describes the shape of the curve.

The crusher model is expressed by a classification function represented by C(x) which is the probability of the selection for breakage of a particle of size x. Figure 20, shows the classification for the crusher model. The general form of the relationship defines a size where all particles are broken C(x) = 1, a size where no particles are broken C(x) = 0 and the particles in between have a probability greater than zero and below one with smaller particles having low probabilities and larger particles higher probabilities. The model is described by three parameters:

C(x) = 1 - for x > K2 (all particles are broken)

C(x) = $1-(k2-x/k2 \quad -k1) * k3$ - for K1 < x < K2

C(x) = 0 - for x < K2 (no particles are broken)

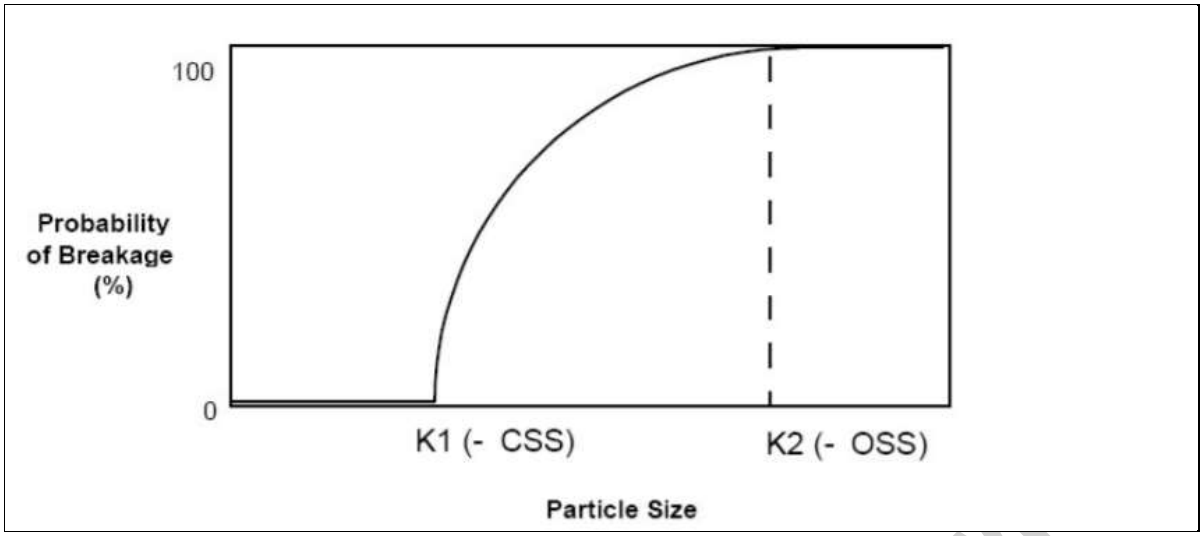

Figure 20: Classification function for the crusher model (Valery et al.,2001)

The crusher operation mostly affects the coarsest part of the material size distribution. The cone crusher operates by compressing the particles between two liner surfaces, thus inducing two different modes of compressive breakage; single particle breakage and inter-particle breakage (Quist.,2017).The eccentric movement of the main shaft axis creates crushing whereby the particles are nipped, compressed and crushed between the mantle and the concave liner (Evertsson.,2000; Napier-Munn et al.,1996). Particle breakage in the cone crusher chamber could either be single particle breakage, where there is particle interaction with the liners, or inter-particle breakage, which takes place between particles (Evertsson., 2000; Wills & Napier-Munn.,2006). This action is due to impact and attrition of a multi-layered portion of particles within the crusher chamber, demonstrates the principle of cone crusher during particle breakage. It was further concluded by Quist (2017) that interparticle breakage is dependent on the feed size distribution, hence results in packed behaviour.

The level of comminution and resultant particle size distribution are largely influenced by the crusher close side setting (CSS). The crusher produces finer product as the gap is closed. In addition, Hulthen (2010) showed that the CSS is used for open loop control in several crushing plants over the world. Due to continuous cyclic motion of the mantle, the distance between the cone and the concave liner changes, thus affecting the particle size distribution, as well as resulting in changes in the crushing ratio and capacity (Hulthen.,2010). The longer the particles stay in the crusher chamber the more compression events they get exposed to (Evertsson.,2000).

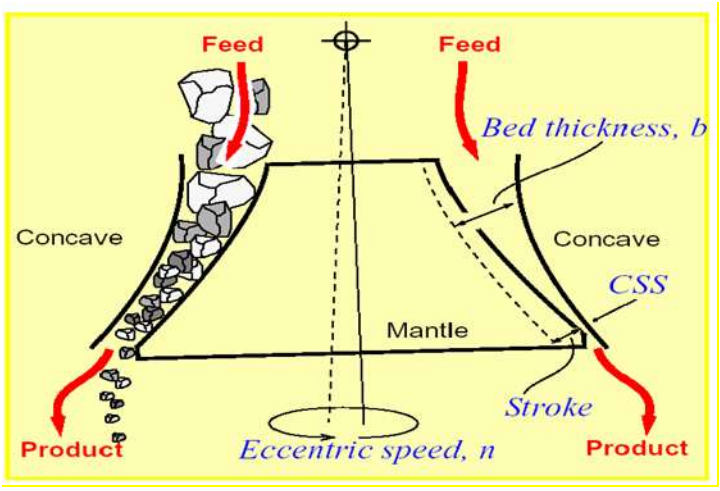

Figure 21:Principle of a cone or gyratory crusher (Evertsson.,2000)

The operational parameters that are discussed in this literature review are only those that have an influence on particle breakage. According to Quist (2012), operational control parameters are those variables that can be altered during the operation of the equipment to control and influence performance.

Eccentric speed has an important effect on the cone crusher product. When the eccentric speed is increased the material is exposed to a higher number of compressive events (Hulthen.,2010; Quist.,2012 ;Jacobson & Lamminmaki.,2013). An increase in the number of compressive events results in a finer particle size distribution, hence the particle takes longer to flow through to the crushing zone (Quist.,2012). Hulthen (2010) showed that by connecting frequency drives the eccentric speed can be attuned throughout the operation.

2.9.3 Transfer points and chutes

As a result of diamond and simulant work done at De Beers Diamond Mines, Rider & Roodt. (2003) has outlined that several practices had to be stopped, modified or phased out due to the following;

- Pneumatic conveying of free diamonds
- Use of impact crushers
- Pumping of diamond concentrates in a water medium is being replaced by jet pumping or modified to reduce tip speeds
- Drop heights for free diamonds are being minimized and construction materials are being changed to minimize the effect of impact

Four distinct mechanisms of size reduction have been identified in fully autogenous mills: attrition, chipping, impact fracture and self-breakage. Attrition is the steady wearing away of comparatively smooth surfaces of lumps due to friction between the surfaces in relative motion. Chipping occurs when asperities are chipped off the surface of a particle by contacts that are not sufficiently vigorous to shatter the particle. Attrition and chipping are essentially surface phenomena and are commonly lumped together and identified as wear processes. Impact fracture occurs when smaller particles are nipped between two large particles during an impact induced by collision or rolling motion. Self-breakage occurs when a single particle shatters on impact after falling freely in the mill. Rates of breakage and the progeny spectrum formed during these processes differ considerably from each other and each should be modelled separately.

A fifth breakage mechanism occurs in a semi-autogenous mill when particles are impacted by a steel ball. Breakage and selection functions that describe this mechanism can be modelled in a manner like those used for the ball mill (King,2000).

In practice three distinct fracture sub-processes are modelled: wear, impact fracture, and self-breakage (Zehra Pinar et al.,2015). Each of these produces essentially different progeny size distributions and the appropriate breakage function must be used for each.

The breakage function for attrition and chipping A(x;y) can be measured in the laboratory in mills that contain only large lumps that are abraded under conditions like those found in operating mills. No general models for the attrition breakage function have been developed (King,2000). The breakage function B(x;y) for the impact fracture process can be modelled using the same model structures that were used for ball milling. The breakage function for self-breakage C(x;y) can be modelled using the t_{10} method that describes single-particle impact fracture using the impact energy equal to the kinetic t_{10} energy of the particle immediately before impact (Taveres.,2007). Particles will have a wide distribution of free-fall impact energies in a real mill and the breakage function for self-breakage is obtained by integration over the impact energy spectrum,

$$C(x;y) = \int_0^\infty C(x;y,h)P(y,h)p(h)dh \tag{15}$$

where C(x;y, h) is the single particle breakage function for self-breakage of a particle of size y in free fall from height h, P(y,h) is the probability that a particle of size y will shatter when falling a vertical height h and p(h) is the distribution density for effective drop heights in the mill or surge bins.

2.10 Simulants and Tracers

Simulants and tracers are a testing tool used by plant metallurgist to optimise circuit performance. They are used in circuits which separate the valuable mineral from the gangue or waste by differences in particle densities (Danoczi,2007).

There are different types of tracers in industry and these includes spiking tracers, Luminescent tracers, ceramic diamond simulants and density tracers.

Spiking Tracers mimic the density of a valuable mineral and are used in situations where the mineral particles are well liberated (Davis et al.,1985a). Their most common application is to test for recovery of free diamonds from an alluvial deposit. They can be inserted in the ore stream anywhere between the pit and the final sorting stage. If that final sorting stage utilizes X-ray sorters, the tracers should luminesce strongly under X-rays to ensure none will be rejected at that point.

Luminescence Index Tracers mimic diamonds in terms of density and luminescence to simulate the response to X-rays of high-luminescent and low-luminescent diamonds. Like diamonds, they should be translucent to light, so that the luminescence is a volume effect, not just a surface effect. The X-ray machine utilizes this property of a diamond to discriminate it from other particles (Danoczi & Koursaris.,2008).

Density Tracers are particles having precise densities to mimic the densities of particles in a plant feed stream (Davis et al.,1985a). Density tracers with densities spanning the range of interest are added to the circuit feed and retrieved from the product and rejects streams, manually or with the assistance of magnets. Tracers are added to the ore in far higher concentrations than the mineral, so providing the mine with greater confidence that the equipment is functioning correctly while also providing statistical information on the mine's recovery efficiency. The most common tracers in use on the mines are the density tracers, which are used to set up density separation equipment such as DMS cyclones, cones and pans. The density tracers are used to evaluate and compare the performance of different density separation equipment as well as the performance of equipment with various operating parameters. (Danoczi & Koursaris.,2008).

The use of diamond simulants makes it possible for the management at mining sites, and particularly at diamond separation and recovery plants, to identify the stages in ore handling or subsequent processing, where stones may be trapped or broken (De beers.,1999 & Danoczi,2007).

Among the simulants and tracers reviewed, it was proper and correct to use the ceramic diamond simulants for identifying and testing areas that are susceptible to diamond breakage within the processing plant because their properties closely mimic the ones of diamonds as demonstrated in Table *2*.

Table 2:Ceramic diamond simulants physical properties compared to diamond properties

Property	Simulant	Diamond
Hardness (Mohs)	9	10
Density (S.G.)	> 3.35 (nominal 3.5)	3.51
Luminescence (colour)	blue	blue
Luminescence Intensity (LI value)	8000 mV 3 mm > 2500 mV 4 mm > 4000 mV	Detectable LI threshold on DebTech x-ray machines > 250 mV
Magnetic	No	No
Acid Resistant	Yes	Yes

2.11 Mass balancing

Mass balancing is a common practice in metallurgy. The mass balance of a circuit is needed for several reasons, to estimate the metallurgical performance of the circuit, to locate process bottlenecks, for circuit diagnosis and to create models of the processing stages.

2.12 Modelling and Simulation

2.12.1 Modelling

Since the 19th century, the quest for models able to predict equipment performance has proven to be a challenge. The fundamental problem has been a difficulty in characterising complex heterogeneous rock materials.

However, models developed post then can be classified into four dominant groups: fundamental models, classical models, black-box models, and empirical models. The last two are reviewed in this section because of their wide use and better predicting abilities (Napier-Munn et al.,1996).

Black Box

In 1877 Charles Brown invented Gyratory crushers which around 1881 were developed by Gates and were then referred to as Gates crusher (Truscott.,1923). The cone crusher is categorised to be the miniature portrayal of a Gyratory crusher (Gupta & Yan.,2006). Figure 21 shows the basic operating principle of a cone crusher (Evertsson.,2000).

The feed material is exposed to repetitive compressive actions inside the crushing cavity as it is comminuted between movable liner (mantle) and fixed liner (concave). The concave chamber is attached to the crusher frame and the mantle to the eccentrically moving main shaft (Itävuo.,2009). The eccentric shaft is nutating around the centre of eccentricity at a fixed distance from the geometric centre point with a constant speed. The rotating cone can be simplified as a bar linkage mechanism (Eloranta.,1995). Evertsson.(2000) characterised the crushing process in a cone crusher by dividing the crushing chamber into diverse crushing zones. This means that the crushing process is discretised, where each crushing zone corresponds to a crushing event performed by a compression that is defined by the ratio of the stroke s and the bed height b (Evertsson.,2000).

The Whiten model is the most generic in the black-box class of models. Indeed, Whiten (1972) assumed that particles entering the crushing chamber could either be broken or dropped through the crusher unbroken. Then, the broken particles can further be crushed or discharged past the crusher. Thus, the crusher can be regarded as consisting of two zones: a single breakage zone and a classification zone in which particles are selected for exit or for re-breakage.

Empirical models

Empirical models have been attained by employing regression techniques while striving to correlate machine variables and crusher performance. An illustration is provided by Karra (1982) who related machine variables, throughput and power consumption:

Throughput = 1.663*(sinθ)*1.224*(throw)*0.773(CSS)0.507

Power consumption = 19.547*(throughput)*0.849*(P_{80})*-0.984

Where P_{80} is the 80% passing size of the product

θ is the vertical angle of the mantle at close side setting

Throw is the stroke of the mantle while rotating and nutating around the eccentric shaft. It is labelled nSTR.

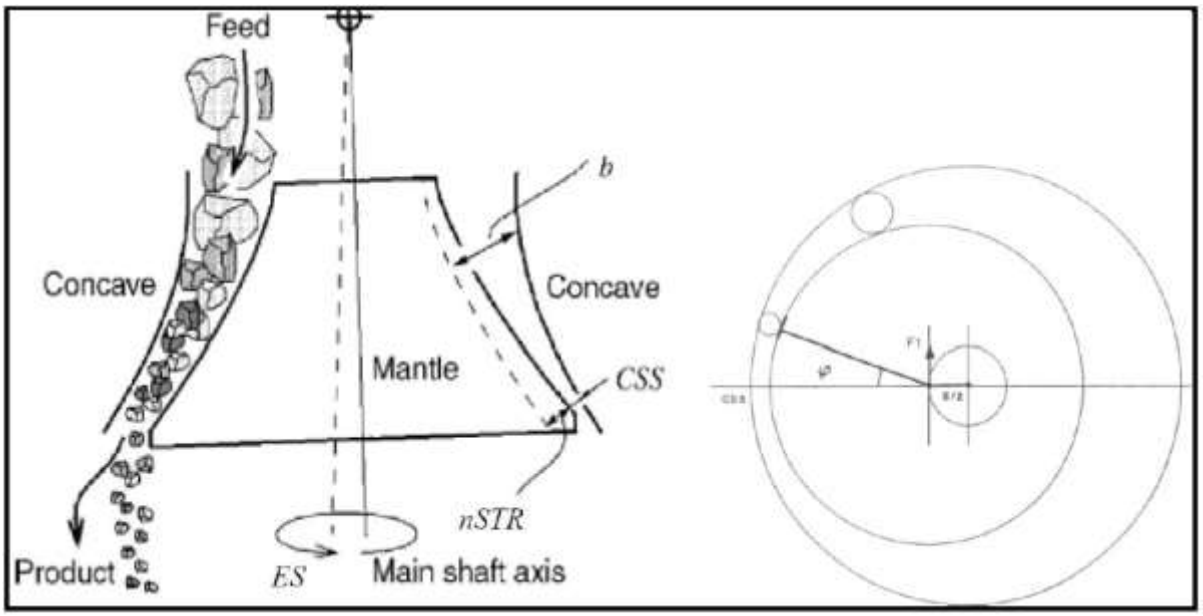

Figure 22:A cone crusher with the machine variables (after Itävuo.,2009) ES is the rotational speed of the eccentric or mantle

Empirical approaches are renowned as quick solutions for industrial challenges and can deliver guidelines for operational purposes. But they are only pertinent to a specific category of crushers and installations. However, they cannot be adopted as generic models.

2.12.2 Simulation

Simulation could be applied as a suitable instrument for investigating the operation and performance of crushing plant circuits. They make the evaluation of various scenarios and the identification of optimum operating conditions easy. Different software packages have been developed and a number have been commercialised with varying degrees of success. This has not deterred the development of simulators for mineral processing units, especially in the last decade.

Typical steady-state software packages are JKSimMet (JKTech.,1989), SIMBAL (CANMET., 1989), USIM PAC (Broussand et al.,1988) and MODSIM (King.,2001).

Steady-state simulation packages have been widely used for crushing plant optimisations (Khosrow.,2001;Luis & Bahena.,2001;Renner & LaRosa.,2005), but are limited to ideal situations. Indeed, any process is subject to change in performance and efficiency with time; steady-state simulators do not cater for this. Dynamic models, on the other hand, evaluate each time-dependent variable, hence the simulation.

Of transient conditions is achievable (Sbarbaro.,2010). That is why the demand for the implementation of dynamic simulations in plant optimisation has been on the rise worldwide.

One of the most widely used platforms for dynamic modelling is the Simulink® environment of the Matlab® software.

Itävuo (2009) successfully created a dynamic process model for a single crushing stage plant implemented in the Matlab/Simulink® environment. The model is a combination of neuro-fuzzy ANFIS networks, steady-state regression, actuators and disturbances. ANFIS is a form of artificial neural network developed upon Tagadi-Sugeno fuzzy inference framework. The simulation period was considerably long, but the outcome was useful in the development of a control system.

CHAPTER 3

3. METHODOLOGY DEVELOPMENT FOR DIAMOND BREAKAGE REDUCTION

Diamond processing involves comminution and physical separation. The study is focused on reducing diamond breakage thus comminution aspect is involved, the place where this is likely to occur. Therefore, only aspects of the process that look at the breakage mechanisms applied in comminution are considered. Due to the security involved in handling actual diamonds, the experimental work could not be performed using real diamonds. However, material with similar properties relating to breakage were procured and used in the test work.

This chapter is concerned with describing the framework that can be used to identify areas where diamonds could break in the process plant and the measurements that can be performed to assist in finding the remedial measures that can be implemented to minimising this problem. The Drop weight test has been used for characterization of diamond ceramic simulants as they are from the manufacture, embedded ceramic simulants in concrete and kimberlite ore mined at the demonstration plant.

This chapter describes the methodology developed for;

1. Identifying areas in the process plant where breakage of diamonds could occur.

2.The type of sampling campaign that be performed around the comminution circuit to calibrate the performance of the circuit.

3. Parametric studies that can be undertaken by varying key operating variables on equipment where the probability for breakage of diamond is considered to be high with a view of assessing the effect on breakage of liberated and unliberated diamonds.

4.Material characterisation that should be performed to understand energy threshold for breakage and link this to places in the process plant where interventions may need experimental setup.

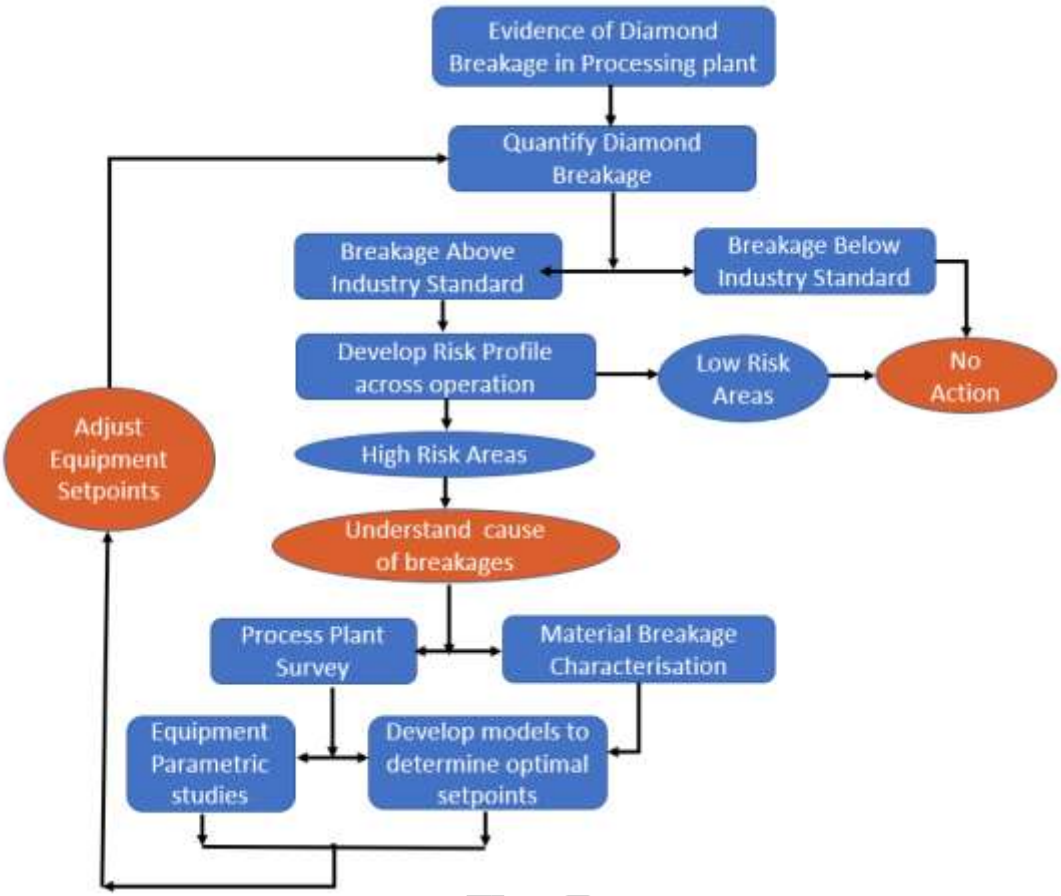

Figure 23: Diamond breakage minimisation methodology

Figure 23,shows the framework methodology developed for minimising the diamond breakage within the operating plant. Each step will be discussed to the demonstrate the practicality of the procedure.

3.1 Evidence of diamond breakage footprint in the process plant

Evidence of diamond breakage in the processing plant was encountered during the assessment and valuation of the recovered diamonds. The diamond above 5caraters(cts) showed a higher extent of breakage. The focus was therefore placed on these +5carater diamonds and bigger stones in respect to their Diamond Sieve sizes.

On the mine chosen as a demonstration plant, it was noted that higher value was attained in the +5cts diamonds during the sale. It was imperative to understand diamond breakage footprint. Since the operation was marginal in revenue generation, diamond breakage had to be minimised to below the industry threshold to preserve the value of diamonds recovered during extraction and maintaining profitability.

Diamond breakage has a significant impact on the average $/ct price as it reduces the quantity of larger diamonds available for sale and causes volatility in the proportion of small diamonds in the sales parcel. The first part in the methodology is to assess if breakage is occurring by

analysing the quality of recovered diamonds. Breakage cannot be assessed from diamond shape alone because of the complex forms that diamonds can exhibit. Diamonds can break during their placement in the kimberlite magma, and those breakage surfaces will also develop distinctive resorption textures. These textures make it possible also to differentiate between natural, resorbed breakage surfaces and mechanically caused unresorbed breakage surfaces that can occur during the mining and extraction processes.

Diamonds that show natural internal weaknesses such as mineral inclusions, gletzs and ruts are more easily broken, so these surfaces are insignificant in the forces required to mechanically break them. A breakage surface associated with a mineral inclusion is notable by the presence kimberlite within the surface, whereas a breakage surface that encountered a rut is classified as etched by the presence of resorption patterns along its boundary. With increasing severity of mechanical breakage, natural weaknesses become less pertinent and distinctive surfaces that are unconstrained by susceptible weaknesses become common. These surfaces include abrasion features, percussion marks and Newton's rings which can form from impact processes. Diamonds exposed to aggressive breakage can shatter resulting in many fragments with all showing fresh breakage surfaces.

3.2 Diamond breakage quantification

The diamond breakage is based on evaluation of the total production of stones above 5cts both on daily and monthly basis. The breakage level is determined based on percent breakage of the total count. Industry standard for diamond breakage is around 5% in which case if breakage levels is lower than 5% no concern is raised and no action is required, If the breakage levels is above the 5% threshold then action is required. In such a case it is necessary to investigate the cause of the breakage and introduce mitigating factors as this could result in value loss.

Also, tracking the percentage of breakages is used to indicate the performance of the process in order to classify as efficient or inefficient. Poor operation of the process leads to plant instabilities and inefficiencies and these has a potential of diamond breakage. If the crusher is not choke fed there is a likelihood that the liberated diamond can fall onto crusher liners and experience impact due to lack of interparticle crushing. The other cause is if the feed to separation stage is not consistent then drop heights can induced impact breakage.

3.3 Diamond breakage risk profile across the processing plant

An assessment is undertaken to develop a risk profile across the operation by seeding tracers with breakages qualities similar to diamonds. For the low risk areas, no action was required.

In high risk sections a detailed investigation is required to understand the cause of the breakage. This part is done systematically so that parts of the circuit where breakage occurs can be identified and the size material that can break in that area can be inferred.

3.4 Processing plant survey (Sampling campaign) and Material Characterisation

Process plant survey is undertaken to evaluate equipment performance in terms of size reduction and assess the flow rates that go through the equipment in the circuit, relative sizes of rocks handled in all parts of the circuit are also extracted. Material characterisation is carried out to study energy thresholds above which the diamonds can break. This is also linked to equipment in the circuit through the model fit performed that is carried out in JKSimMet. The models are used to calibrate the performance of the circuit and evaluate optimal setpoints of the operation. Process adjustment to equipment optimal parameters and alignment of the model output can then lead to re-quantifying diamond breakage.

3.5 Parametric modelling in Diamond processing plant

Parametric modelling is used to define a dimension's ability to change the shape of model's geometry immediately when the dimension value is modified. In this project, the objective is to generate a relationship between detailed physical conditions within the unit and its process outcome. Figure 23, shows a closed-circuit type of framework because the process under consideration is continuous and requires re-evaluating the methodology as the inputs variable changes that is feed material from mining as well as changing operational parameters such as close side settings on the crusher.

Once the model has been established, it must be used in simulation to solve practical challenges in diamond processing operation hence providing direction to parameter adjustment for circuit optimisation

CHAPTER 4

4. EXPERIMENTAL PROGRAMME

This chapter describes the procedures that were carried out to test if the methodology developed in chapter 3 can be applied successfully to minimise diamond breakage on an operating mine. The procedures followed include use of painted rocks to determine survival changes of different size rocks in the coarse end of the comminution circuit. Seeding of ceramic diamond simulants at different stages of the process to assess where breakage could occur.

A full circuit survey was also performed to determine flow of materials and collect data to develop a circuit model for the use in assessing comminution equipment operating parameters that would minimise diamond breakage. In addition to this material characterisation tests were performed to understand energy thresholds that would lead to diamond breakage.

4.1 Identifying areas that are susceptible to diamond breakage

The method to identify areas where diamond breakage could occur involved seeding the ceramic diamond simulants at different stages of the process flowsheet. The diamond ceramic simulants were used from sinks screen (Recovery section) upstream of the process to identify areas that are prone to breakage. It is very important to note the that breakage is based on the categorisation as it was developed by De Beers Mines in 1978 as shown in Figure 47.

UNBROKEN	CHIPPED	LIGHTLY BROKEN	HEAVILY BROKEN	
Class 1	Class 2	Class 3	Class 4	Class 5
Whole stone	Chipped	Lightly Broken	Heavily broken	Fragment
100% Remaining	99.99% to >90% Remaining	89.99% to >75% Remaining	74.99% to >25% Remaining	Less than 25% Remaining. Generally no natural faces left
Quick Guide ►	Less than 10% Missing	Aprox 25% Missing	Aprox 50% Missing	Aprox 75% Missing
Golden rule - Consensus required - if unsure or unknown, leave as unbroken				
			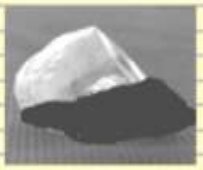	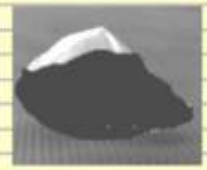
UNBROKEN	CHIPPED	LIGHTLY BROKEN	HEAVILY BROKEN	FRAGMENT

Figure 24:Diamond breakage classification developed by De Beers (1978).

The simulants were introduced in the processing plant upstream in a sequential order so that it would be easier to identify where they got broken. These areas where the simulants were seeded includes; the recovery sinks screens, coarse & fines DMSs, coarse & fines DMS surge bins and secondary crushers and tertiary crushers. Figure 25, shows the positions at which the ceramic diamond simulants were seeded during baseline establishment. These areas are highlighted in red dots.

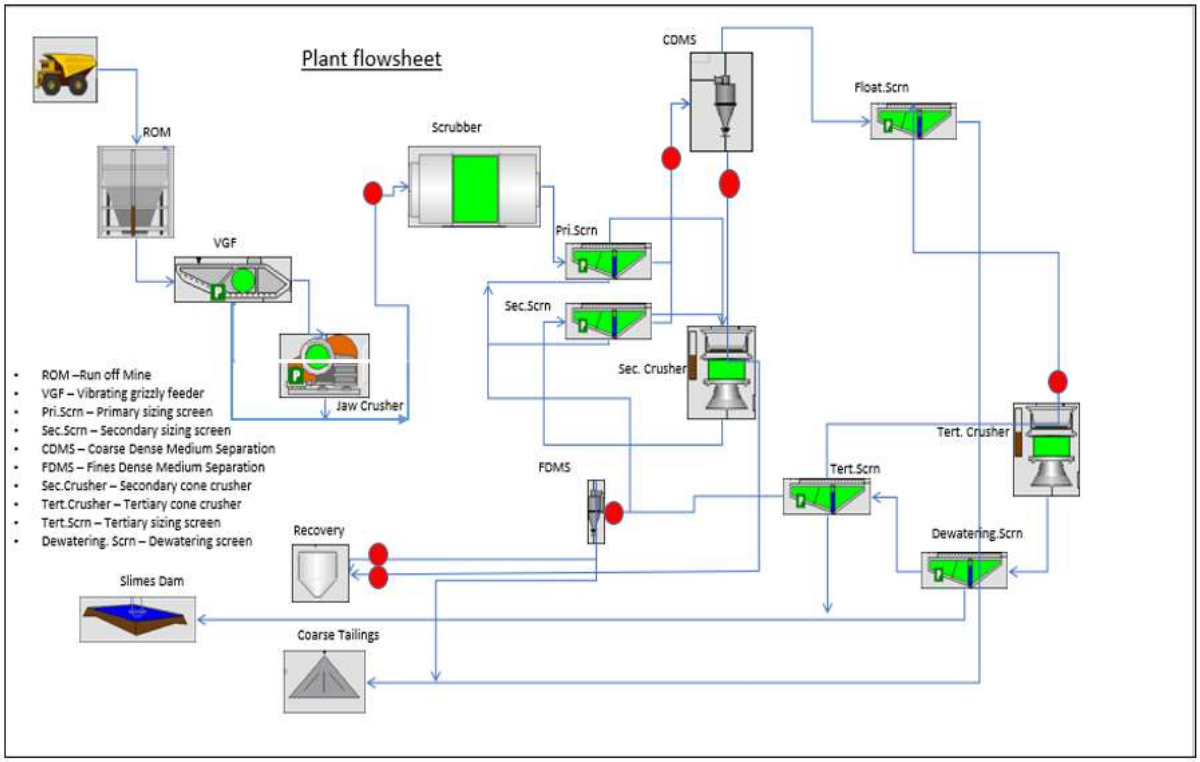

Figure 25: Plant flowsheet with points of seeding ceramic diamond simulants during baseline establishment

The flowsheet under review indicates the units involved in the assessment of areas that are susceptible to diamond breakage. The sampling campaign was performed around the comminution section to calibrate the performance of the circuit. This survey was carried out under normal operating conditions.

For modelling and simulation studies, it is important to ensure that all the necessary data is collected carefully and where possible redundant data is collected to provide proper mass-balancing of streams and checks on the prime data. The general methodology which has been used successfully on many plants was employed in this work.

The data required to perform modelling and simulation studies includes the rate of flow of solids and the size distribution of the solids for all key streams around the circuit. The total feed to circuit was obtained by measuring the solids feed rate. The size distributions and flow rates around all the circuit streams were obtained by sampling the streams and performing careful sizing of these samples. Size gradings were obtained from a comprehensive set of screenings over the full-size range of the solids.

The painted rocks as could be seen in Figure 26, were seeded in the scrubber to determine if there was any size reduction and as well as assessing the risks of diamond breakage. The simulants were also seeded in the scrubber.

Figure 26:Painted rocks before seeded into the scrubber

A further study of this involved seeding ceramic diamond simulants into the feed process stream. This formed a proxy for the behaviour of liberated diamonds. It can be seen on Figure 27, the ceramic diamonds simulants pre-seeded in the scrubbers.

Figure 27: Ceramic diamond simulants seeded in the scrubbers

4.2 Plant Survey

4.2.1 Plant Survey and Sampling methods

The sampling methodology adopted for the comminution circuit under review has been outlined in this section and is based on the general standards developed for survey procedure. The proposed sampling points for plant survey are highlighted on Figure 28.

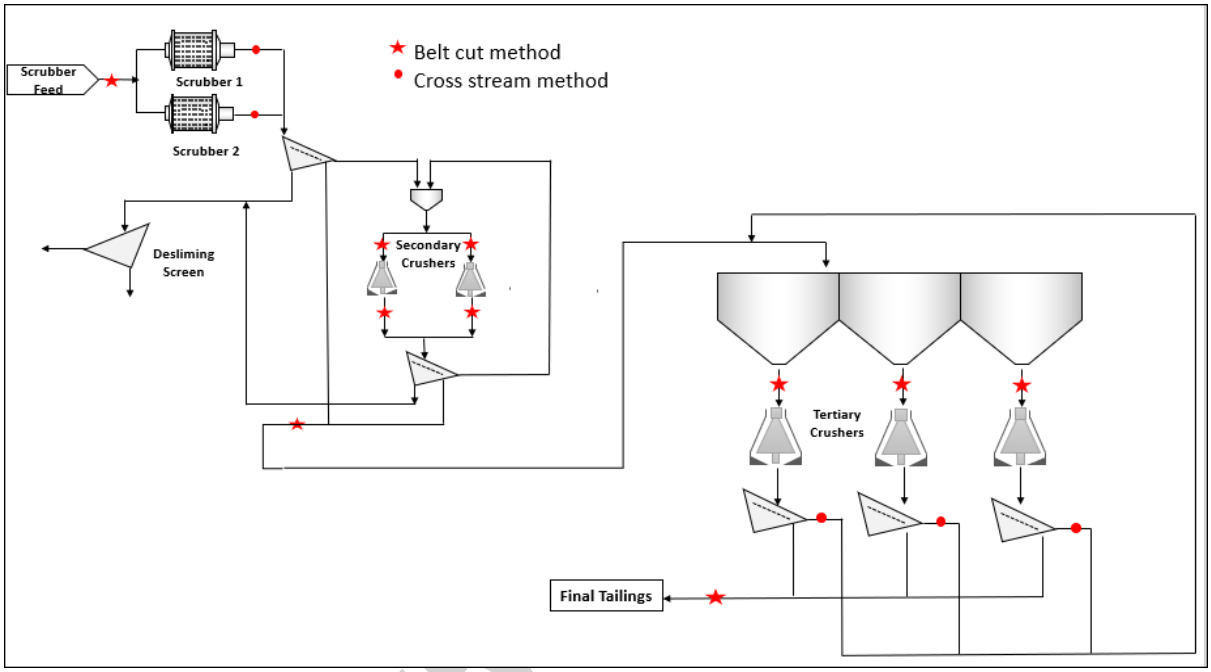

Figure 28:Plant flow diagram showing comminution circuit with sampling points

4.2.2 Plant Survey procedure

During the survey, it was preferable to only stop one equipment at a time because only individual equipment calibration is important in this survey. Mass balancing was performed to identify bottlenecks in the flow and equipment. The plant was operated at conditions as close to steady state operation as possible by monitoring key instrumentation tags over a period of at least three residence times of the scrubbers before stopping the relevant scrubber for sampling and inspection.

The team was given access to the control room to monitor progress. The base case survey was performed at conditions close to the plant's recommended operating set points. After reaching steady state, sampling of scrubber product was conducted over a period of at least 30 minutes followed by a crash stop of the scrubber being assessed. Inspection of the scrubber internals and belt cut sampling of the scrubber feed was then be undertaken during the stoppage.

The crusher survey procedure involved taking representative belt cut samples of the feed and product streams of each crusher unit at known closed side settings (CSS). The base case survey was conducted at the normal operating CSS for all crushing plants, as well as normal filling rates for the scrubber units.

Following the completion of the base case survey, additional surveys on the secondary and tertiary crushers were conducted with four other CSS different from the base case settings.

4.2.2 (a) Cross cut sampling – scrubber discharge stream

Figure 29:Scrubber discharge sampling point

The scrubber is a special type of tumbling mill, operated to promote gentle breakage of the ore. Like most tumbling mill installations, the sampling points for the drum scrubber discharge units are not easily accessible as shown in Figure 29, due to a combination of ergonomics and exceptionally high flow rates. A specially designed sampler that was supported and conveyed by an overhead crane assembly was designed as could be seen in Figure 30. It is important to ensure that the operation of the sampler is such that the entire stream should be accessed by the sampling device.

The sampler material was made from a stainless-steel cutter with a thin gauge to make it relatively light. The base was perforated with a mesh size of approximately 1mm. The mesh is allowed in this case because the interest lies in capturing stones larger than this nominal size.

Figure 30:Specialised sample cutter discharge high flow stream

4.2.2 (b) Cross cut sampling

To ensure accurate representation of all size fractions in the sampling of coarse material using the belt cut approach, a method that improves the statistical representation of coarse material in the final particle size distribution was used.

The approach, listed in most standards, is to extract all material from a portion of the belt that is as wide as at least three-times the expected size of the largest particle on the belt. However, for material such as crusher and scrubber feed, the upper size of material can be appreciably large, therefore a customized procedure was applied. The number of particles larger than approximately 53 mm in the standard belt cut is not enough to statistically represent the correct constitution of this coarse fraction in the overall particle size distribution of the material conveyed. Collecting more coarse particles over a larger measured length of belt would

provide more particles to augment the statistics associated with the composition of the coarse fraction in the overall material Particle size distribution.

To achieve this, it was recommended that the procedure should be in two main stages as follows;

A length of belt that is at least 3 times the expected top size of material on the belt and remove all material within the marked section to constitute a primary sample for coarse and fine screening. Due to the material loading on the belt, a standard 2 meter belt cut was instituted to give enough material for analysis as shown in Figure 31.

Figure 31:Belt cut sampling on a secondary crusher product

The full belt cut sample was weighed, then sun-dried on a clean plastic sheet as seen in Figure 32 and weighed again. The big rocks are screened using hand sizers from big rocks and at 212 mm down, sieves were used. The fines as well as rocks below 53 mm were screened from 37.5 mm down to sub 1.25 mm. The technique for coarse sample screening was used, as explained in detail above. The resulting fractions the size intervals that were packed separately were up to 13.2 mm. Below 13.2 mm they were packed into one bag.

Figure 32:Samples drying in the sun

Collection of coarse material larger than approximately 53 mm from the crusher pan feeders was performed according to the cross cut method. The sample was collected cross-sectionally to gather enough material. This is the crusher feed sample in Figure 33.

Figure 33:Crusher pan feeder being sampled using cross cut method

4.2.3 Crash stop measurements

Crash stop and Inspection of the drum scrubber units

Crash stops are required to determine the volumetric load level and to obtain slurry level measurements which are critical in scrubber optimization studies (Clermont & de Haas.,2010). The scrubbers were crash-stopped after the base case test to obtain the volumetric percentage filling of the charge in the mill. That required good organization to ensure that all the responsible people were in place before the crash stop. This was necessary to reduce the down time and to avoid disturbing the conditions in the mill by allowing water to be absorbed due to the characteristics of the kimberlite ore.

Crash stop procedure

A crash stop was performed at the end of survey and the person coordinating the survey ensured that the appropriate conditions were achieved and that the plant was in a relatively stable condition prior to such a stoppage.

The interlock was temporarily removed from the scrubber discharge pumps (under direction of plant operation personnel. Inlet water to the scrubbers was closed, as the inlet water reading dropped the feed and the scrubber were stopped simultaneously.

Scrubber entry procedure

The scrubbers were locked out following the guidelines of lock out procedure. Scrubber lock-out register was completed by personnel that entered the scrubbers for measurements and inspections and those from the team entering the scrubbers. Each person entering the scrubber had to apply an individual lock after the power was isolated. Entry was via the discharge outlet once the scrubber had stood still. Torches were provided in order to inspect the scrubber interior. The team ensured that all the required internal measurements were obtained as quickly as possible to avoid unnecessary downtime. About 10 minutes was required for stops where volumetric filling only was being measured. One entry of about 40 minutes was required to measure the scrubber internals. Total downtime is mainly a function of mill stop, lockout and start procedure.

Crash stop measurements

It is important to avoid keeping the mill running after the feed ore and mill inlet water are simultaneously stopped. If the mill is kept running a portion of the mill load will be ground out and the crash stop measurements obtained will not represent the conditions under which the test was performed.

It is good practice to photograph the charge after the crash stop and a careful study of these can provide some insights on any crash stop problems encountered. Photographs of the charge surface at eight different locations in the mill are preferred. Sometimes the presence of slurry in the charge after the crash stop indicates that the stoppage performed was reasonable and the crash measurements can be used to provide the load and slurry level for the test. However, one must make sure that the water is shut as the mill (drum scrubber) stops because if not shut properly, the mill may appear to contain a slurry pool which may be misleading.

The measurements obtained during the crash stop include the internal mill dimensions (mill diameter, belly length, trunnion diameters, grate measurements, and pulp lifter depth), charge level and slurry measurements (the height above the charge, the level of slurry below the rock charge).

Figure 34:Charge in the scrubber during crash stop

4.2.4 Sizing of the samples

The screen sizes that were required for all the samples are listed in the screen sizes tables. As the method of screening is important in obtaining a high-quality set of sizing data suitable for modelling of process units, it is laid out in detail here. Internationally accepted laboratory

techniques are used, with some improvements for the coarse rock processing, to reduce the risk of errors and sample mixing.

Sizing of coarse material

A systematic approach is required to obtain consistent and accurate results. This is especially important for the large run-of-mine feed sample. The general procedure is laid out as follows;

Sun dry sample on a clean plastic sheet or dry in the oven for an hour or two. Tare at least 20 buckets and write the tare on each bucket. Line up the screens and hand sizers in a long row on top of buckets or drums. Label each bucket as sub (screen size) plus (next screen size down), e.g., below the 53 mm screen the bucket is labelled–53 mm +38 mm. This is to avoid confusion as with this technique the contents of each bucket are the size passing the screen, not retained on it – as is normal practice.

Start with the smallest (1.25 mm) screen and place a portion of the material on that screen, so that it is not overloaded and can easily be shaken. Remove larger rocks by hand immediately, brushing off any fines into the bucket, and pass along the row of screens. A rock must always be tested on the screen size below the final one it passes through, to ensure it is in the correct size fraction. If a bucket fills up, then place a fresh bucket in front of it and continue screening into that. Do not remove any buckets until the entire sample has been screened.

Then start from one end and work your way along, weighing each size fraction at a time. This prevents the samples from being mixed up. If the samples are not required for further analysis or breakage testing, then as you finish weighing each sample it can be decanted back into the original drum for discarding.

Weigh the minus 1.25 mm bucket and remove for fine screening. Immediately add up all the masses to do an integrity check with the total dry mass, if the individual masses add up to close to the total mass then the sample can be accepted. If there is a discrepancy then it can be checked immediately, before the sample is discarded. Do not wait until a few weeks later to check sample masses, it is then too late to locate and correct errors. The mass integrity check is quick and simple and an excellent check.

There must be 100% passing the largest screen size. The series of screens used must range to above the largest rock size, and the fact recorded that no mass (0 kg) was retained on the largest screen used.

4.3 Ceramic diamond simulants seeding in the process

The ceramic diamond simulants of different sizes (25 mm,20 mm,12 mm and 8 mm) as seen in Figure 35 were thrown in-line with the material (Kimberlite ore) at the concentrate bins in the sorthouse and were collected after two days which was assumed those that were missed they would have exited the process. The same method of seeding the simulants in the sorthouse concentrate bins was employed to the following sections; UV drier feed hoppers, DMS sinks screens, DMS mixing boxes, DMS surge bins, Tertiary cone crushers, Secondary cone crushers and the Scrubbers.

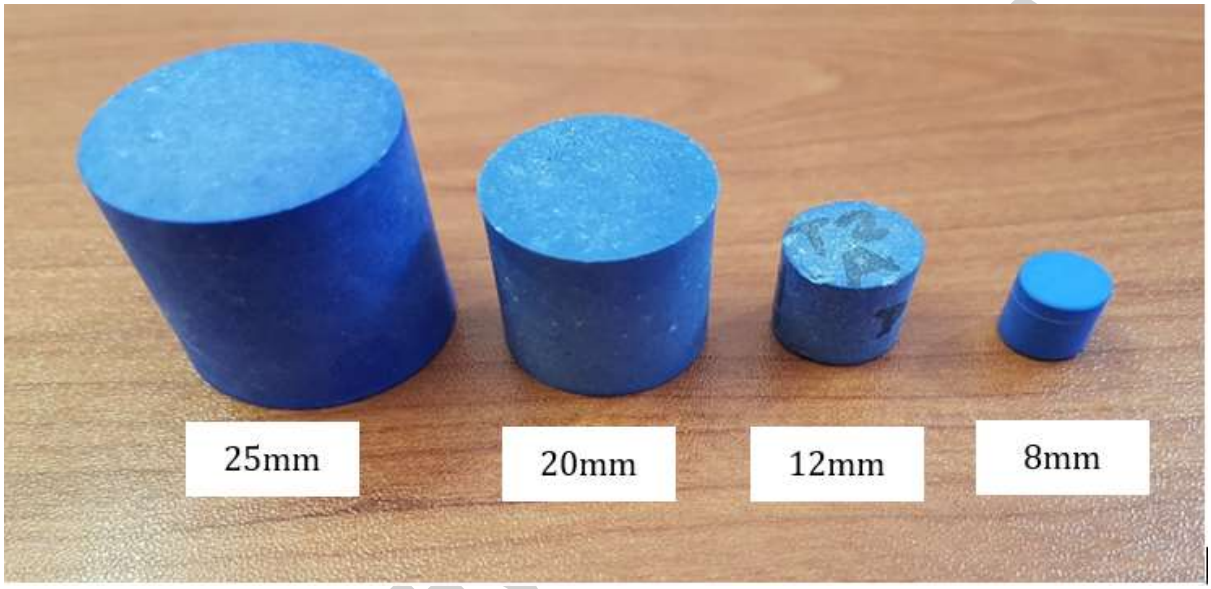

Figure 35:Ceramic diamond simulants used to identify where diamond breakage is susceptible

4.3.1 Seeding of Liberated and Embedded ceramic diamond simulants

The ceramic diamond simulants have the hardness of 10 on the Mohs scale of hardness and they mimic diamond properties (DebTech, Doc.no.K09-000001-776 Rev 1.0). Simulants that were seeded in the plant as they were from the supplier were referred to as liberated and those that were encapsulated in the concrete mix were referred to as locked. The ceramic diamond simulants both in their liberated and locked form were seeded at the key feed point of the major equipment in the process and they were collected on the product end of the unit.

These simulants were seeded in the crusher while the crusher was operating at choke feed levels and seeding in the scrubber took place when the head feed was 500 t/h nameplate capacity.

4.3.2 Seeding of simulants during varying of the operational variables (Effect of change on CSS)

The close side setting (CSS) is the most important machine control parameter for the cone crusher (Cleary et al.,2017). It can vary due to wear or intentionally as a result of operator or machine control decisions. The tests were conducted on equipment where the probability for breakage of diamond was considered to be high with a view of assessing the impact on breakage of liberated and unliberated diamonds.

The effect of changes in the CSS on the flow and crusher performance tends to be very significant. Unsurprisingly the product becomes coarse showing no reduction on the particle. Table *3* below shows the gap settings for both the secondary and tertiary cone crushers. It also indicates at what crusher gap were the simulants seeded either liberated or imbedded in the concrete blocks.

Table 3:Summary of crusher tests (Parametric studies)

Stage	Crusher #1 CSS (Set point) [mm]	Crusher #2 CSS (Set point) [mm]	Ceramic diamond simulants in the feed stream [Y/N]
Secondary	35	35	Y
	39	39	N
	43	43	Y
	47	47	N
	51	51	Y
Tertiary	13	13	Y
	15	15	N
	17	17	Y
	19	19	N
	21	21	Y

The product from the secondary crushers was taken from the product belt with the method described in the previously. Since the belt usually contained the product from both crushers, the samples were taken while running the crushers one at a time, to ensure that the belt only contained product from one crusher. The tertiary crusher product was sampled from the edge of the dewatering screen. This was done by moving a bucket along the edge as seen in Figure 35.

Figure 36:Taking the tertiary crusher product

4.4 Material characterisation tests

Material characterisation was performed to understand the energy thresholds in key comminution equipment to break the diamonds. The information was going to be used to identify areas in the flow sheet where diamond breakage can occur and to provide insights how breakage can be minimised by operating the equipment with contacts that may lead to reduced energy input. The characterisation was performed for ceramic diamond simulants as supplied by the manufacturer representing liberated diamonds, ceramic diamond simulants embedded in concrete matrices of different strengths to mimic unliberated diamonds encapsulated in a rock of different properties and the kimberlite ore. The equipment used were JKRBT and drop weight test.

4.4.1 JK Rotary Breakage Tester (JKRBT)

The product size distribution resulting from impact breakage for ore or material type depends on the specific input energy and particle size (Shi & Kojovic.,2007; Banini.,2000). The effect of these two factors on the particle size distribution was investigated to determine the impact breakage parameters.

In RBT, simulants were fed into the rotary breaker, accelerated and impact a wall at a specified speed as discussed by Zuo & Shi.(2016). The progeny is collected, sieved and used in t_{10} calculations to characterise the hardness of the simulants. Similarly, in drop weight test the

weight of a known mass is dropped from a measured height onto stationary particle on an anvil and the resultant daughter fragments were then sieved and used for t_{10} calculations, the highlighted followed the principle outlined by Napier-Munn et al.(1996); Genc, Ergun & Benzer. (2004).

There is a non-linear relationship between the degree of breakage measured by the percentage material passing 1/10th of the original feed size (t_{10} parameter) and specific input energy (Narayanan.,1985). Due to the non-linearity of specific input energy and particle size, the standard hardness characterization test requires three energy levels however due the limited amount of the ceramic diamond simulants two energy levels were used (1 kWh/t and 2.5 kWh/t). In addition, the standard rotary test requires four particles size classes (Zuo &Shi.,2016) however two particles size classes were considered (-22.4 mm + 19.0 mm) and (-16.0 mm + 13.2 mm) due to limited size of the simulants from the manufacture, this led to a narrow JKRBT testing conditions(Zuo & Shi.,2016).

The ceramic diamond simulants used for the JKRBT tests were of different sizes as could be seen in Figure 37. They are manufactured by Deb Tech. The sample preparation for the impact breakage test conducted at Lonmin metallurgical research and development laboratory is described in this section.

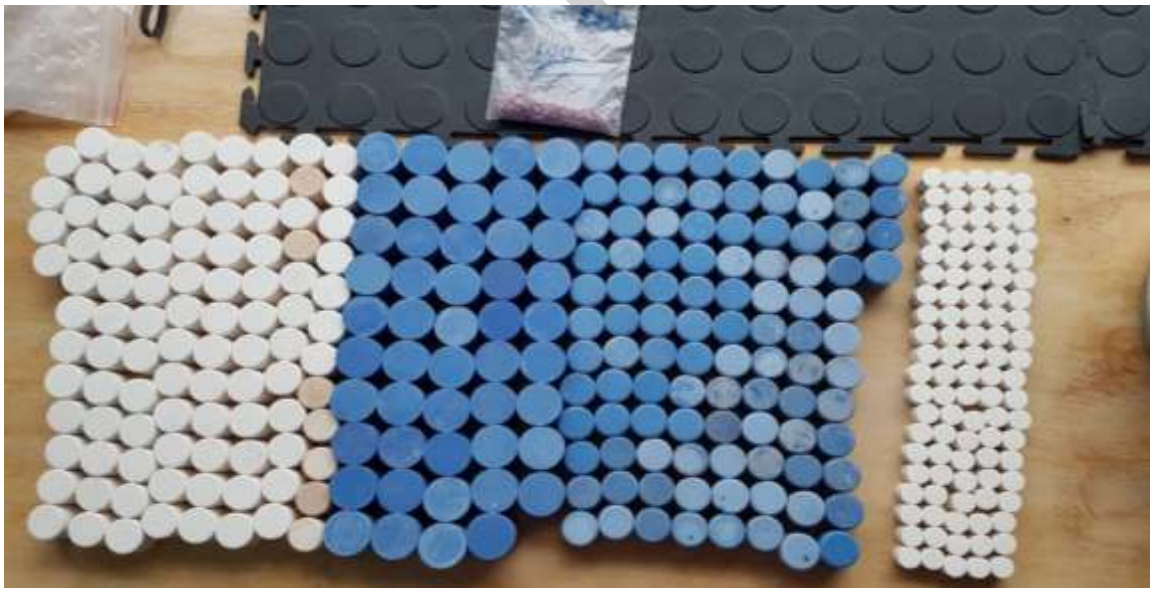

Figure 37: Image of ceramic diamond simulants used for the impact breakage test on JKRBT

The components used for the standard breakage characterisation test on the ceramic diamond simulants are; JKRBT test machine, Endecell D50 vibrating screen shaker. The application of √2 series of 200mm diameter screen with apertures sizes ranging from 0.106 mm to 45 mm and Precisa BJ6100D weighing scale and collecting trays and samples bags.

The ceramic simulants were classed based on the colour and size and because of the cost implication it was decided to use 10 pieces per energy level. The standard test requires four classes thus being(-45 mm+37.5 mm, -31.5 mm+26.5 mm, -22.4 mm+19 mm and -16 mm+13.2 mm)(Shi et al., 2009).

The image in Figure 38 shows the JKRBT unit used at Lonmin metallurgical research and development laboratory in South Africa.

Figure 38: JK Rotary Breakage Tester (RBT) installed at the Lonmin Concentrators Technical Centre in Marikana with the lid closed (a) and open (b) positions

The ceramic diamond simulants in the classes were subjected to impact breakage by two energy levels as shown on the Table 4.

Table 4: Impact breakage tests at different energy levels

Size (mm)	Energy levels (kWh/t)		No. of Particles per test	
			White	Blue
-45+37.5	-	-	-	-
-31.5+26.5	-	2.5	-	20
-22.4+19	1	2.5	10	10
-16+13.2	1	2.5	10	10

The following steps are conventional to the operation of the JKRBT as stipulated in the JKMRC rotary breakage tester manual; Upon completion of initial start-up procedure, the oil and air pressure were checked. The mist separators were drained of any vapour or moisture by pressing the discharge button on the side of the filters.

Figure 39 shows that the required energies and rotor speeds were set on the control panel by inputting the desired energy input in (kWh/t) or in revolution per minute (rpm).

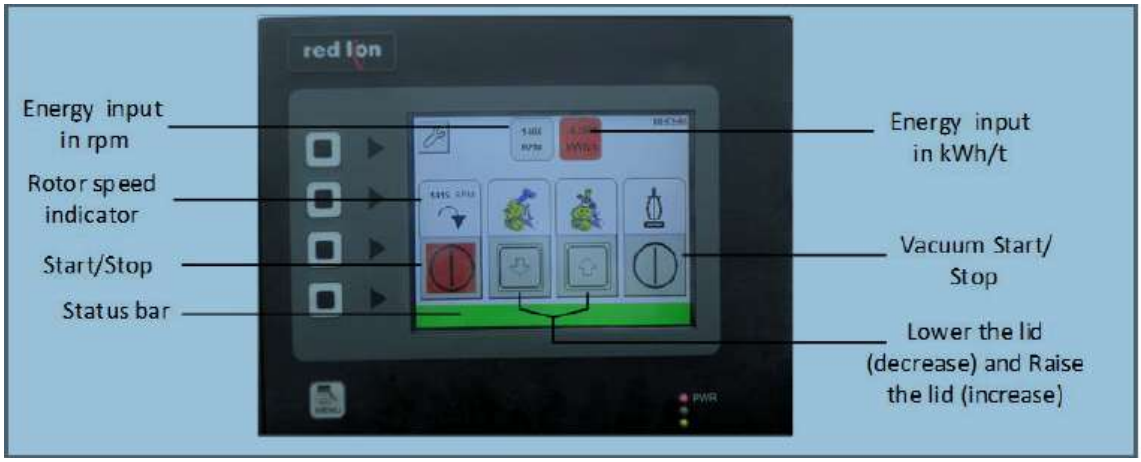

Figure 39: The image displaying the control panel of the JKRBT

To perform the test the desired speed was set, and the start button was pressed, the rotor accelerated to the required speed. There is a light indicator on top of the RBT that signalled a stabilised rotor speed has been achieved. The revolutions per minute to achieve energy levels required for this work are given in Table 5

Table 5: RBT rotor speed for breakage tests at different energy levels

	Required RPM for target Ecs Values			
	White		Blue	
Size (mm)	1.00 kWh/t	2.50 kWh/t	1.00 kWh/t	2.50 kWh/t
-45+37.5				
-31.5+26.5				4 067
-22.4+19	2 618	4 067	2 618	4 067
-16+13.2	2 618	4 067	2 618	4 067

The weighted ceramic diamond simulants were fed to the JKRBT at the rate of two particles per second using a hand driven feeder. This provided surety of single particle impact breakage in the unit. Figure 40, shows the JKRBT with its key components.

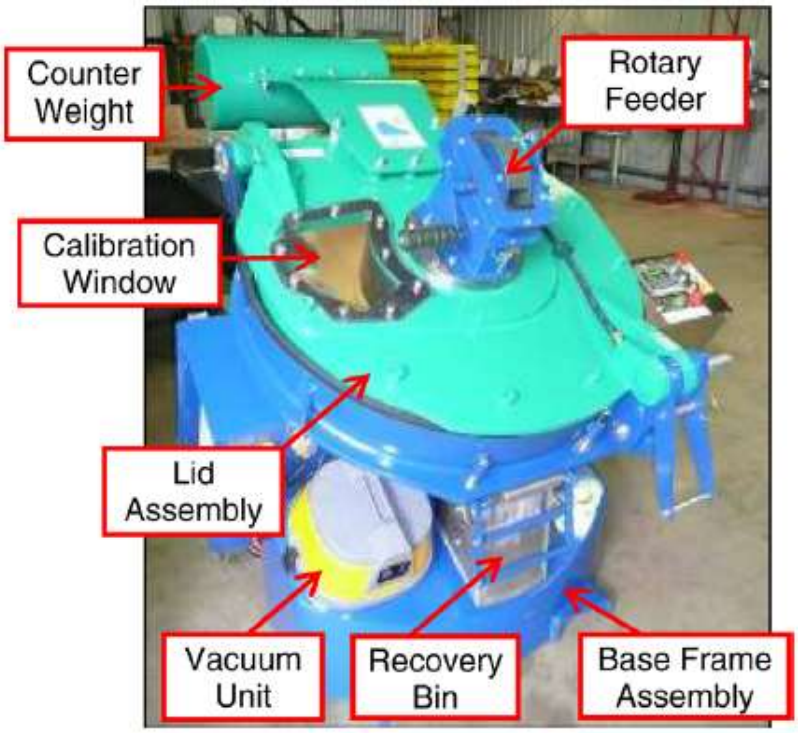

Figure 40: The JKRBT showing different components

The stop button was pressed to stop the rotor, then automatically the vacuum pump switched on when the flywheel reduces the speed below 1500 rpm to collect the product in the bin.

The top lid of the RBT was opened after the rotor had stopped to access the impact chamber for cleaning and collecting remaining fragments from the anvil and around the flywheel.

All the collected product particles were passed to the next stage of sample processing which is screening. The daughter particles of each test were screened with √2 series of sieves (Napier-Munn.,1996). The progeny particles were collected and weighed before screening to mass loss during the screening process.Figure 41,shows the Endecells D50 vibrating screen shaker that was used to screen the samples utilizing the √2 screen series ranging from 0.106 mm to 45 mm for a period of 10 minutes.

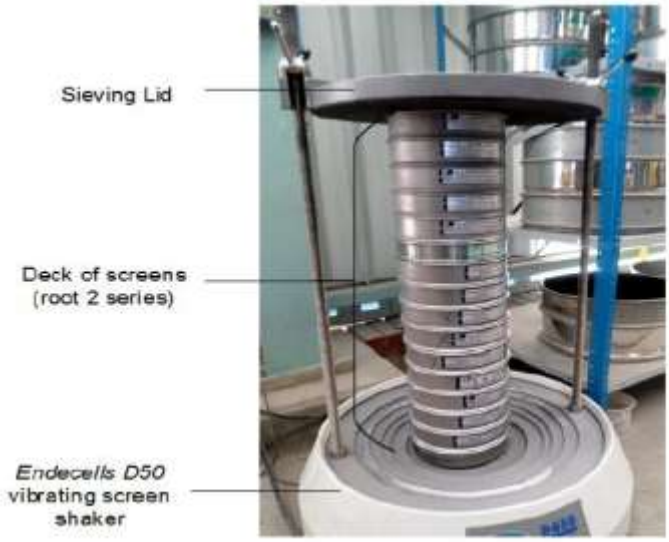

Figure 41: Endecells D50 vibrating sieve shaker packed with a deck of root 2 series of screens

The mass retained on each screen was recorded and percentage passing was therefore calculated.

4.4.2 Drop Weight Test

The drop weight test was developed at JKMRC to replace the twin pendulum apparatus for assessing impact breakage characteristics of ores (Brown.,1992) as cited by Napier-Munn et al.(1996). Both King (2001) and Tavares (2007) used the drop weight test to determine the single particle breakage function and as well investigate the breakage characteristics of materials.

Many researchers have used drop weight test. Test results from this technique were evaluated through the breakage distributions of different size fractions at various impact energy levels (Genc, Ergun&Benzer,2004). Breakage parameter t_{10} (Narayanan.,1986) is used to represent the degree of size reduction which is assumed to be representative of the breakage product size distribution obtained from drop-weight tests. Relation between specific comminution energy level and breakage index number (t_{10}) was established on the size fractional base so that the variation in impact breakage characteristics of different materials can be evaluated.

As shown in section 3.2.3 for the standard requirements of the size classes of the JKRBT, the drop weight test also has its own requirements of the size classes. Standard drop weight test requires five size classes thus being (-16 mm+13.2 mm, -22.4 mm+19 mm, -31.5 mm+26.5 mm, -45 mm+37.5 mm & -63 mm+53 mm). Materials used for breakage test using Drop weight test device as seen in Figure 42.

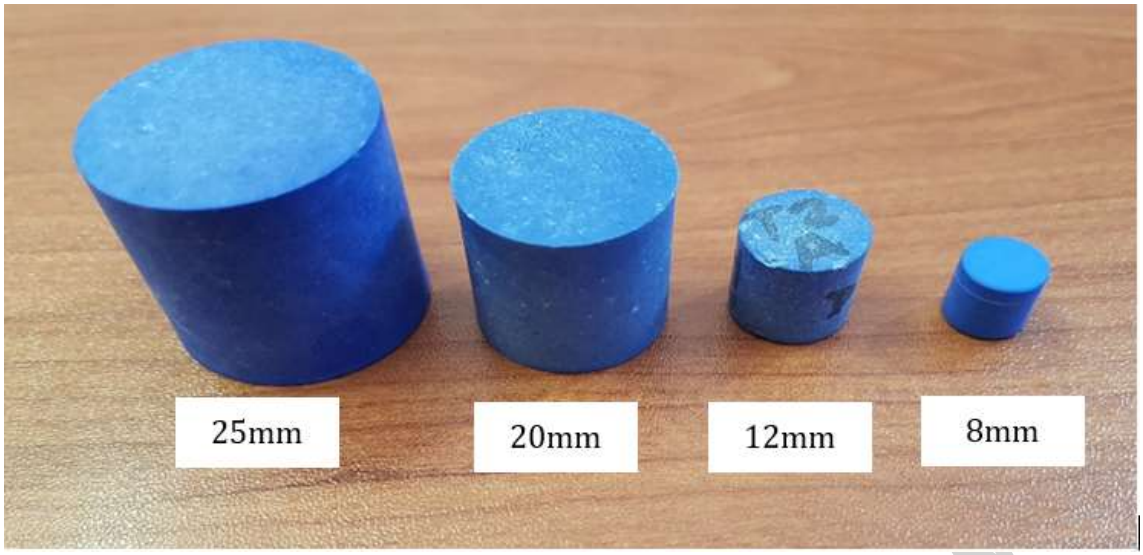

Figure 42: Ceramic diamond simulants used on drop weight test representing liberated diamonds

The ceramic diamond simulants were also embedded in concrete matrix strength of 77 Mpa, 55 Mpa and 34 Mpa shown in Figure 43 were characterised by using drop weight test. These embbeded simulants represents the locked diamonds in the diamond host rock at different sizes.

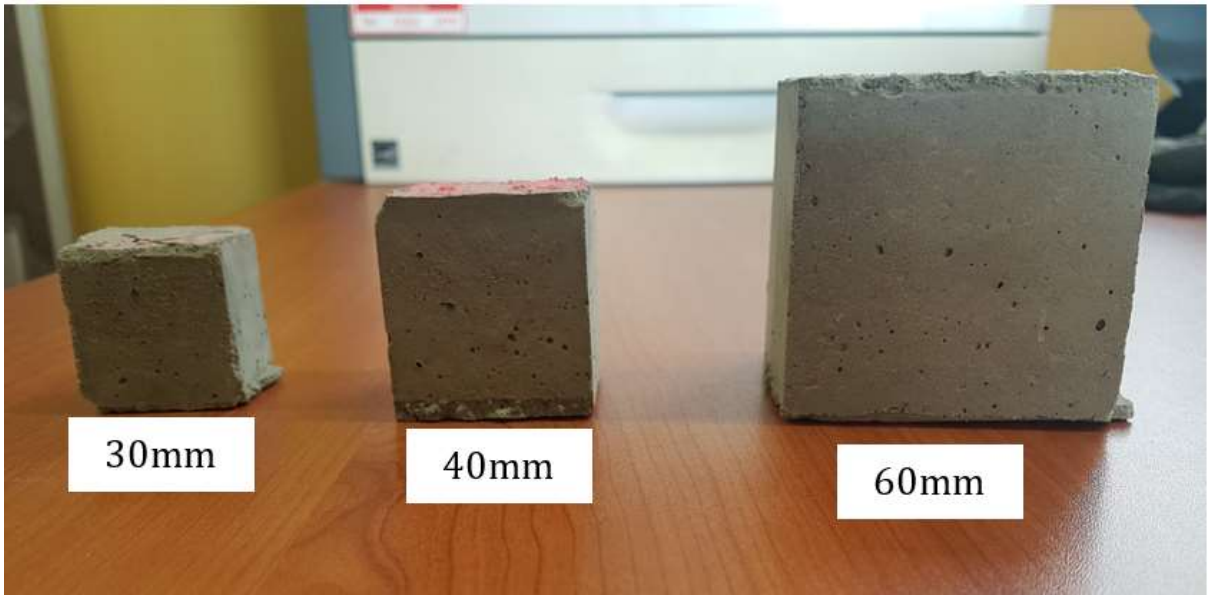

Figure 43: Embedded ceramic diamond simulants in concrete to represent unliberated diamonds

Ore samples that were collected during plant survey were used for the drop weight test after being prepared according to the standard JKMRC procedure for drop weight test however the particles below 13.2 mm were not used refer to Figure 44.

Figure 44: Kimberlite ore samples for drop weight test before preparation

The drop weight test device in Figure 45, has been used onsite for single particle breakage characterization of ceramic diamond simulants in their original form from the manufacturer representing liberated diamonds, embedded simulants representing unliberated diamonds and kimberlite ore.

The components used for the material characterization in a drop weight test are; drop weight test unit, steel weights, √2 sieve series of 200 mm and 450 mm diameter screen and collection sample trays. Scale for weighing the sample mass

The experimental procedure for undertaking drop weight test has been outlined by sample preparations (Ceramic simulants, embbeded simulants in concrete and Kimberlite ore samples). Categorise the samples into the 5 sieve classes for a particular energy level, randomly pick 30 particles for each sieve class. Weigh the 30 particles to obtain the mean particle mass (in grams). Use the mean particle mass to calculate the drop height (at given Energy and drop mass). Measure drop height from the base of the anvil and place the steel weights. Secure the steel weights at the top and take 30 particles from each sieve class, relating to an energy level. Place a particle in the middle of the anvil (ensure that the particle is not protruding on the side of the anvil). Two people stand on either side of the apparatus and the steel weights carrier is released (the two people will guide it to the required height) and once the carrier is at the required height, the weights are released at the same time. The carrier is lifted to the drop height and the anvil is cleaned of the progeny particles.

The process is repeated from the point when the carrier is lifted to the drop height until all the particles have been crushed for each sieve class. Place the progeny into a plastic bag after the crushed particles are sieved using the root 2 series sieve. Repeat the procedure for each sieve class at different energy levels

Due to time and financial constraints, only 10 particles were used for both the embedded simulants (representing locked diamonds in the host rock) and simulants in their original form, as supplied by the manufacturer (representing liberated diamonds). According to the JKTech laboratory services (1992), impact breakage testing procedure states that ten to thirty particles are required in each size fraction for each energy level, depending on the particle mass.

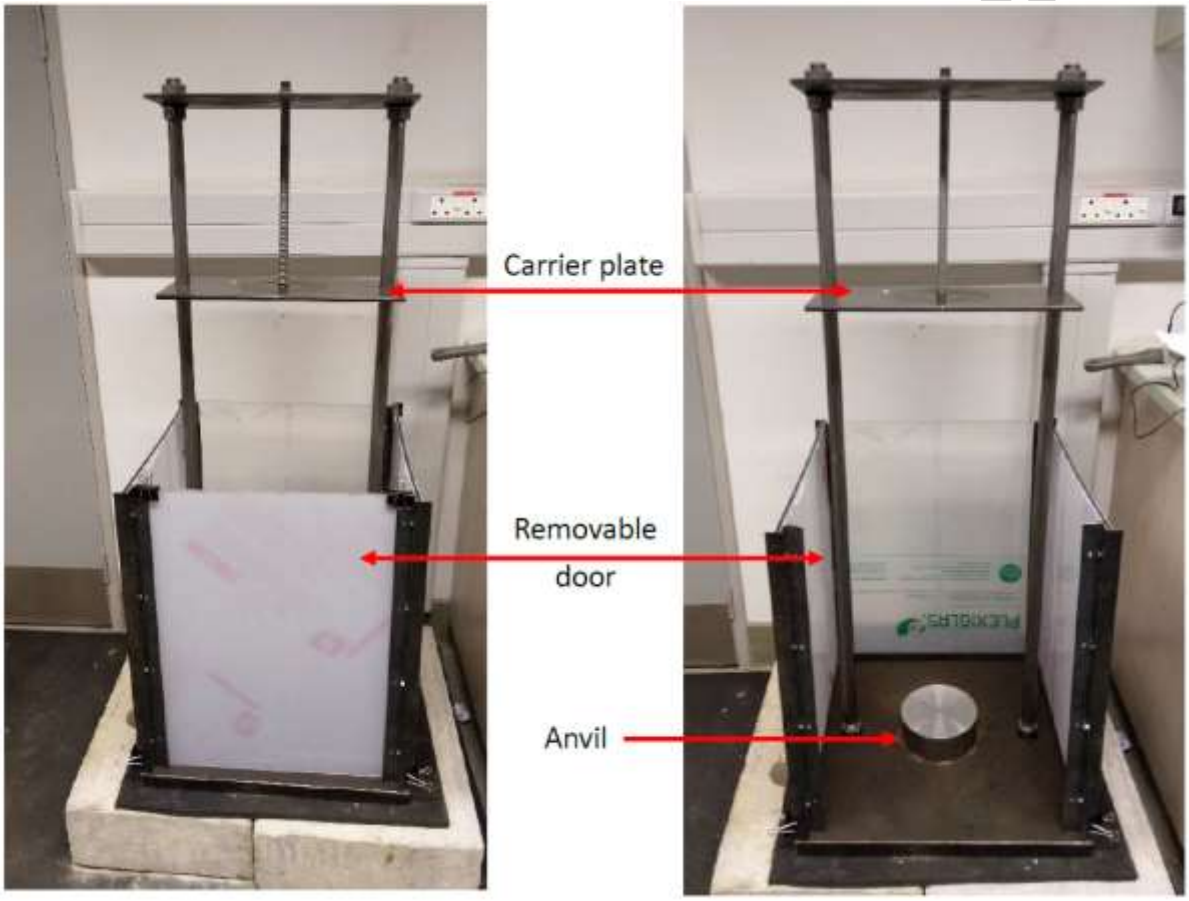

Figure 45:Drop weight test device (Adapted from Napier-Munn et al.,1996)

Figure 46:Weights used to make mass combination for the drop mass

The drop weight tests were performed on the following samples; scrubber feed, secondary cone crusher feed and concrete blocks at the following strengths 77 Mpa, 55 Mpa and 34 Mpa.

Experimental procedure for casting the concrete mixture to embed the ceramic simulants was to take Sikacrete 214A mix with Sikacrete 214C to a free-flowing consistency. The PVC strip was divided into 60x60 mm, 40x40 mm and 30x30 mm lengths. These strips were arranged into squares, that would contain the Sikacrete mixture and each block was filled to the brim with the mixture (any excess was scraped off). Simulants were embedded into the mixture, Table 6 shows the size of concrete blocks per simulants size.

The mixture was cured according to the desired strength (77, 55 and 34 MPa) for each block size. The curing times were 28, 7 and 2 days for the 77, 55 and 34 MPa respectively. Once the curing time had lapsed, the blocks were removed from the molds.

Table 6: Demonstrating simulants with concrete blocks per size

Block size (mm)	Size of diamond ceramic simulant (mm)
60x60	20
40x40	12
30x30	8

Figure 47:Ceramic diamond simulants being embedded into concrete blocks

Figure 48: Concrete blocks impregnated with ceramic diamond simulants per size

Table 7 to Table 12 outlines the conditions at which each test was carried out.Each table with its material type.

Table 7:Scrubber feed samples

Size (mm)	Mean particle mass(g)	no. of particles	kWh/t	Calc Height(cm)	Rest Height Adj(cm)	Actual Drop Height(cm)	Total Drop Mass(kg)
63.0 x 53.0	**284,00**	30	0,1	68	3,17	**71**	**15,4**
	293,67	30	0,25	78	2,97	**81**	**34,5**
	275,33	30	0,4	81	2,84	**84**	**49,97**
45 x 37.5	**119,00**	30	0,1	88	2	**90**	**4,97**
	115,33	30	0,25	69	2,3	**71**	**15,4**
	91,60	30	1	67	2,4	**70**	**49,97**
31.5 x 26.5	**34,90**	30	0,25	65	0,45	**65**	**4,97**
	35,37	30	1	64	0,66	**65**	**20,2**
	35,27	30	2,5	82	0,58	**82**	**39,738**
22.4 x 19.0	**13,73**	30	0,25	57	1,14	**58**	**2,23**
	12,90	30	1	46	0,57	**47**	**10,23**
	12,53	30	2,5	57	0,32	**57**	**20,2**
16.0 x 13.2	**6,10**	30	0,25	27	0,81	**28**	**2,04**
	5,57	30	1	92	0,5	**92**	**2,23**
	4,53	30	2,5	84	0,27	**84**	**4,97**

Table 8:Cone crusher samples

Size (mm)	Mean particle mass(g)	no. of particles	kWh/t	Calc Height(cm)	Rest Height Adj(cm)	Actual Drop Height(cm)	Total Drop Mass(kg)
63.0 x 53.0	**347,67**	30	0,1	83	3,17	**86**	**15,4**
	334,67	30	0,25	89	2,97	**92**	**34,5**
	366,67	30	0,4	108	2,84	**111**	**49,97**
45 x 37.5	**111,67**	30	0,1	83	2	**85**	**4,97**
	116,00	30	0,25	69	2,3	**72**	**15,4**
	116,67	30	1	86	2,4	**88**	**49,97**
31.5 x 26.5	**36,80**	30	0,25	68	0,45	**69**	**4,97**
	38,77	30	1	71	0,66	**71**	**20,2**
	42,23	30	2,5	98	0,58	**98**	**39,738**
22.4 x 19.0	**14,17**	30	0,25	58	1,14	**60**	**2,23**
	17,67	30	1	63	0,57	**64**	**10,23**
	12,40	30	2,5	56	0,32	**57**	**20,2**
16.0 x 13.2	**6,57**	30	0,25	30	0,81	**30**	**2,04**
	7,10	30	1	117	0,5	**118**	**2,23**
	6,47	30	2,5	120	0,27	**120**	**4,97**

Table 9:Concrete blocks made of sikacrete - 214 at 34Mpa

Size (mm)	Mean particle mass(g)	no. of particles	kWh/t	Calc Height (cm)	Rest Height Adj(cm)	Actual Drop Height(cm)	Total Drop Mass(kg)
60x60	**519,00**	10	0,1	75	3,17	**79**	**25,284**
	510,00	10	0,25	76	2,97	**79**	**61,768**
	510,00	10	0,35	106	2,84	**109**	**61,768**
30x30	**75,10**	10	0,1	51	0,45	**52**	**5,38**
	72,70	10	1,0	77	0,66	**78**	**34,495**
	71,70	10	2,0	85	0,58	**86**	**61,768**

Table 10:Concrete blocks made of sikacrete - 214 product at 55Mpa

Size (mm)	Mean particle mass(g)	no. of particles	kWh/t	Calc Height (cm)	Rest Height Adj(cm)	Actual Drop Height(cm)	Total Drop Mass(kg)
60x60	**510,00**	10	0,1	74	3,17	**77**	**25,284**
	504,00	10	0,25	75	2,97	**78**	**61,768**
	503,00	10	0,35	105	2,84	**108**	**61,768**
30x30	**74,40**	10	0,1	51	0,45	**51**	**5,38**
	76,30	10	1,0	81	0,66	**82**	**34,495**
	74,90	10	2,0	89	0,58	**90**	**61,768**

Table 11:Concrete blocks made of sikacrete - 214 at 77Mpa

Size (mm)	Mean particle mass(g)	no. of particles	kWh/t	Calc Height (cm)	Rest Height Adj(cm)	Actual Drop Height(cm)	Total Drop Mass(kg)
30x30	**72.8**	30	0.1	51	3.17	**54**	**5.29**
	72.56	30	0.25	53	2.97	**56**	**12.49**
	73.52	30	1	77	2.84	**80**	**35.05**
40x40	**168.44**	30	0.1	50	2	**52**	**12.49**
	175.34	30	0.25	79	2.3	**81**	**20.49**
	172	30	1	103	2.4	**105**	**61.67**
60x60	**548.42**	30	0.1	80	0.45	**80**	**25.3**
	542.18	30	0.25	81	0.66	**81**	**61.67**

Table 12:Ceramic diamond simulant for drop weight test

Size (mm)	Mean particle mass(g)	no. of particles	kWh/t	Calc Height (cm)	Rest Height Adj(cm)	Actual Drop Height(cm)	Total Drop Mass(kg)
25x25	**42,90**	10	1	62	3,17	**66**	**25,284**
	43,60	10	2,5	65	2,97	**68**	**61,768**
20x20	**23,20**	10	1	159	0,45	**159**	**5,38**
	23,10	10	2,5	62	0,66	**62**	**34,495**
12x12	**4,90**	10	1	33	0,45	**34**	**5,38**
	5,00	10	2,5	13	0,66	**14**	**34,495**
8x8	**1,40**	10	1	10,427	4,97	**15**	**5,38**
	1,50	10	2,5	4	0,66	**5**	**34,495**

CHAPTER 5

5. RESULTS AND DISCUSSIONS

This chapter discusses the results of the methodology developed for identifying where diamond breakage occurs. The first part of the methodology is to review areas where diamond breakage is likely to occur in the process flowsheet. Secondly, to demonstrate the methodology aimed at minimizing diamond breakage in a conventional diamond processing plant.

The analysis and interpretation of the results are reported in the following categories:

I. Classification of diamond breakage risk level.

II. Baseline establishment of diamond breakage within the processing plant using the ceramic diamond simulants.

III. Seeding of ceramic diamond simulants “As-Is” and in encapsulated form in concrete to assess areas that are susceptible to breakage.

IV. Material breakage characterization of kimberlite ore obtained from the feed sample during the survey, concrete blocks impregnated with ceramic diamond simulants and the ceramic diamond simulants themselves (“As-Is”). The material breakage characterization tests were performed with JK rotary breakage tester and Drop weight tester and the models.

V. Energy thresholds for the simulants to break were obtained from examining the progeny at various energy levels, if they are liberated or imbedded in concrete.

VI. The effect of operating cone crushers close side setting on the breakage of the embedded simulants was assessed.

5.1 Classification of diamond breakage risk level

The risk level ranking used to classify parts of the circuit was based on the risk of breakage of liberated, partially locked and locked diamonds in each equipment or activity considered.The three ranking classification used were “high” for equipment and areas where the risk was considered to be very high, “medium” where the risk was deemed to moderate and “low” where the risk was potentially negligible.Table 14 shows, the ranking that was carried out at the demonstration site.

Table 14: A summary of possible risks of diamond breakage in the mining operation

Equipment/Activity	Liberated	Partially locked	Locked
Drilling	High	High	High
Blasting	High	High	High
Primary Crusher	Low	High	Low
Scrubbers	High	High	Low
Secondary crusher	High	High	High
Coarse DMS Bins	High	High	Low
Coarse DMS Cyclone Feed Pump	Low	Low	Low
Tertiary Crusher	High	High	High
Fines DMS Feed pump	Low	Low	Low
Coarse Recovery transfer points	High	Medium	Low
Fines Recovery transfer points	High	-	-
Sort house	Low	-	-

5.2 The simulants that were used for baseline were recovered chipped, as shown in Figure 49
(a) Sink screens

(b) Coarse DMS

(c) Fines DMS

(d) and (e) both in Coarse DMS surge bins.

It is very important to note that breakage is based on the categorisation that was developed by De Beers Mines in early 1978 refer Figure 24, which demonstrated details of the assessment.

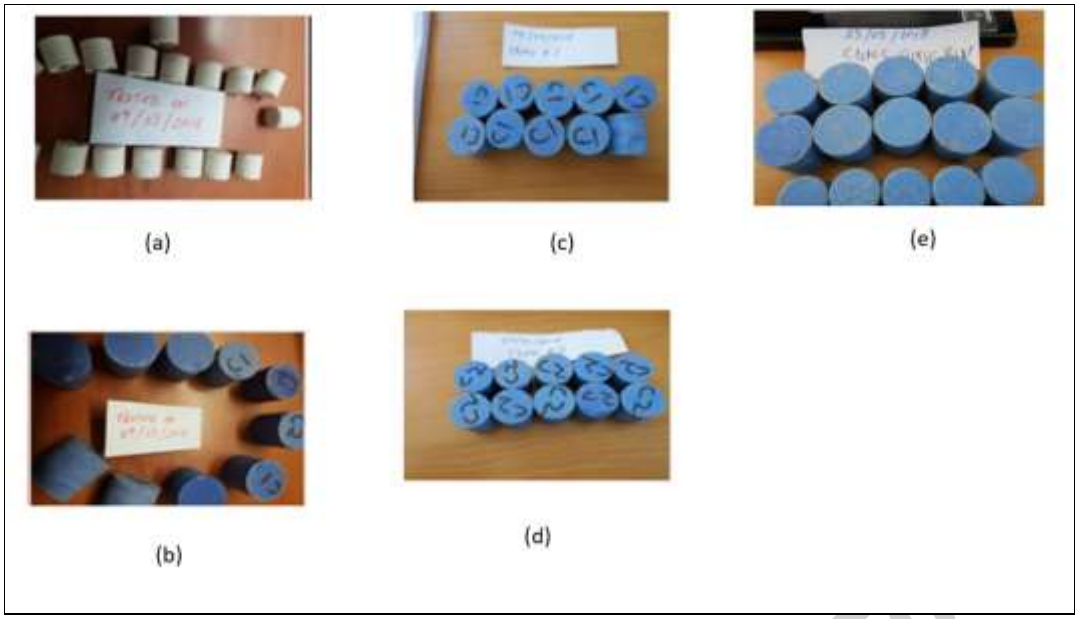

Figure 49:Chipped diamond ceramic simulants introduced on the sinks screen, CDMS, FDMS & CDMS Surge bin.

The simulants that were seeded in secondary crusher #1 & #2 can be seen in Figure 50a) and (b). Chipping was observed on some of the simulants recovered from the secondary crushers, but these appeared on very few pieces.

Figure 50:Chipped diamond ceramic simulants introduced on both secondary crusher #1 & #2.

Figure 51 shows photographs of simulants recovered from the tertiary crushers. Two sizes of simulants were seeded at the tertiary crushers. The 12 mm shown in Figure 51(a) and 8 mm in Figure 51(b). Most of the 12 mm simulants were broken and some breakages on the 8 mm

were observed. The 12 mm ceramic diamond simulants are most broken because at the time of the test the crushers were operating at a close side setting of 12 mm.

The tests carried out by seeding the ceramic diamond simulants, showed that a higher number of 12 mm simulants were broken compared to 8 mm simulants at the close side setting of 12 mm. It was deduced that the close side setting could have been small for simulants with size of 12 mm or larger to go through without breaking.

Figure 51:Heavily broken ceramic diamond simulants introduced on the tertiary crushers.

From these set of tests, it was concluded that diamond breakages were most likely to occur at this point. It was however decided to approach the problem holistically by looking at the comminution circuit and its performance. The results from simulants provided information on areas to put more focus on when defining possible remedial measures to alleviate diamond breakage.

5.3 Comminution circuit calibration for unit performance assessment

A full survey was performed covering the whole comminution circuit. Information from all key streams was obtained including particle size distributions of feed and product streams. The data from the survey was mass balanced to assess the data quality and obtained flow rates for streams where it could not be measured. The results obtained are presented in this chapter.

5.3.1 Drum scrubber (Autogenous mill)

During the scrubbing stage the particles are reduced in size by a combination of impact and abrasion mechanisms (Wills.,2005). The scrubbers are Mechprotech products with 3 metre diameter and 6.8-meter length.

The volumetric filling of 35.4% was obtained for scrubber 1 and 35.1% was scrubber 2. The similar operating volumetric filling is an indication that they are set up to achieve the same size reduction performance.

Figure 52,shows the particle size distribution for the scrubber feed and product. Since there was no notable particle size reduction in both the scrubbers,the particle size distributions of the product streams are similar to the feed streams. Therefore, it can be concluded that only liberated diamonds can be broken in the scrubbing units. The breakage of the liberated diamonds can be as a result of high impact energy from the rocks in the toe region.

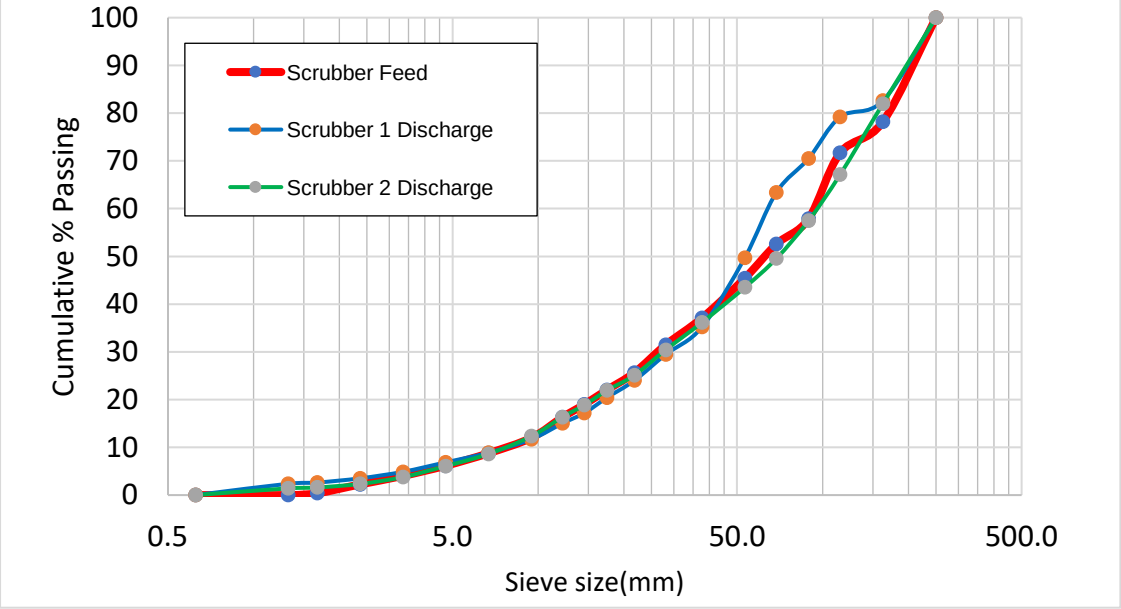

Figure 52: Scrubber feed and discharge particle size distribution

Figure 28, shows the flowsheet with the positions where the samples were collected. The particle size distributions graphs are also plotted to demonstrate insignificant size reduction in Figure 52.

Figure 53,shows the ceramic diamond simulants that were seeded in the scrubber feed. It can be seen that there was very little impact on the simulants and this observation agrees to what had been seen on the particle size distribution on Figure 52.

Figure 53: Ceramic diamond simulants recovered post seeding in the scrubber

5.3.2 Mass Balancing for comminution circuit

Mass balancing was performed to assess the quality of the data and to supply missing information such as flow rates and particle size distributions that could not be measured during the test work. The data from the survey conducted were mass balanced using JKSimMet, a steady state simulator. JKSimMet considers particle size distributions and solids flow rates when performing the mass balance. JKSimMet considers all the information available in arriving at reconciled results. JKSimMet requires data collected under conditions as close as possible to steady state. The input data required for mass balancing includes mass flow rates of solids and particle size distributions for solids and slurry streams.

For the comminution circuit in diamond plants only the scrubbing units requires water therefore the flow rates from all other water addition points were not considered. Particle size distributions were obtained from processed samples while the plant feed mass flow rate was obtained from the weightometer readings, along with measurements involving belt cuts of

known length for known conveyor belt speeds. It was desirable to collect redundant data during the test so that a proper a mass balance can be performed and checked.

The mass balance was performed in two stages; the first stage included the scrubbers and secondary crushing circuit and the second stage focused on the tertiary crushing circuit. The experimental data is closely to the balanced data and that shows the sampling survey was undertaken while the plant operated close to steady state.

Figure 54 and Figure 55 shows a comparison of balanced and experimental data for the streams around the scrubbers. It can be seen that the balanced data matches to the experimental data hence it can be concluded that the system was operating as expected.

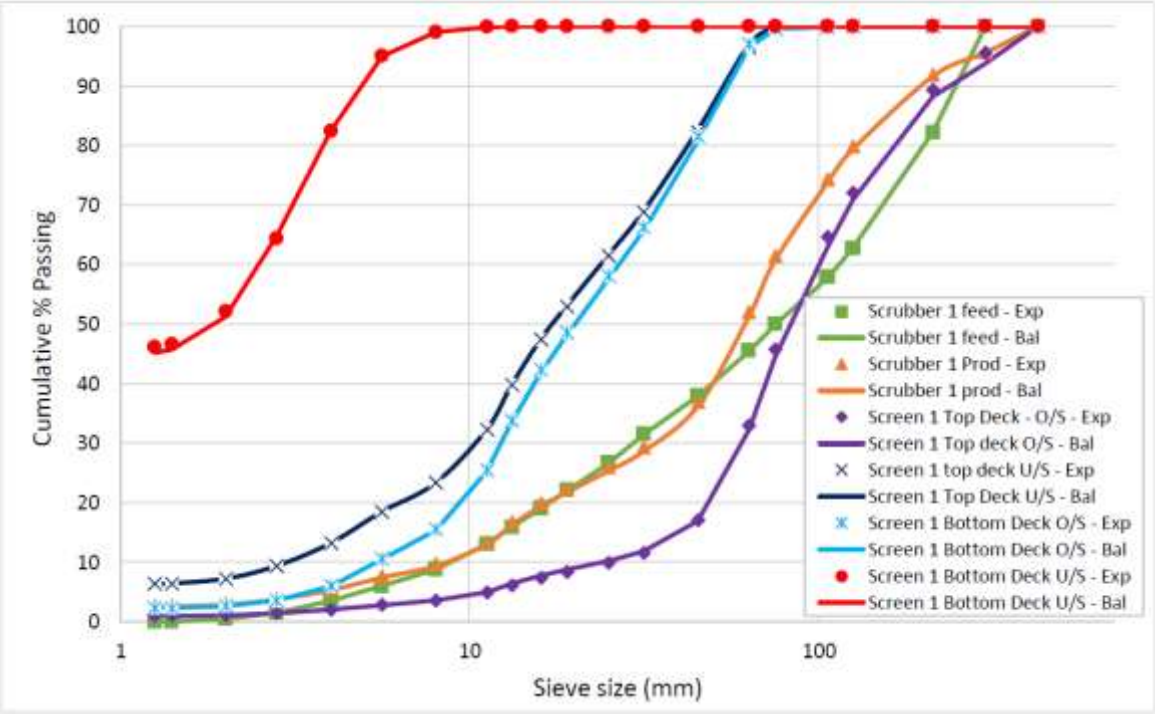

Figure 54: Particle size distribution for balanced and experimental data for scrubber #1.

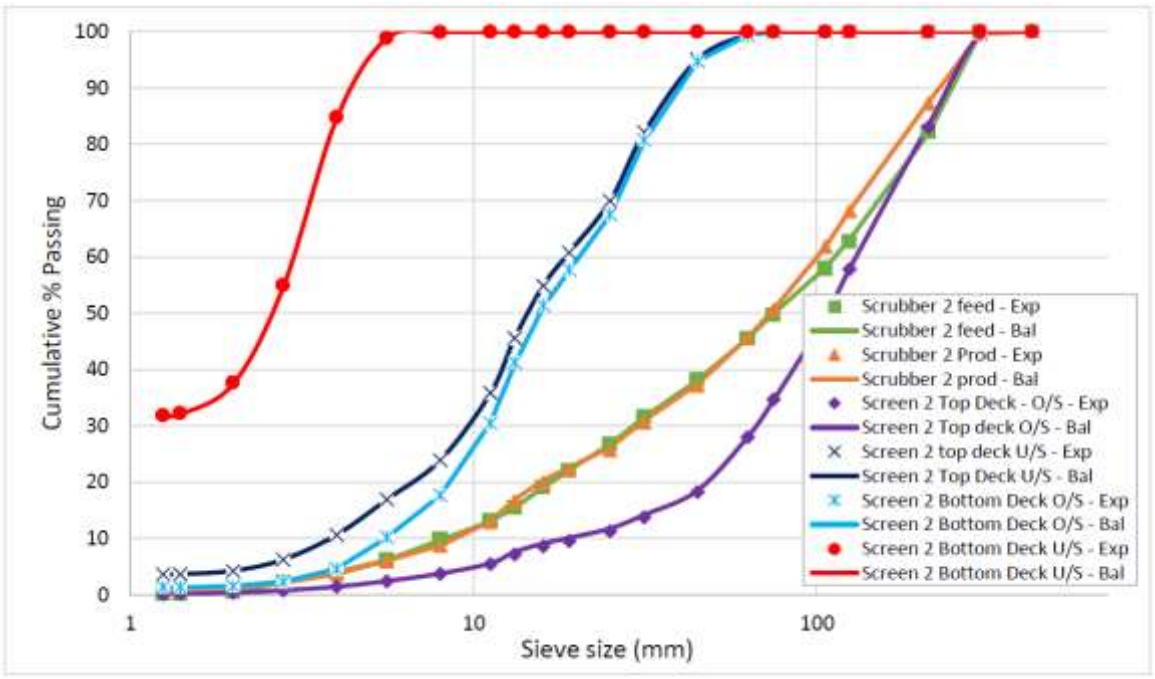

Figure 55: Particle size distribution for balanced and experimental datafor scrubber #2.

Figure 54 and Figure 55 are derived from the experimental and balanced data from the survey conducted. The data shows that there is no notable size reduction within the scrubber units.

A comparison of balanced and experimental particle distribution size for the scrubbers and secondary crushing circuit is given in Figure 54, Figure 55 and Figure 56. It can be seen that the balanced data matches the experimental data hence the process operated close to the expectation.

The particle size distribution samples taken around the secondary crushers shown in Figure 56, suggest that the performances of both the crushers are the same in terms of size reduction of the material. It can be seen on Figure 56, that the percent material passing the sub fractions of 32 mm, 10 mm and 1.25 mm were very low and since the close side setting on this stage of crushing was 35 mm, it can be concluded that diamond breakage at this stage was negligible.

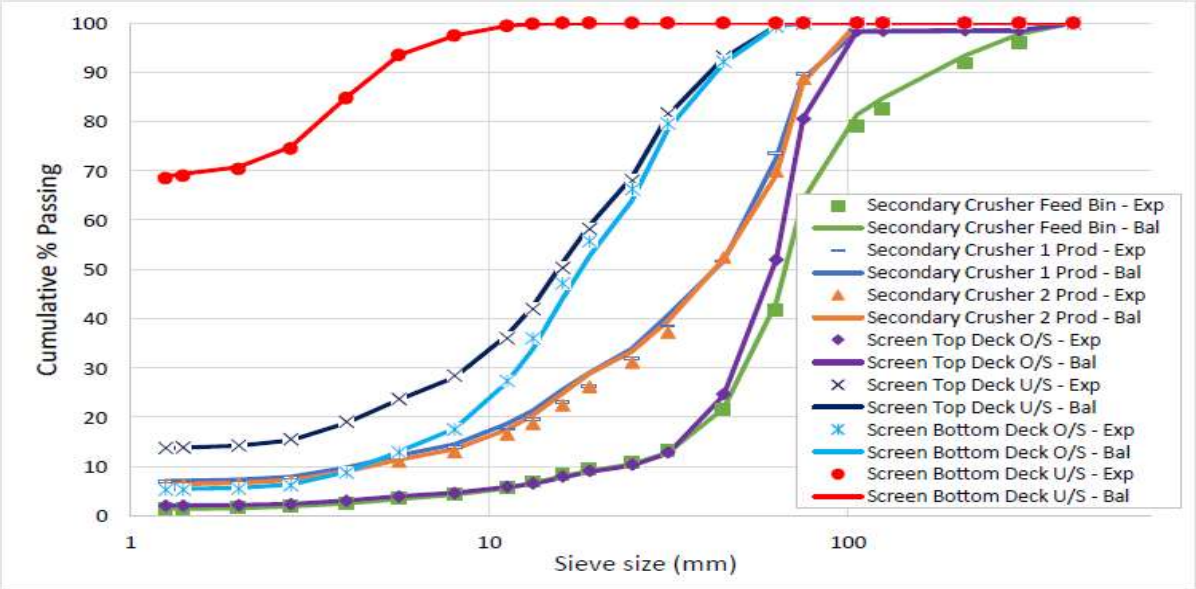

Figure 56: Mass balance and experimental particle size distribution for the secondary crushers.

A comparison of balanced and experimental particle distribution size for the tertiary crushing circuit is given in Figure 57.

The particle size distribution for the tertiary crushers are shown in Figure 57. The feed particle size distribution for the crushers were similar, hence only one is shown. It can be seen on Figure 57, the percent sub 32 mm particle size there is a likely possibility of diamond breakage due to the close side setting being below 32 mm. It is concluded that breakage would likely be on any particle above the operating close side setting of 13 mm. On the sub 10 mm and 1.25 mm the material would pass through the close side setting as those fractions are smaller than the operating crusher gap therefore diamond breakage is unlikely.

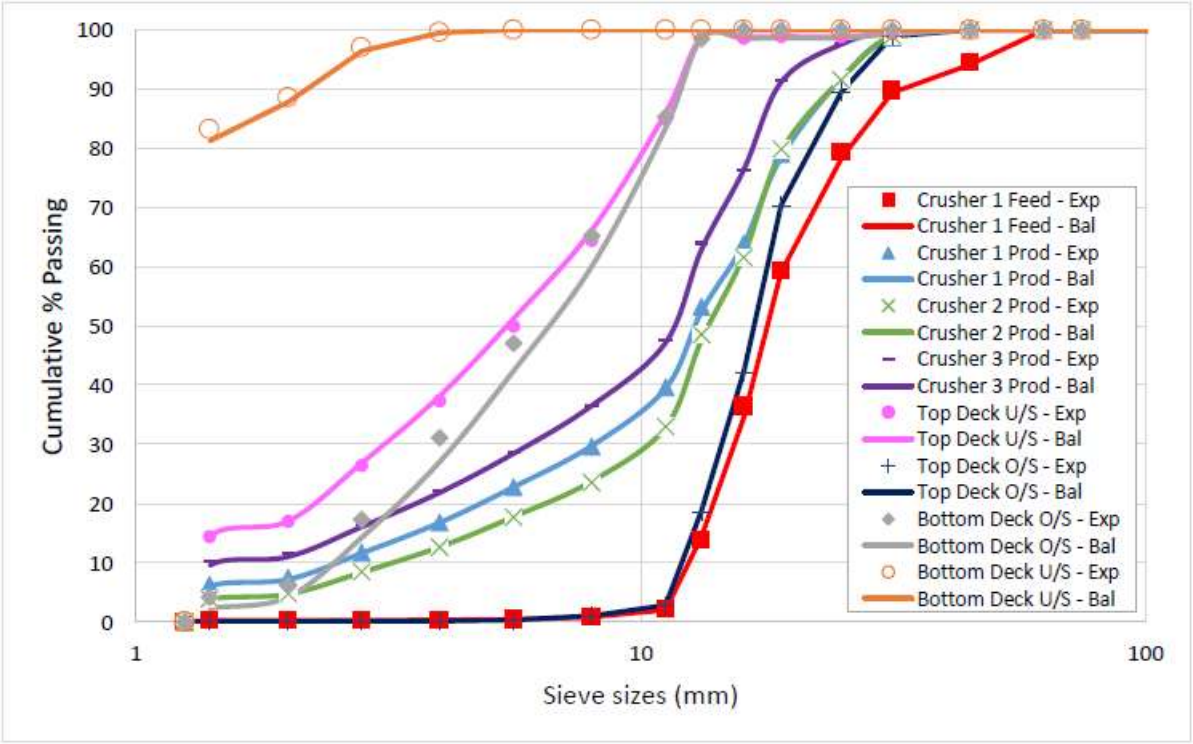

Figure 57: Mass balance and experimental data for tertiary crushing circuit.

Figure 57, shows all the tertiary crushers produce particle size distributions with similar profiles, with crusher 3 producing a slightly finer product than crusher 1. Crusher 2 had the coarsest product. The bottom deck of the tertiary sizing screen undersize reports to the slimes and degrit stream. The bottom deck of the oversize goes to fines DMS while the top deck oversize is recirculated back to the tertiary crushers. The circulating load around the tertiary crushers was calculated as 125% for the duration of the survey, this suggests some extent of inefficiency on the crushing.

5.3.3 Simulations on tertiary and secondary cone crushers

The controllability and correlative outcome of feed material were examined for both tertiary and secondary crushing circuit. The simulated feed material and manipulated variable were assigned rational ranges derived from the experimental data with an assumption that the simulated parameters were only bare to natural variations.

During the simulation for the disturbances caused by selected operating parameters, a close side setting variable is adjusted independently, by effecting step changes from the nominal operating point. The nominal operating points were selected with an objective of giving realistic ranges for variables as much as possible.

The crushers were modelled in JKSimMet using the Andersen/Whiten crusher model. A summary of the model fit parameters for the tertiary and secondary crushers are given in Table 13 and Table 14 respectively.

Table 13: Summary of tertiary crusher model fit

Crusher	Tertiary 1	Tertiary 2	Tertiary 3
TPH	312	315	314
F80, mm	25.36	25.36	25.36
K1 CSS(mm)	0.6	0.65	0.22
K2 CSS(mm)	4.5	5	4.5
K3 Const	2.3	2.3	2.3
T10	13.47	12.96	20.37

The parameters that resulted in a good fit are all in the same range with crusher 1 and 2 having fairly similar parameters and the performance for the two crushers is similar. The K1 CSS constant for crusher 3 is smaller than those from crusher 1 and 2 and the influence can be seen in the significant amount of the sub 11.2 mm material produced. Figure 57 shows the results of the simulated feed and products at different close side settings, this shows the bigger the gap the coarser the product becomes hence could result in inefficient liberation of diamonds.

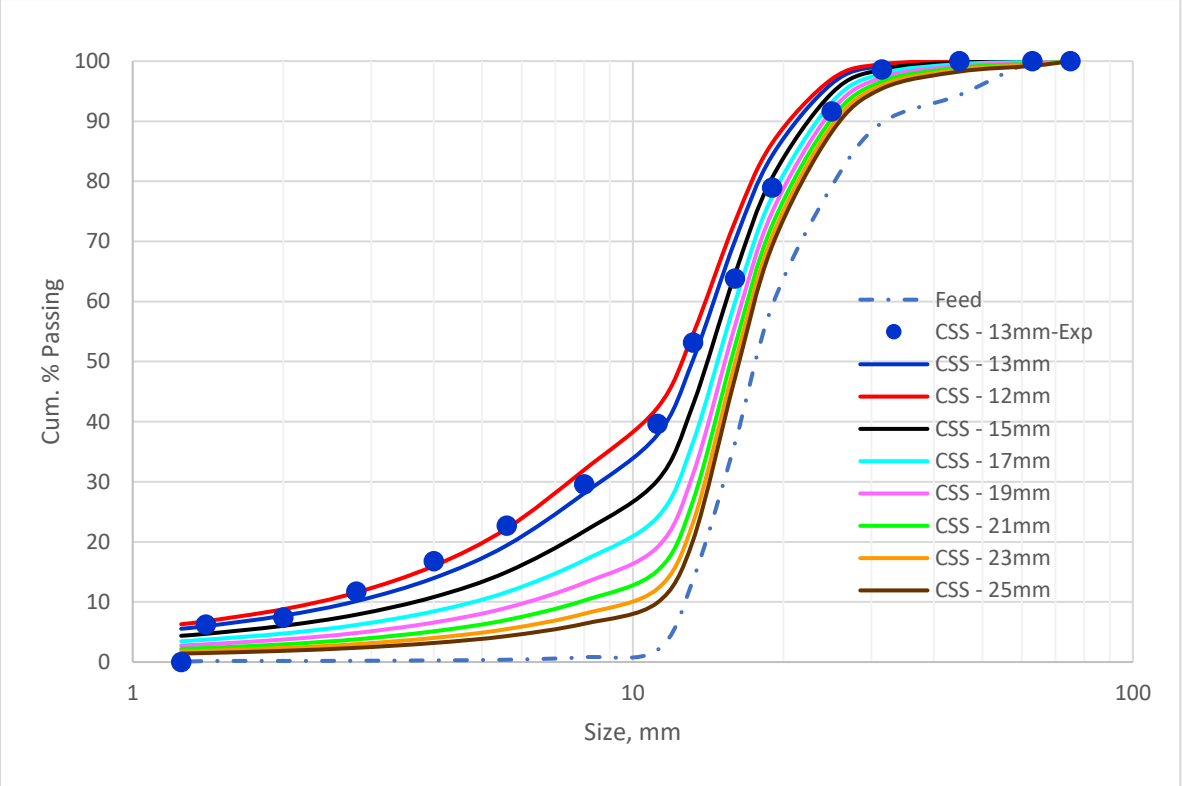

Figure 58: Summary of predicted particle size distribution post simulations at different close side settings

Table 14: Tertiary crushers power consumption and simulated P80 at varying close side settings

Tertiary crusher	No: 1		No: 2		No: 3	
CSS(mm)	Power, kW	Simulated P_{80}, mm	Power, kW	Simulated P_{80}, mm	Power, kW	Simulated P_{80}, mm
12	189	17.49	174.6	18.28	232.6	16.43
13	176.1	18.13	162.7	18.87	219.1	17.03
15	155.1	19.18	143.4	19.84	197.3	18.05
17	138.8	20.01	128.5	20.58	180.4	18.87
19	125.9	20.65	116.9	21.15	167	19.52
21	115.7	21.17	108.2	21.6	156.1	20.05
23	107.8	21.58	101.6	21.96	147.2	20.49
25	101.7	21.92	96.57	22.26	139.7	20.85

Table 18 and Table 19 illustrates that the model shows that the performance of secondary crushers are similar. The deficiency in the model developed is that the same average feed was used for both crushers in the model. The parameters that resulted in the good feed are close indicating that the performance is similar.

Table 15:Summary of secondary crusher model fit

Crusher	Secondary 1	Secondary 2
TPH, tph	312	315
F80, mm	111	111
K1 CSS (mm)	2	2
K2 CSS (mm)	1.9	2
K3 Const	2.3	2.3
T10	13.52	12.99

Table 16: Secondary crushers power consumption and simulated P80 at varying close side settings

Secondary crusher	No: 1 and No:2	
CSS(mm)	Power, kW	Simulated P80, mm
31	129.4	50.98
35	114	55.98
39	103.2	61.75
43	99.14	66.25
47	95.12	70.49
51	91.11	74.75

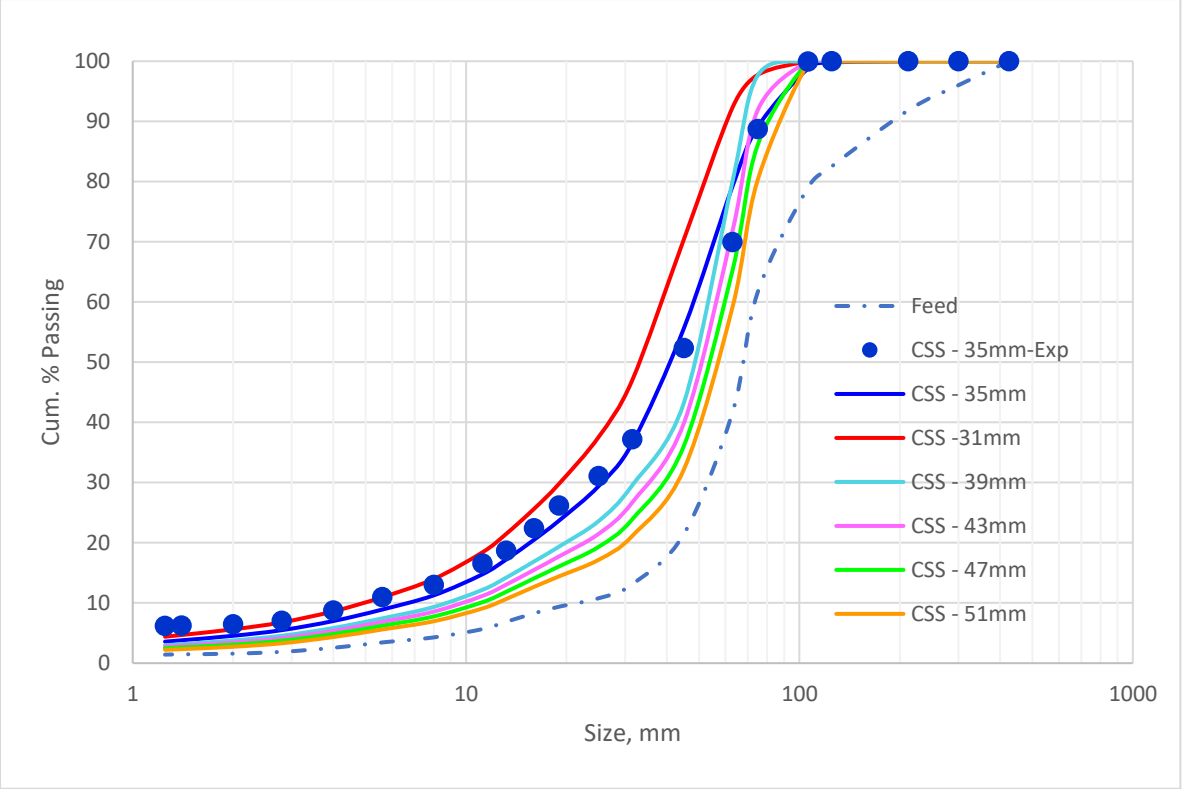

Figure 59: Summary of predicted particle size distribution post simulations at different close side settings on secondary crushers

From the perspective of control design, the difference in the reactions of the product on the manipulated variable can be noted. This suggests that a control strategy using the closed side setting has the potential to improve the control of the size distribution but also reduce diamond breakage. As a simple example of control strategy, the close side setting could be used for obtaining a suitable shift to size distribution.

A suitable criterion for control design is likely to include minimizing the power draw of the crusher under some boundary condition on product flow and size distribution. Modelling the dependence of the power draw on the operated variables, the size distribution and hardness of the crusher feed is therefore a necessary step.

5.4 Parametric studies of Secondary and Tertiary cone crusher tests

5.4.1 Secondary cone crushers

Few parameters are considered when engaging in cone crusher performance assessment as discussed in chapter 2. One of the most important operating set points for the crushers is the close side setting. The influence of the close side setting was assessed in this study by operating the crusher at different close side settings. Figure 60 and Figure 61, shows the particle size distribution from different close side settings (CSS) tests performed on secondary crusher 1 and 2 respectively.

It can be seen from Figure 60 and Figure 61, that the product becomes finer with decrease in the CSS, considering P_{80} of the highest CSS on secondary crusher #1 being 49 mm while the P_{80} of the smallest CSS on the same crusher is 31 mm. Secondary crusher #2 has a P_{80} of 48 mm on the highest CSS, while on the smallest is 30 mm. Therefore, operating at very small CSS level would result in diamond breakage however; the tests performed using the ceramic diamond simulants showed a low probability of breakage in the secondary crushers. This could be due to operating the secondary crushers at CSS levels much higher than the simulants.

It is important to note that for this assessment there are two aspects to be given cognizance and they both presents a tension on the operation of the crushers, that is mineral liberation for preserving the value (Herbst et al.,2008), and particle size reduction without causing damage to the valuable mineral as cited by Evertsson.(2000).

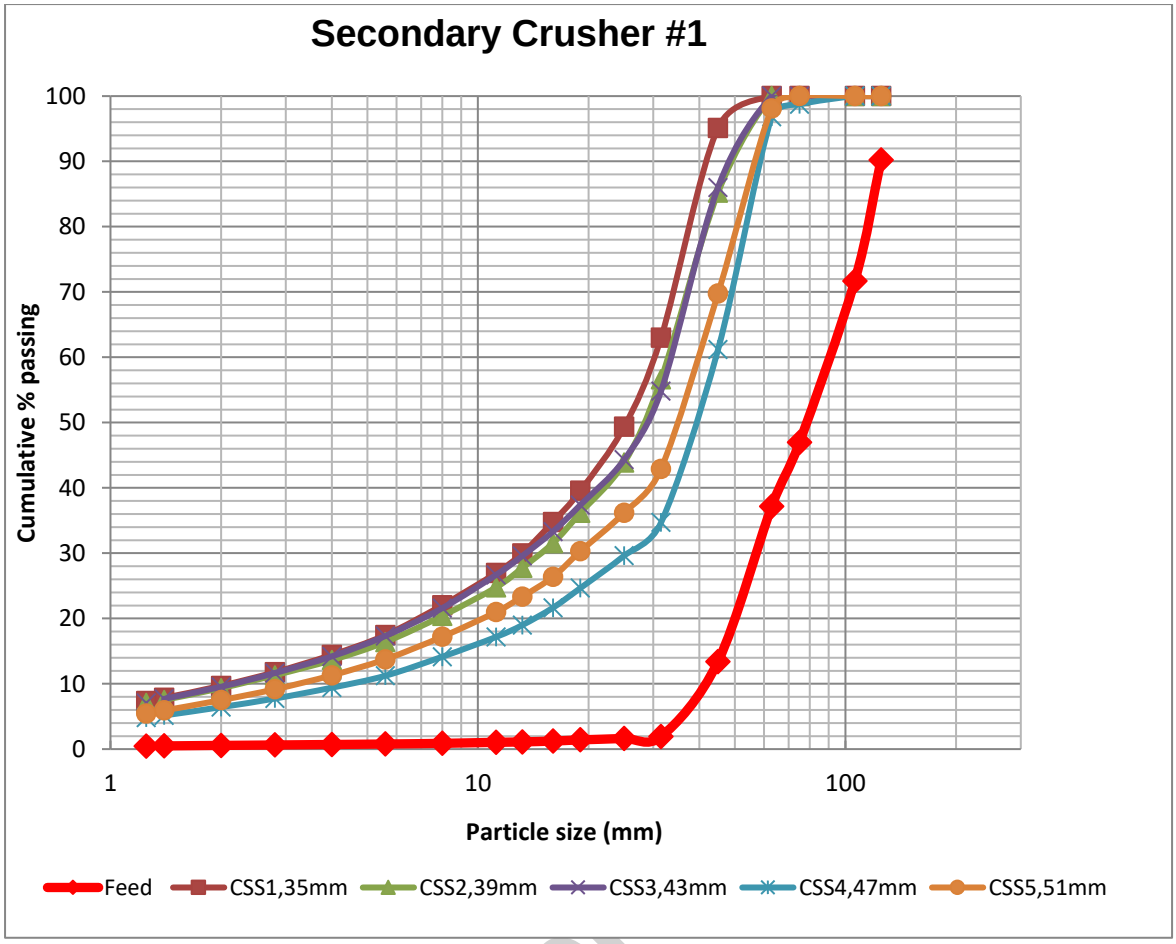

Figure 60: Secondary crusher #1 particle size distribution with feed and products at different close side settings.

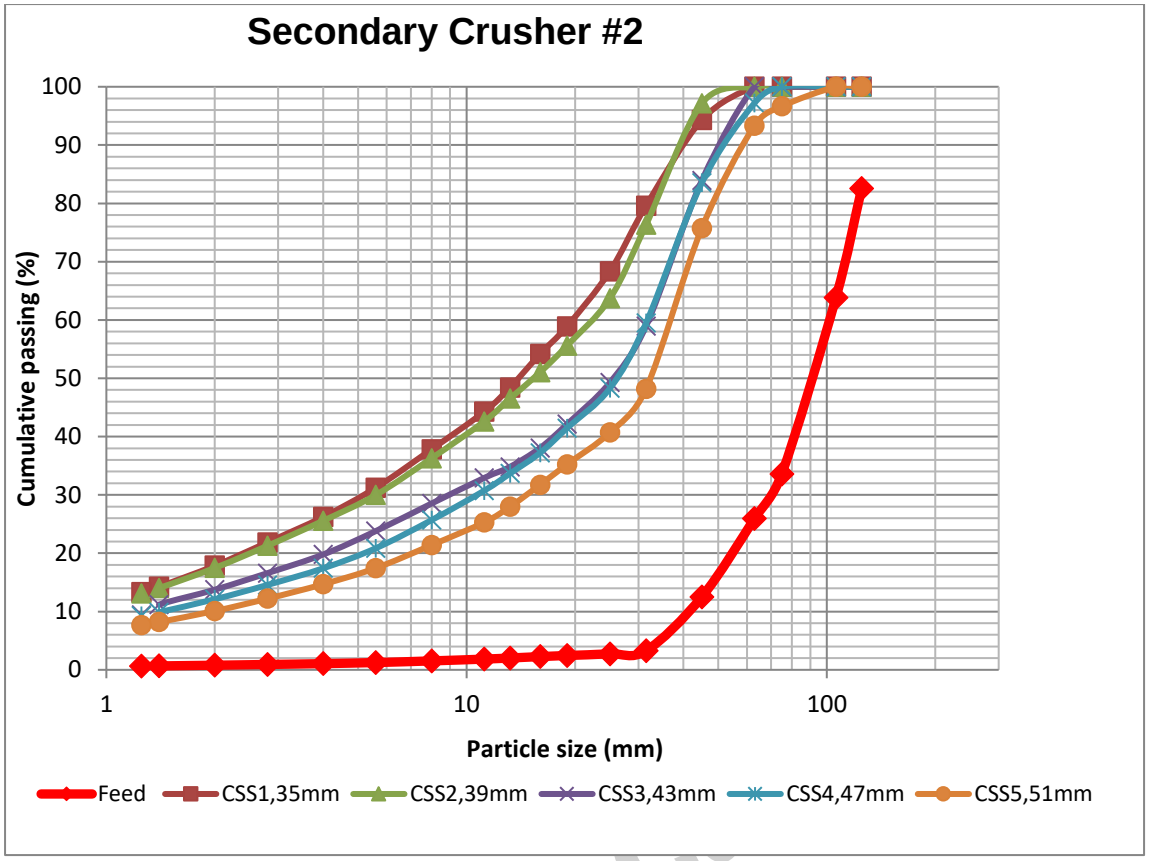

Figure 61: Secondary crusher #2 particle size distribution with feed and products at different close side settings.

The reduction ratios were extracted for P_{50} and P_{20} to assess the impact of close side setting on size reduction. Figure 62 and Figure 63 shows the reduction ratio and close side setting. It can be seen that operating the secondary crusher at small close side setting result in high reduction ratios. This agrees with Quist (2012) who showed that the reduction ratio has a negative trend when increasing the close side setting. This is also in agreement with the observation made by Cleary (2017) that the output of the cone crusher is controlled by the close side setting (CSS). The reduction ratio of secondary crusher #1 is lower than that of secondary crusher #2 because of preferential feeding of coarse material on crusher #2 while operating on the same close side setting with crusher #1.

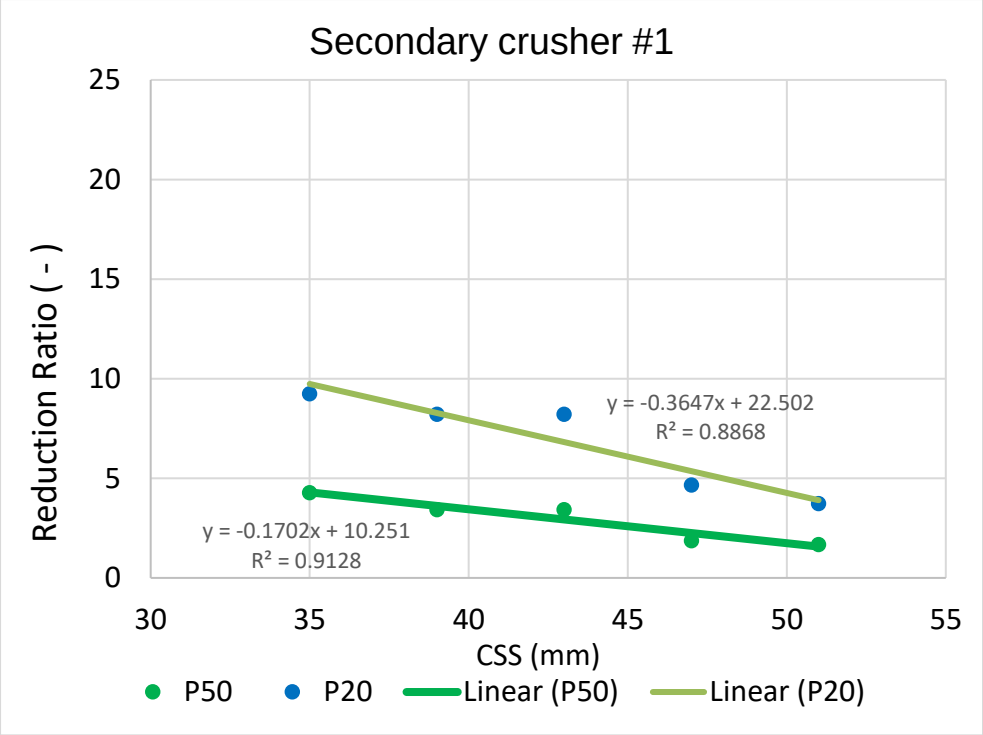

Figure 62: Reduction ratio on secondary crusher #1 showing a negative trend when increasing the close side setting.

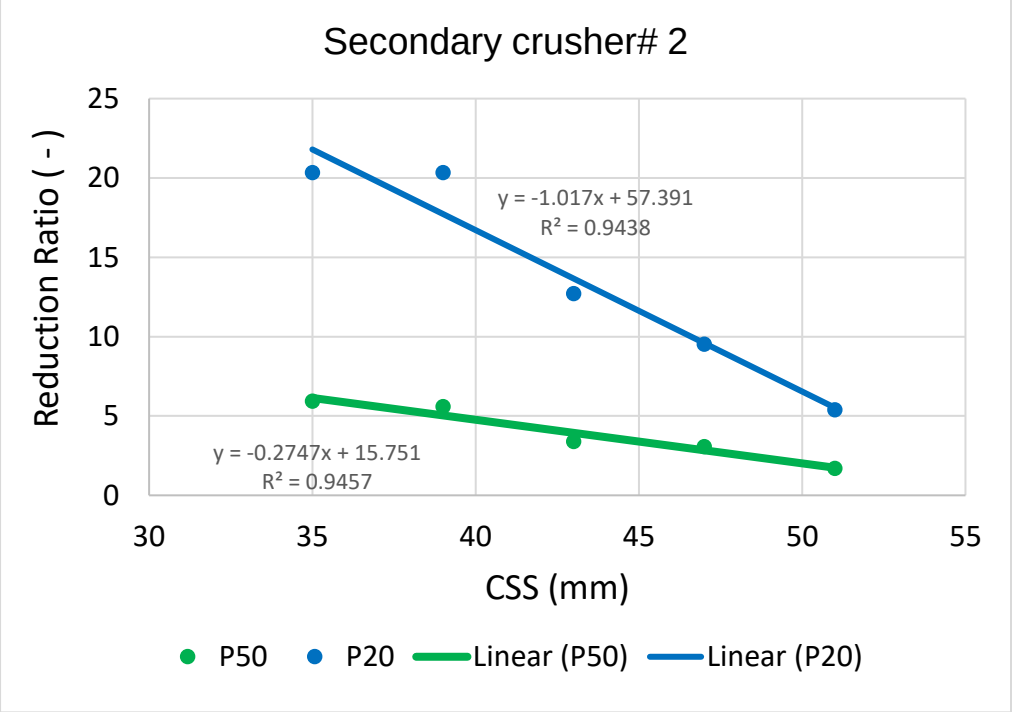

Figure 63: Reduction ratio on secondary crusher#2 showing a negative trend when increasing close side setting.

5.4.2 Tertiary cone crushers

The experiments involving varying the close side settings were performed on two of the three crushers available at the demonstrated plant. The CSS were varied systematically from 13mm to 21mm for the crushers.

The size reduction in the tertiary crushers increased with the decrease in CSS. The largest CSS gap tested resulted in very little size reduction of the material where significant reduction was observed for the smallest setting as shown in Figure 64 and Figure 65. The product becomes finer with decrease in the CSS, considering P_{80} of the highest CSS on tertiary crusher #1 being 26 mm while the P_{80} of the smallest CSS on the same crusher is 18 mm. Tertiary crusher #2 has a P_{80} of 25 mm on the highest CSS, while on the smallest is 16 mm. The reduction ratios for both the crushers are given in Figure 66. It can be seen that the results are not in any close proximity this is due to the orientation of the feed bin where material experiences segregation upon entrance in the crusher bowls. Based on the results attained from the tests, it can be concluded that tertiary crusher 2 has a higher potential of breaking the diamonds.

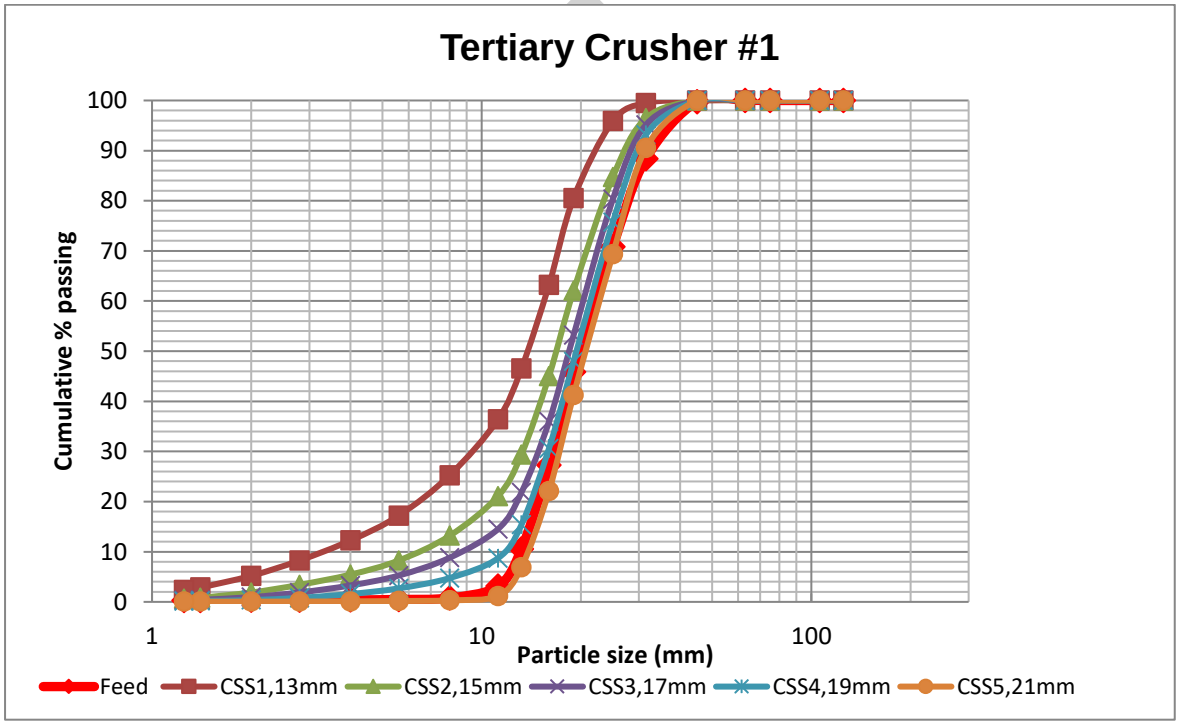

Figure 64: Tertiary crusher #1 particle size distributionwith feed and products at different close side settings.

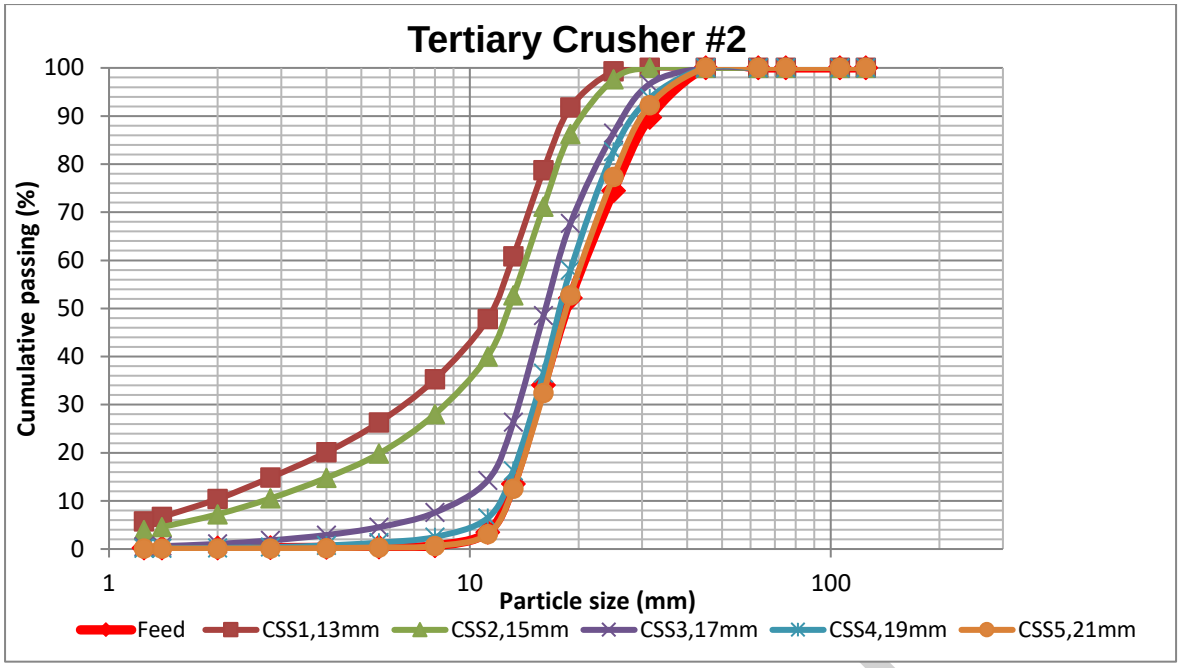

Figure 65: Tertiary crusher #2 particle size distribution with feed and products at different close side settings.

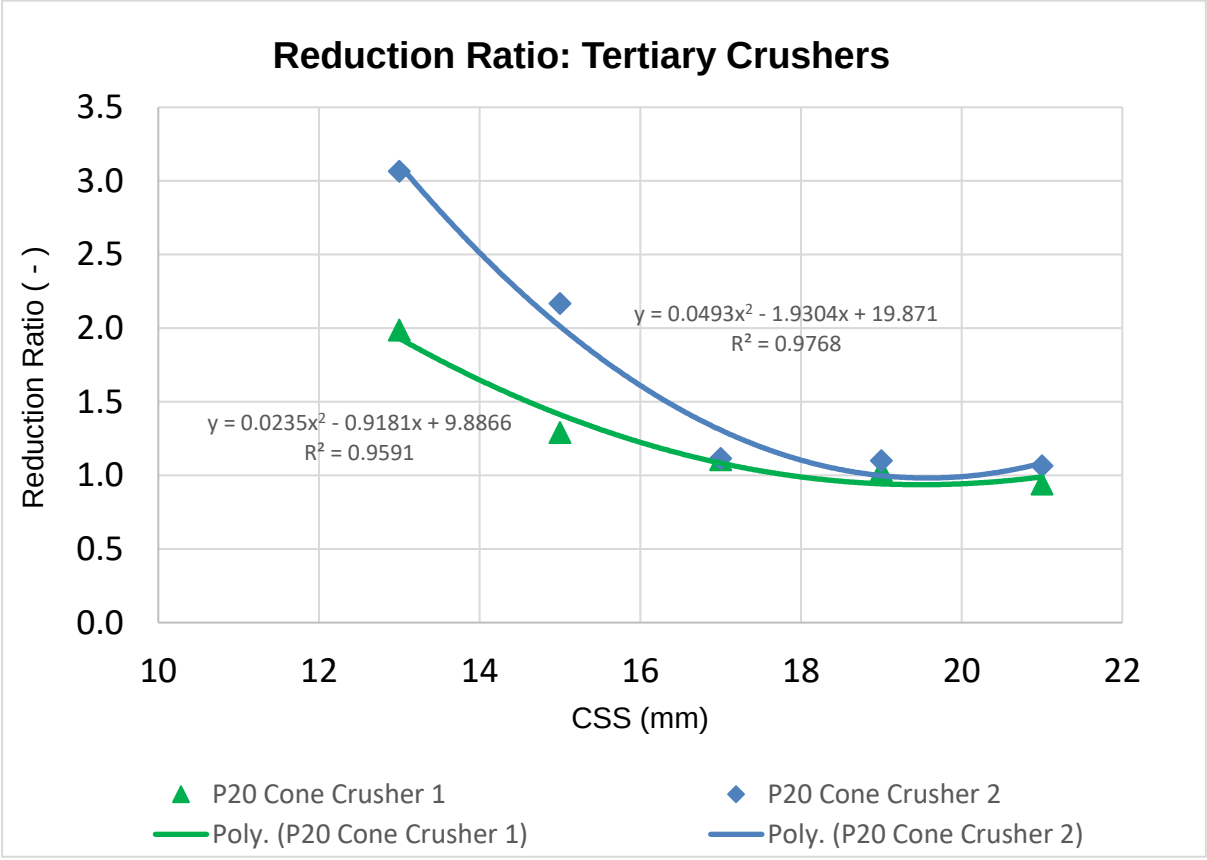

Figure 66: Reduction ratio on tertiary crushers #1 and #2

The reduction ratio for two of the tertiary crushers is shown in Figure 66. The data shows that 19mm and 21mm CSS values resulted in very little size reduction of the material. The operation of crushers at different close side setting was to establish the optimum operating gap that delivers better liberation and reduces the diamond breakage. As noted by Evertsson (2000), that the reason to keep the cone crusher choke fed from an aggregate point of view is to produce a better material shape, while from a diamond liberation perspective choke feeding promotes more interparticle comminution which leads to better liberation for a given particle size distribution.

5.5 Material breakage characterisation

The problem that the thesis focused on was the minimising of diamond breakage in the diamond beneficiation plant. It is therefore important to understand the breakage characteristics of the material that are being comminuted in the plant. Two methods were chosen for this; impact breakage using JKRBT and impact breakage using JK Drop weight tests. The two methods were chosen based on the particle size range encountered in the comminution circuit.

The breakage experiments performed covered the following samples;

- Ceramic diamond simulants representing liberated diamonds
- Embedded simulants in concrete matrix of different strengths, which represented diamonds, encapsulated in the host rock of different facies.
- Actual kimberlite ore.

5.5.1 Breakage characterization tests

Breakage characterisation studies of the ore and ceramic diamond simulants were conducted using the JKRBT and the Drop weight tester. These included tests on ceramic diamond simulants “As-Is” (manufactured from the supplier), simulants embedded in concrete blocks and Kimberlite ore obtained from the crushed scrubber feed. The breakage characteristics of the ceramic diamond simulants were determined by the JK Rotary Breakage Test (RBT) and the Drop weight test (DWT).

The analysis performed to obtain breakage characteristics indices were:

- Extraction of the t_{10} values
- Obtaining the A and b indices by fitting the t_{10} model
- Fitting the Shi-Kojovic model to obtain parameters for size dependent effects

5.5.2 Degree of breakage (t_{10})

Degree of breakage represented by the parameter t_{10} defines the extent of breakage or fineness of the progeny particle size distribution resulting from the applied energy. t_{10} is defined as the cumulative percentage passing one tenth of initial mean particle size (Napier-Munn et al., 1996).

A tenth of the original particle geometric mean size (t_{10} screen size) for each of the size fractions used in the standard impact breakage tests was calculated to aid in the determination of t_{10}. The t_{10} parameter was determined by interpolating the cumulative percent passing data between the two closest sieve sizes to the t_{10} screen size and in consideration of the geometric mean of the particle. The three materials tested had distinct breakage characteristics and produced progeny of different particle size distributions at the same energy.

Figure 67 and Figure 68, shows the progeny particle size distribution obtained from breakage test experiments of ceramic diamond simulants, concrete blocks and kimberlite ore in the -16+13.2mm and the -31.5+26.5mm size fractions, respectively.The concrete block of 34Mpa strength and applied energy of 2 kWh/t produces the most fines and the simulants produce the same particle size distribution even at different applied energies.

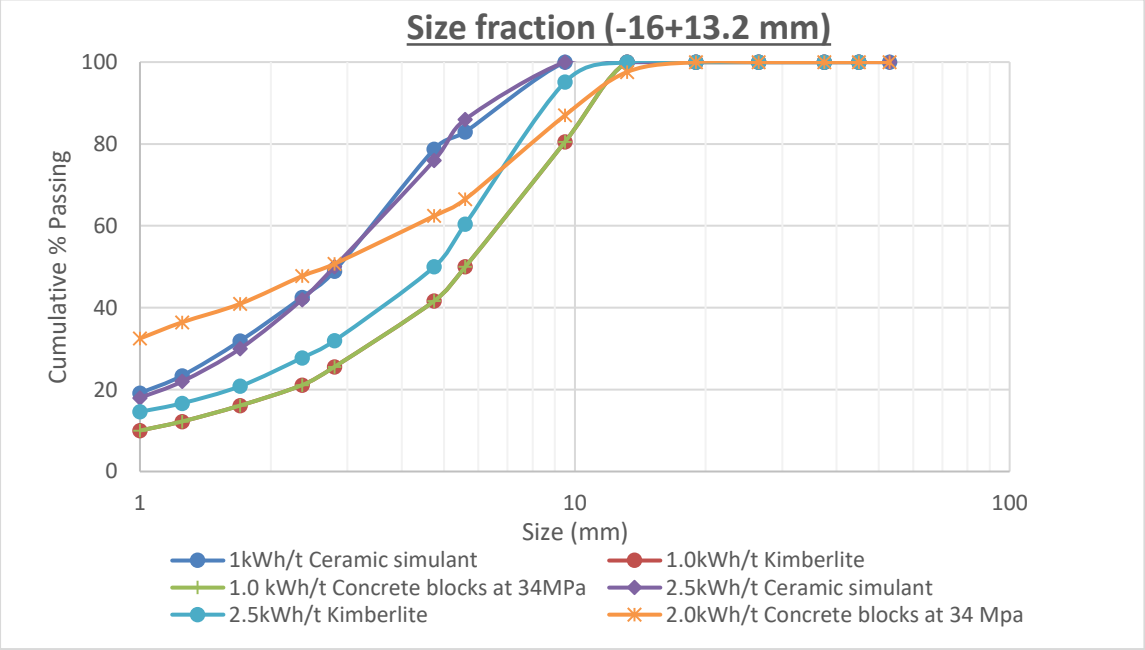

Figure 67: Progeny particle size distribution for ceramic diamond simulants, concrete blocks and kimberlite ore in -16+13.2mm size fraction.

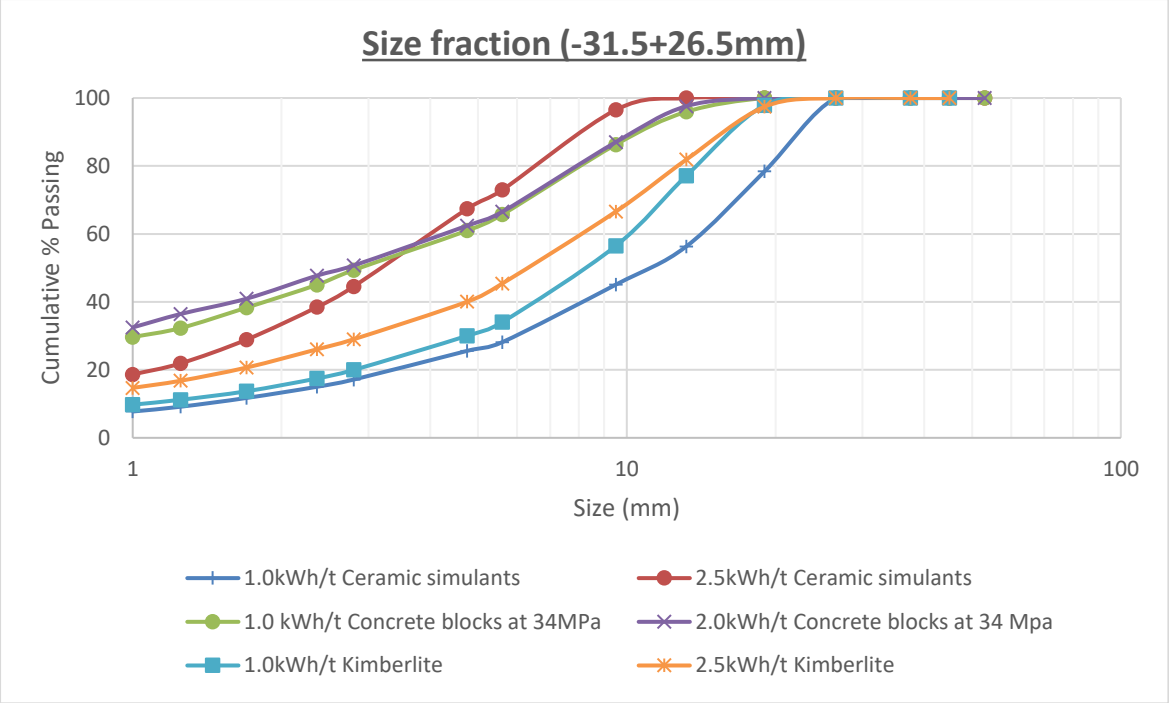

Figure 68: Progeny particle size distribution for ceramic diamond simulants, concrete blocks and kimberlite ore in -26+31.5mm size fraction.

5.5.2 (a) JK Rotary breakage test

Photographs of the ceramic diamonds simulants were taken before and after each test. This included tests on ceramic diamond simulants “As-Is”, simulants embedded in concrete blocks and Kimberlite ore. The breakage characteristics of the simulants were determined by the JK Rotary Breakage Test (RBT).Figure 69 and Figure 70, shows the extent at which the progeny particles are post the test work.

Figure 69: (a)12mm and (b)20mm size ceramic diamond simulants used in the JKRBT tests.

Figure 70: Ceramic diamond simulants after undergoing JKRBT tests, (a) progeny particles at 1.0kWh/t ,(b) progeny particles at 2.0kWh/t and (c) progeny particles at 2.5kWh/t

Breakage is often characterised using the t_{10} model (Genc, Ergun &Benzer (2004); Napier-Munn et al (1996) and Zuo &Shi (2016)). After the breakage tests were completed, the progeny was sieved, and each size fraction was weighed. The percentage of material that is one tenth the size of the original particle is recorded as the t_{10} value, which occurs at the specified energy. The model is fit to the data using the parameters, A and b as seen in (16).

$$t_{10} = A(1 - e^{-bE_{CS}}) \tag{16}$$

Here, A represents the asymptotic value of the t_{10} curve, the maximum measure of breakage. The value Axb indicates the resistance to breakage. The data and model fit results for the simulant tests are shown in Figure 71. The parameters were fitted as A = 47.04 and b = 0.396, making Axb = 18.6. It can be seen from Figure 71, that the ceramic diamond simulants had a good fit on the t_{10}-E_{cs} model.

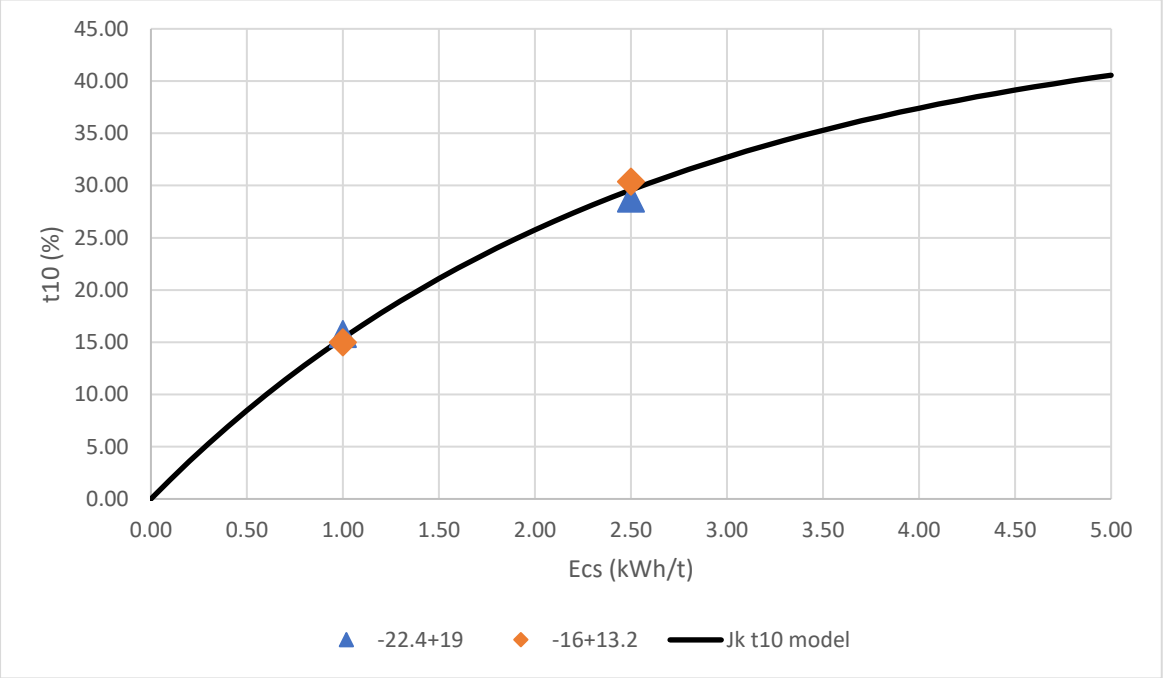

Figure 71: Results of t_{10} -E_{cs} model for simulants in the JKRBT.

5.5.2 (b) Drop weight test

The drop weight was used to characterise the kimberlite rocks and the ceramic diamond simulants embedded in concrete of different strengths. The drop weight tester was used because it was the only unit that could be readily available onsite during the test work.

The material that was tested under drop weight test were subjected to the impact breakage at different energy levels. The daughter fragments were examined to evaluate the magnitude of breakage to the particles by single impact. The two size classes of interest were(-16+13.2mm) and (-31.5 +26.5mm).

Based on the observation made by Genc.O,Ergun.L & Benzer.H (2004) and Chickochi (2017) both on JKRBT and DWT, breakage product size distributions indicates that, an increase in breakage energy level increases the fineness of the breakage distributions whereas, size distributions start to become closer at higher energy levels indicating no more size reduction.

Table 17 shows the t_{10} values obtained when fitting the model per material type. The material size on other energy levels makes it impossible to get the correct required data. In areas that were that were not filled, the model fit was not yielding any satisfactory conclusion. The work could be investigated in future studies.

Table 17: t_{10} values in relation to the size fraction per material type.

		t_{10}		
		1.0kWh/t	2.0kWh/t	2.5kWh/t
-16+13.2	Ceramic diamond Simulants	16.87	-	27.83
	Concrete blocks	-	-	-
	Kimberlite ore	14.35	-	18.95
-31.5+26.5	Ceramic diamond Simulants	16.77	-	19.93
	Concrete blocks	60.45	61.89	-
	Kimberlite ore	29.56	-	39.54

The concrete blocks seem to be finer than ceramic diamond simulants and kimberlite at the tested energy levels. Zuo & Shi (2016), has also a similar trend of a finer product at higher energy levels. Chikochi (2017), has also evaluated the specific input energy on the PGM associated ore and observed a similar trend where higher energy produces a finer product, depending on the initial particle size.

5.6 t_{10} breakage model

The Whiten t_{10}-E_{cs} model was fitted to all the breakage data using solver in excel to obtain the breakage indices A and b. Figure 72, Figure 73 and Figure 74, show the fitting of the whiten t_{10}-E_{cs} model to ceramic diamond simulants “As-Is”, embedded simulants in concrete and kimberlite respectively.

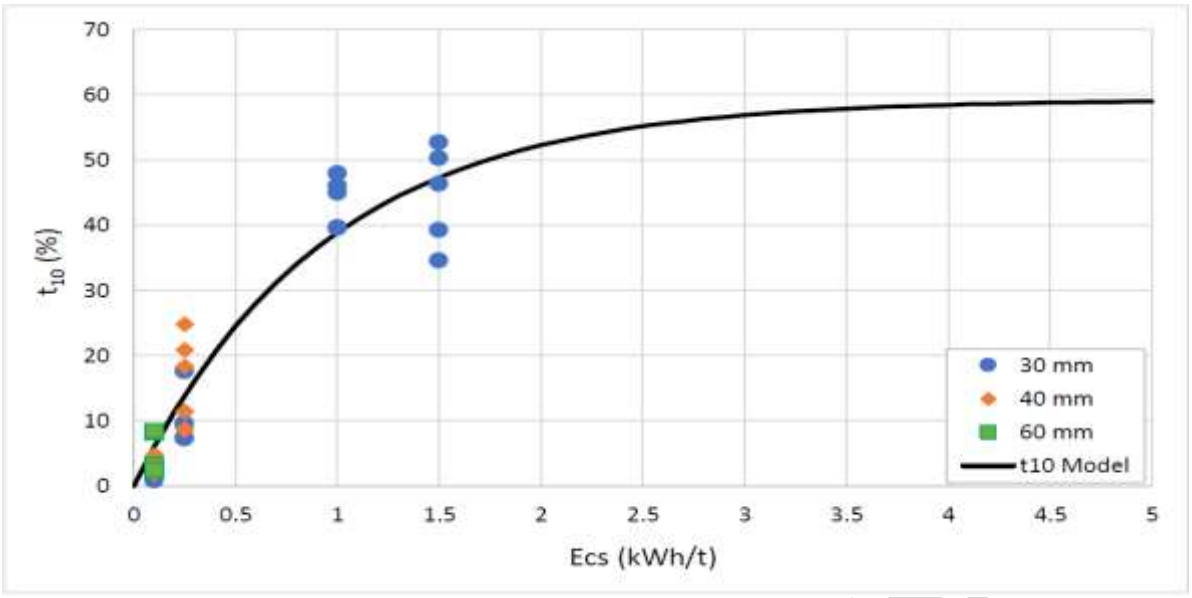

Figure 72: t_{10} model fit for embbeded simulants test

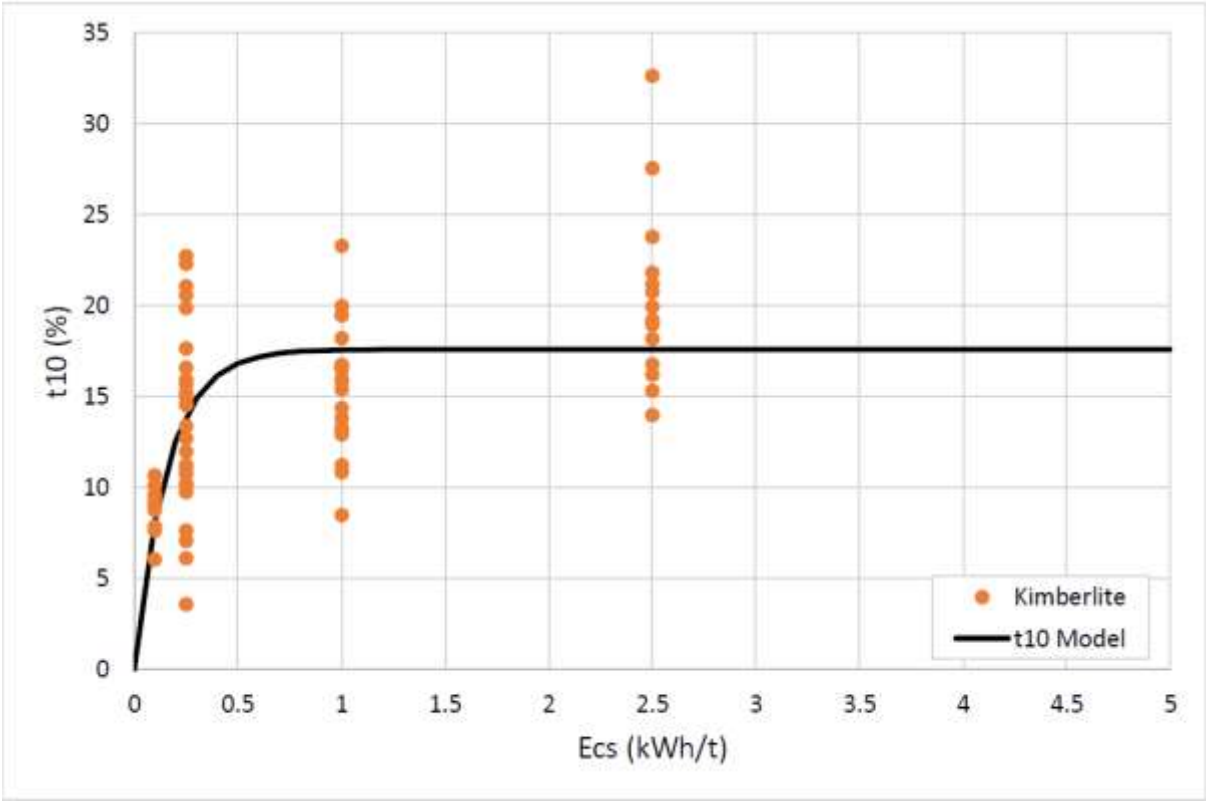

Figure 73: t_{10} model fit for kimberlite ore tests

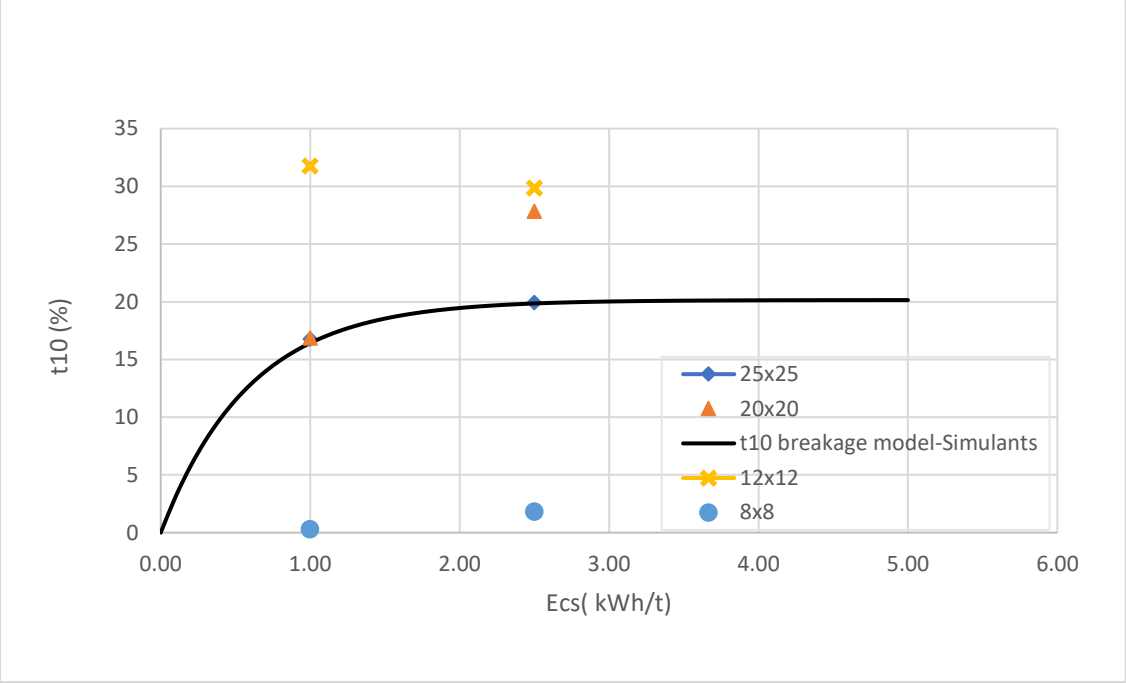

Figure 74: t_{10} model fit for ceramic diamond simulants tests.

It can be seen from Figure 72 to Figure 74, that the Whiten t_{10}-E_{cs} model fitted the data very well for ceramic diamond simulants "As-Is" and embedded simulants in concrete blocks. However, scatter was observed in the fitting of the kimberlite ore which could be due to size dependence and variable breakage behaviour with the kimberlite material. The observation motivated to fit the model that has size dependence parameters develop by Shi & Kojovic.(2007). Table 18 shows a summary of breakage parameters extracted from the fitting of the ceramic diamond simulants, embedded simulants in concrete at different compression strength and kimberlite ore.

Table 18: Material hardness parameters A,b and Axb for the material used in drop weight test.

Material type	A	b	Axb	RMSE
Kimberlite ore	22.75	4.75	108.13	24.69
Ceramic diamond simulants	20.15	1.69	34.05	31.4
Sika-Crete 214 (34MPa)	65.62	1.89	124.02	11.9
Sika-Crete 214 (55MPa)	59.06	1.98	116.94	13.32
Sika-Crete 214 (77MPa)	59.28	1.07	63.43	17.03

The breakage parameters in Table 18, can be interpreted using the guide by Napier-Munn (1996) as demonstrated in Table 19.Table 19 shows, material characterisation based on t_{10} model. From the A parameter which represent the highest t_{10} value at the asymptote of the fitted curve on the Whiten t_{10}-E_{cs} relationship. It can be concluded that the concrete at 34 and 55Mpa are in the same classification as the kimberlite ore. This is advantageous because the embedded results are applicable to the demonstration plant.

Table 19:Material characterisation based on t_{10} model.

	Very Soft	Soft	Medium	Hard	Very Hard
Axb	> 127	67 - 127	43 - 67	30 - 43	< 30

Photographs of the parent concrete blocks, and the progeny particles from the drop weight test are shown in Table 20. It can be seen that in some cases the embedded simulants are broken while others are simply liberated without being broken. Partially liberated ceramic simulants were also observed.

Table 20, image (a), (b) and (c) showed the concrete blocks after being manufactured in their respective sizes 30 mm, 40 mm and 60 mm respectively. The drop weight test was performed at 0.1 kWh/t, 0.25 kWh/t and 1.0 kWh/t. The progeny particles at 0.1 kWh/t at all concrete block sizes were not finely fragmented as could be seen on picture (d), (e) and (f) this could be due to the particle orientation during the test, however comparing the particle product at 0.25 kWh/t then it can be seen that the progeny particles are finer. The test undertaken at 1.0 kWh/t has resulted in more finer progeny particle as seen in picture (i) and (j). It was therefore concluded that the test carried out in higher energy levels produces finer product. Size dependency also was considered and had been explored in section 5.7.

Table 20: Concrete blocks with embedded simulants and results of drop weight tests.

Ecs (kWh/t)	30mm	40mm	60mm
	 (a)	 (b)	 (c)
0.1	 (d)	 (e)	 (f)
0.25	 (g)	 (h)	
1.0	 (i)	 (j)	

5.7 Size dependent breakage model

Since the combination from Rumpf's similarity consideration (Rumpf,1973) and the Weibull statistics of fracture mechanics (Weibull,1951), Vogel and Puekert (2003,2004) established a breakage probability model. It was noted by Banini (2000), that the JK breakage model does not take in consideration the particle size effect on the breakage index t_{10} instead it uses one set of *A, b* parameters to represent all particles sizes (Shi,2016).

It was, however, noted that in the work of Vogel-Peukert breakage probability model the particle size (x) was incorporated with anticipation that the particle size can be accommodated using the fundamental breakage model structure. The Vogel-Peukert breakage probability model was therefore revised to describe the breakage index t_{10} by Shi & Kojovic (2007).

The breakage model developed by Shi and Kojovic (2007) incorporating the effect of size to describe the degree of breakage was fitted to the breakage data by non-linear regression techniques. For the fitting, the number of impacts, k, was taken to be 1 as no incremental breakage tests were performed. The energy threshold (E_{min}) below which infinite impacts will not result in fracture was taken to be zero as suggested by Zuo and Shi (2015). This was a valid assumption since high t_{10} values were obtained by a single impact even at low energies.

The parameter, f_{mat} is a size dependent material property which characterises the resistance of particulate material against fracture in impact comminution (Zuo & Shi, 2015; Vogel & Peukert, 2004). f_{mat} for each size class and a global M (maximum t_{10} for a material subjected to breakage) for each specific test, were fitted to provide the least root mean square error (RMSE). The model fittings for kimberlite ore, ceramic diamond simulants and embbeded concrete blocks of 34 MPa ,55 MPa and 77 MPa are presented in Figure 75 to Figure 79.

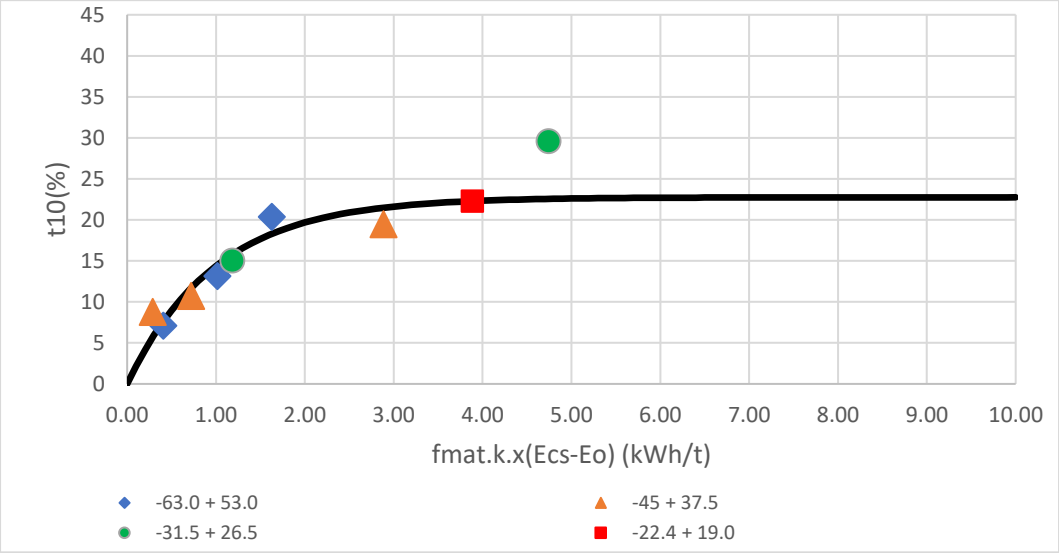

Figure 75:Size dependent breakage model fitting to kimberlite ore particles.

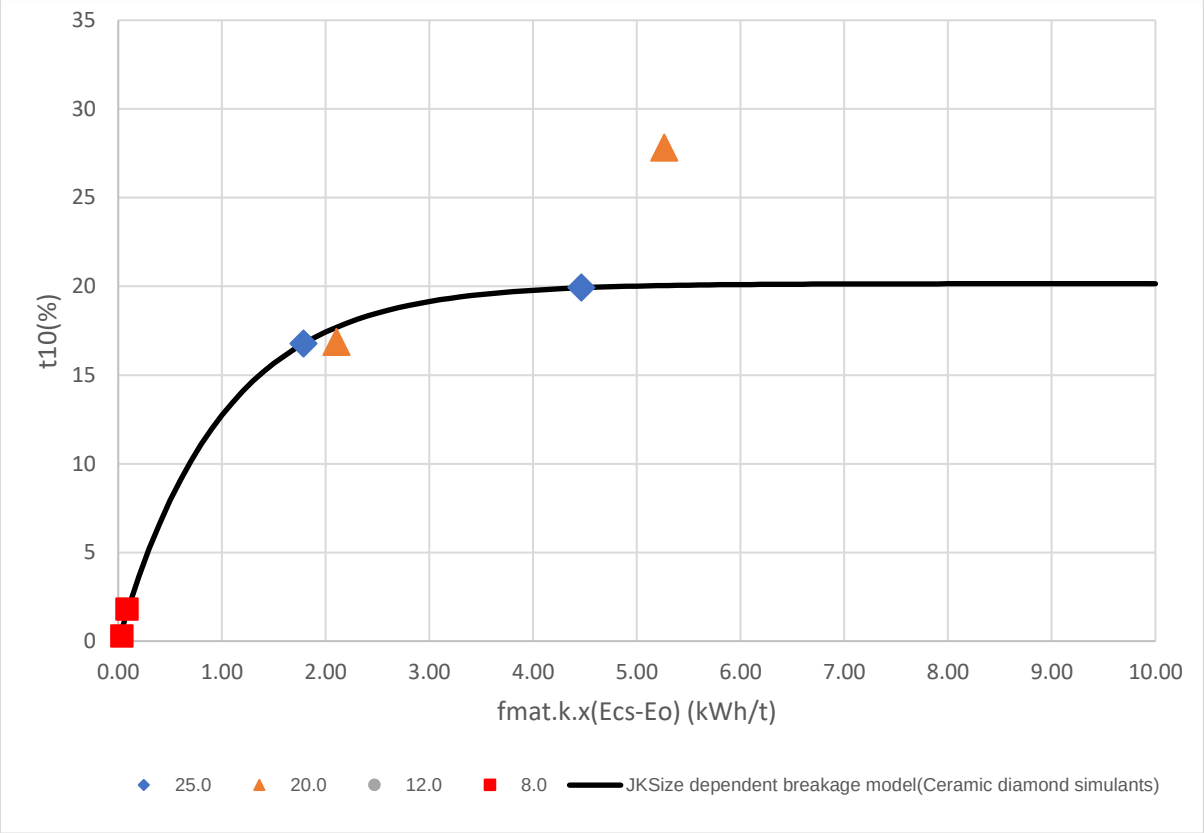

Figure 76:Size dependent breakage model fitting to ceramic diamond simulants.

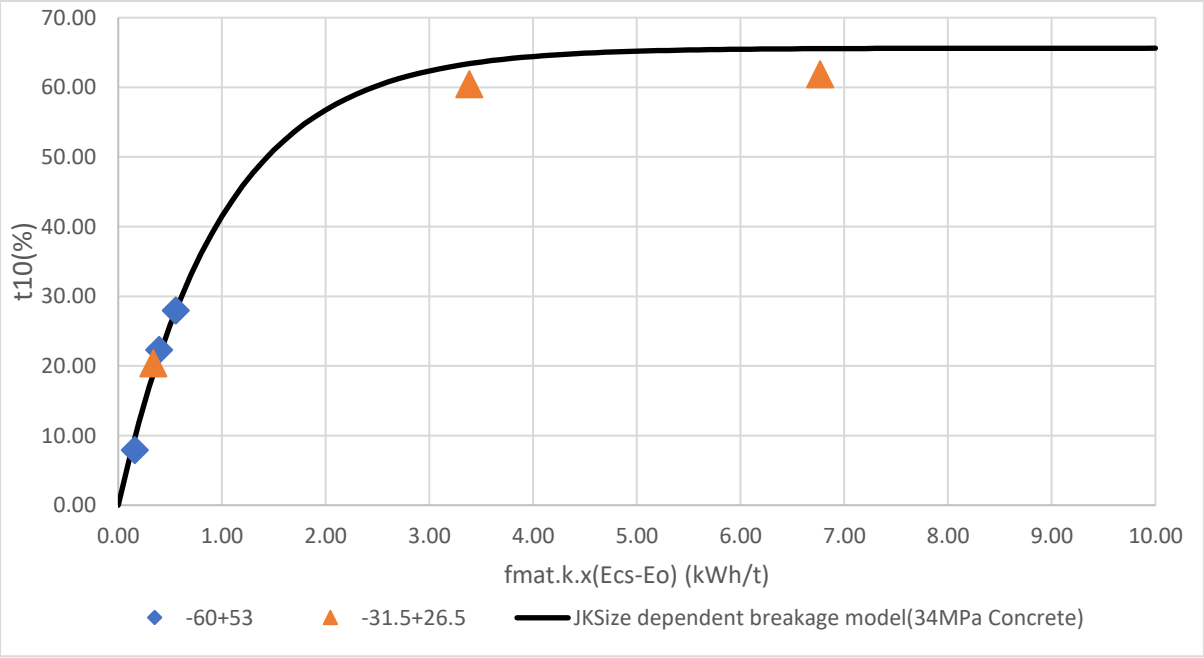

Figure 77:Size dependent breakage model fitting to concrete blocks at 34MPa.

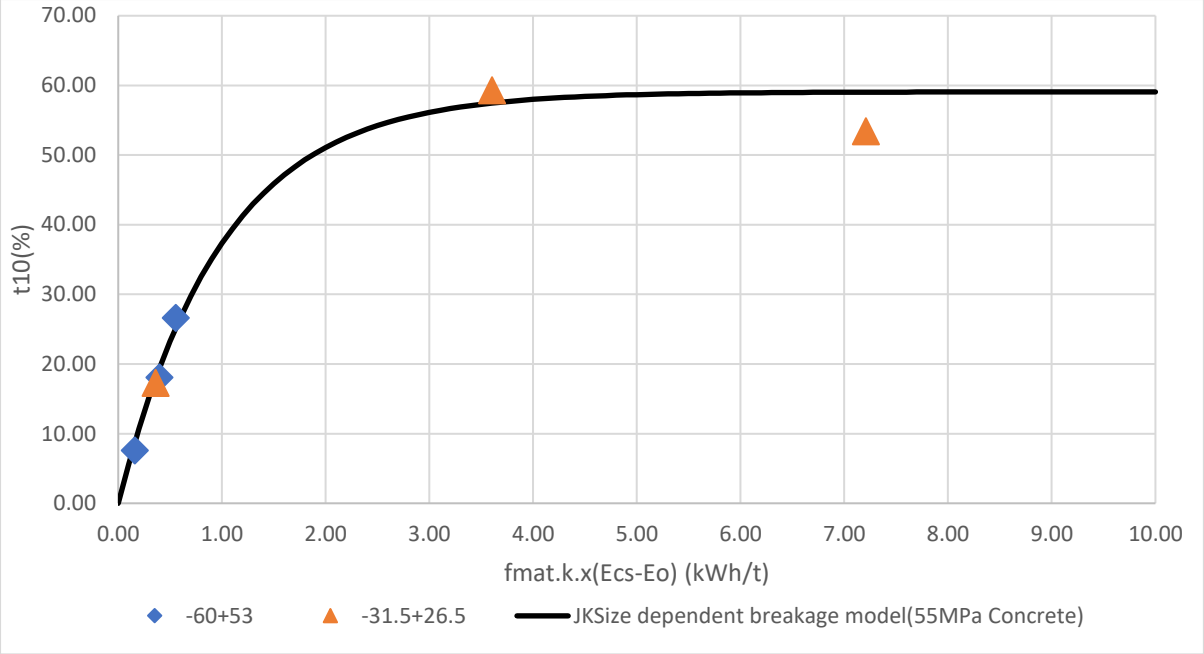

Figure 78:Size dependent breakage model fitting to concrete blocks at 55MPa.

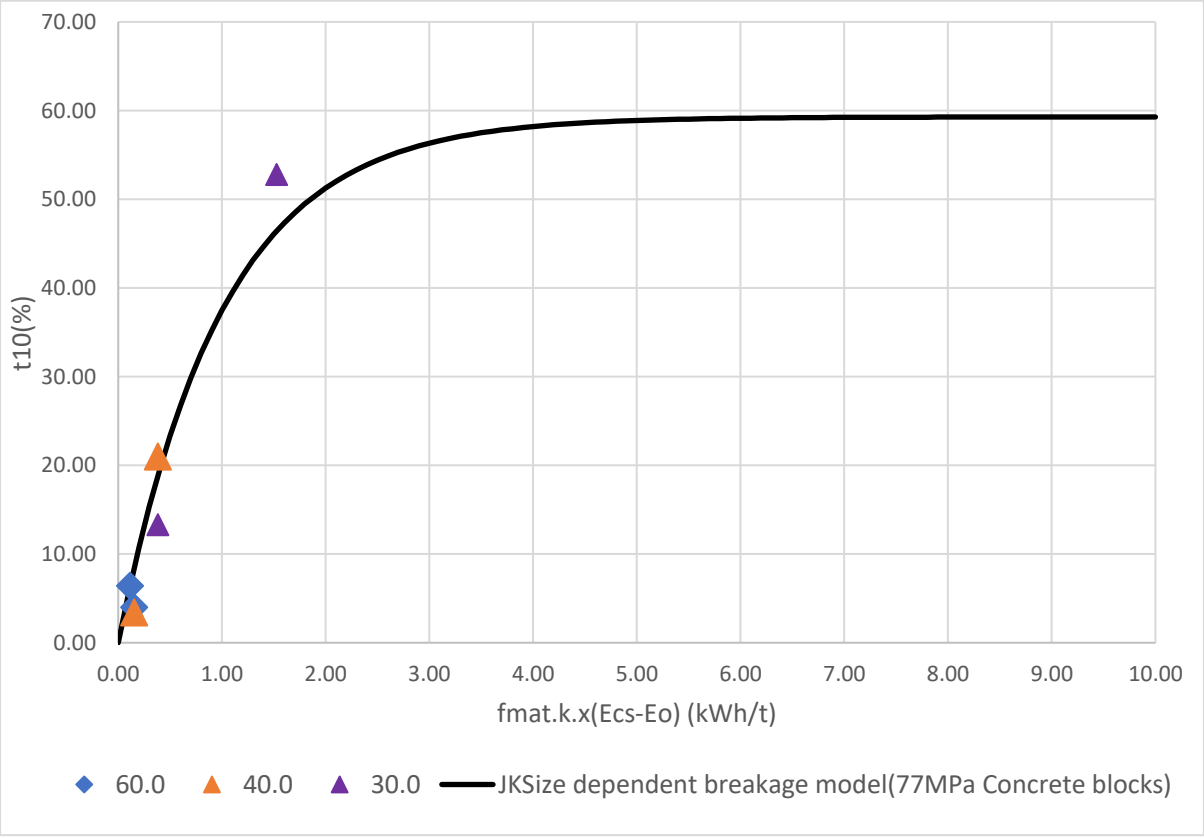

Figure 79:Size dependent breakage model fitting to concrete blocks at 77MPa.

The size dependent model fitted the data well for all material as shown in figure 72 to figure 76.The model parameters obtained by fitting the size dependent breakage model for kimberlite ore, ceramic diamond simulants and embedded concrete blocks are summarised in Table 21.

Table 21: Breakage characterisation parameter for the tested material determined by fitting the breakage data to the size dependent model.

Material type	M(%)	Particle mean size(mm)	f_{mat} ($Kg.J^{-1}m^{-1}$)	RMSE
Kimberlite ore	22.75	57.8	0.07039	23.27
		41.1	0.07026	
		28.9	0.16424	
		20.6	0.75357	
		14.5	6.67853	
Ceramic Diamond Simulants	20.15	25	0.07142	17.03
		20	0.10527	
		12	1.33890	
		8	0.00425	
Sika-Crete 214 (34MPa)	65.62	56.4	0.02808	5.29
		28.9	0.11713	
Sika-Crete 214 (55MPa)	59.97	56.4	0.02808	6.31
		28.9	0.12477	
Sika-Crete 214 (77MPa)	59.28	60	0.01907	10.96
		40	0.03811	
		30	0.05093	

Values of A and M(%) which represent the maximum t_{10} for the t_{10} breakage model and the size dependent model respectively are the same as indicated in Table 18 and Table 21. The value of M had adopted the similar pattern of A. The high values of M were attained from the embedded concrete blocks for all the three strengths tested as shown in Table 21.

Figure 77, Figure 78 and Figure 79 show that the t_{10}-E_{cs} curve for the embedded concrete samples had a deeper gradient compared to the kimberlite and ceramic diamond simulants in Figure 75 and Figure 76 respectively. The slope of the t_{10}-E_{cs} is closely related to the material's property f_{mat} (Zuo & Shi, 2015). Size dependency of f_{mat} is also observed with the parameter increasing with the reduction of particle size. It was however seen that the ceramic diamond simulants did not follow the pattern only on the smallest particle tested shown in Table 21.

The root mean square error for the size dependent model in Table 21 can be seen to be lower compared to the values achieved in the t_{10} breakage model in Table 18.

CHAPTER 6

6. MODELS TO EXTRACT EQUIPMENT PARAMETERS IN CIRCUIT

6.1 Model fitting

Model fitting was done using the Model Fit Mode in the JKSimMet software. Each unit in the system is described by a model. The unit models that were used for fitting the circuit are described by Napier-Munn et al (1996).During model fitting, JKSimMet estimates the model parameters by calculating the difference between the predicted and experimental data and then adjusting the model parameters such that the squared sum of the differences is a minimum (JKSimMet Version 6 Manual,2014). The model fitting process was carried out for the crushers and associated vibrating screens. No significant size reduction was achieved in the scrubbers.

6.2 Model Descriptions

6.2.1 Crusher model

The crusher model is expressed by a classification function represented by C(x) which is the probability of the selection for breakage of a particle of size x. The general form of the relationship defines a size where all particles are broken C(x) = 1, a size where no particles are broken C(x) = 0 and the particles in between have a probability greater than zero and below one with smaller particles having low probabilities and larger particles higher probabilities. The model is described by three parameters:

$$C_{(x)} = 1 \qquad \text{for X>K2 (All particles are broken)} \qquad (17)$$

$$C_{(x)} = \frac{K2-x}{K2-K1}\, x\,(K3) \qquad \text{for K1 < X < K2} \qquad (18)$$

$$C_{(x)} = 0 \qquad \text{for X < K2 (No particles are broken)} \qquad (19)$$

The fitting involves adjusting the constants K1 to K3 for the cases described in the three equations.

6.2.2 Vibrating screens

All the screens were modelled using a simple efficiency curve, which is described by three partition curve parameters:

α - sharpness of the split

C - Water split to undersize

d50c - cut-size, approximately equal to the effective aperture size

6.3 Model fitting results for plant surveys

The parameters used to describe the demonstration plant circuit are in Table 22.

Table 22: A summary of the plant crusher circuit and screening,JKSimMet model parameters.

Equipment	Model Used	Parameter	Value
Primary Screen 1	Double deck screen based on efficiency curve	Efficiency Curve – α - Top Deck	8
		Efficiency Curve - α - Bottom Deck	5.6
		Corrected D50 (mm) - Top Deck	51
		Corrected D50 (mm) - Bottom Deck	12
Primary Screen 2	Double deck screen based on efficiency curve	Efficiency Curve - α - Top Deck	5.2
		Efficiency Curve - α - Bottom Deck	4.8
		Corrected D50 (mm) - Top Deck	48
		Corrected D50 (mm) - Bottom Deck	10
Secondary Crusher 1	Andersen/Whiten	K1 - Constant	70.06
		K2 - Constant	70.76
		K3 - Constant	2.3
Secondary Crusher 1 Screen	Double deck screen based on efficiency curve	Efficiency Curve - α - Top Deck	12
		Efficiency Curve - α - Bottom Deck	12
		Corrected D50 (mm) - Top Deck	45
		Corrected D50 (mm) - Bottom Deck	16
Secondary crusher 2	Andersen/Whiten	K1 - Constant	70.06
		K2 - Constant	70.76
		K3 - Constant	2.3
Secondary Crusher 2 Screen	Double deck screen based on efficiency curve	Efficiency Curve - α - Top Deck	12
		Efficiency Curve - α - Bottom Deck	10
		Corrected D50 (mm) - Top Deck	45
		Corrected D50 (mm) - Bottom Deck	16
Tertiary crusher 1	Andersen/Whiten	K1 - Constant	8.41
		K2 - Constant	71.0
		K3 - Constant	2.3
Tertiary Crusher 1 Screen	Double deck screen based on efficiency curve	Efficiency Curve - α - Top Deck	5
		Efficiency Curve - α - Bottom Deck	1.2
		Corrected D50 (mm) - Top Deck	8
		Corrected D50 (mm) - Bottom Deck	1.4
Tertiary crusher 2	Andersen/Whiten	K1 - Constant	13.73
		K2 - Constant	35.5
		K3 - Constant	2.3
Tertiary Crusher 2 Screen	Double deck screen based on efficiency curve	Efficiency Curve - α - Top Deck	4
		Efficiency Curve - α - Bottom Deck	1.6
		Corrected D50 (mm) - Top Deck	9
		Corrected D50 (mm) - Bottom Deck	1.2
Tertiary crusher 3	Andersen/Whiten	K1 - Constant	11.21
		K2 - Constant	36.0
		K3 - Constant	2.3
Tertiary Crusher 3 Screen	Double deck screen based on efficiency curve	Efficiency Curve - α - Top Deck	4
		Efficiency Curve - α - Bottom Deck	1.1
		Corrected D50 (mm) - Top Deck	10.5
		Corrected D50 (mm) - Bottom Deck	1.2

From the model developed, the crusher parameters, K1 and K2, for the secondary and tertiary crushers are all within the expected range. For this model, K3 was kept constant at a recommend value of 2.3. In the scrubber and secondary crusher part of the circuit, the top deck screen parameters, α and $D50_c$ values indicated that the screens were working efficiently. The α values were all above 4 and the D50 values were close to the aperture sizes. For the tertiary crusher, the top deck screen had α values above 4 and the D50 values close to the aperture sizes indicative of efficient performance.

However, the bottom deck screens had very low α values in the region of 1 to 1.6 and D50 values between 1.2. The α value shows that the separation on these screens is not as sharp as one would expect for screening operations. This could be due to overloading of the screens.

This model can be applied to simulate various optimisation routes including assessing circuit capacity with changes in fragmentation from the mining section.

CHAPTER 7

7. EVALUATING METHODOLOGY AND PROPOSED REMEDIAL MEASURES

This chapter discusses the recommended remedial measures and provides the outcome of implementing the recommendations that were arrived at after applying the methodology developed in this thesis discussed in chapter 3. The details of what has been implemented in the processing plant after all the test work had been done and the results of the methodology developed systematically are provided.

7.1 Remedial Measures

The remedial measure will be narrated in parts as they were all implemented in sequential order to determine the areas prone to diamonds breakage. It was important to implement the remedial measure in stages in order to gain the confidence of the staff at the operating plant. This was important because the aspect of the work required disrupting the operations of the plant to perform test work and implement recommended changes. Other aspects required the plant to provide funds and without gaining confidence, they would not provide resources for the project.

7.1.1 Recovery plant

The recovery plant x-ray machines concentrate pipe installed were of stainless-steel pipes and they were replaced with the HPDE (High density polyethylene) material to minimize the free diamonds impact on hard surface as shown on the pictures in Figure 80.The concentrate holding bins in the sort house were also rubber lined to provide a more friendly surface that will reduce impact. The work from seeding ceramic diamond simulants showed that some breakage of liberated diamonds could occur in this part of the process. The concentrate drying system was also improved by installing the drying humidifier as it was initially noticed that some level of breakage could be as a result of thermal shock.

Figure 80: Illustration of stainless steel pipes in(a) being replaced by HDPE pipes in (b).

7.1.2 Secondary and tertiary cone crushers control philosophy.

The crushers were initially set up with a pan feeder to start slowly and gradually increase the speed until such a point where it could easily be controlled. To maintain choke feed condition was however inversely instituted to run the pan feeders at high speed upon startup to reach the choke feed conditions faster. It has been seen in previous studies that choked feed enhances interparticle crushing (Evertsson., 2000). The interparticle crushing is well preferred because it is believed that it reduces diamond breakage because of reduced particle to metal contact.

The crushers in a conventional plant use compression and impact forces between two steel surfaces to break the feed material. Although the crushers are optimized to operate at the maximum possible crushing gap, there is still the potential for breaking diamonds between the steel surface liners. Through simulation, the influence of close side setting was evaluated and parametric studies with diamond ceramic simulants were performed for use in deciding the close side setting to use in operation to minimise diamond breakage.

7.1.3 Surge bin drop heights

The surge bins are the most likely culprits that cause breakage through drop heights. In the current conditions the low level of the bin was set to a 40% mark just to make sure that any breakage is minimized. As demonstrated by King (2000), breakage function for self-breakage C(x;y) can be modelled using the t_{10} method that describes single-particle impact fracture using the impact energy equal to the kinetic t_{10} energy of the particle immediately before impact

(Taveres.,2007). Particles will have a wide distribution of free-fall impact energies in a real mill and the breakage function for self-breakage is obtained by integration over the impact energy spectrum where C(x;y, h) is the single particle breakage function for self-breakage of a particle of size *y* in free fall from height h, P(y,h) is the probability that a particle of size y will shatter when falling a vertical height h and p(h) is the distribution density for effective drop heights in the mill or surge bins. The level was changed to minimise drop height of material hence a reduction in impact resulting from dropping material.

7.2 Diamond breakage monitoring

Diamond breakage is an inherent risk within any diamond processing plant, however there were proposed interventions to minimise the breakage. Figure 81, shows the monitoring graph since middle 2017 when it was observed the +5carater diamonds stones were showing high breakage level. Initiatives were put in place to investigate and address the diamond breakage issues. The diamond breakage aspect had to be considered with understanding unit operation coupled with material properties. Material characterization was extensively investigated and thus provided guidelines to addressing the breakage seen within the processing plant.

The 5% mark seen on Figure 81, is the set threshold, which the breakage levels should not be exceeded as benchmarked against industry standards. The percentage breakage is based on the total count of the stones above 5 caraters and calculating the broken stones from the total number recovered.

Since the July 2017 the breakage levels were above 5% and the interventions were executed in order to reduce the breakage. By May 2018, some of planned interventions were completed and it can be seen on the graph in Figure 81, that the percentage breakage was declining. In June 2018, all key interventions were completed, and the diamond breakage levels had been below the threshold.

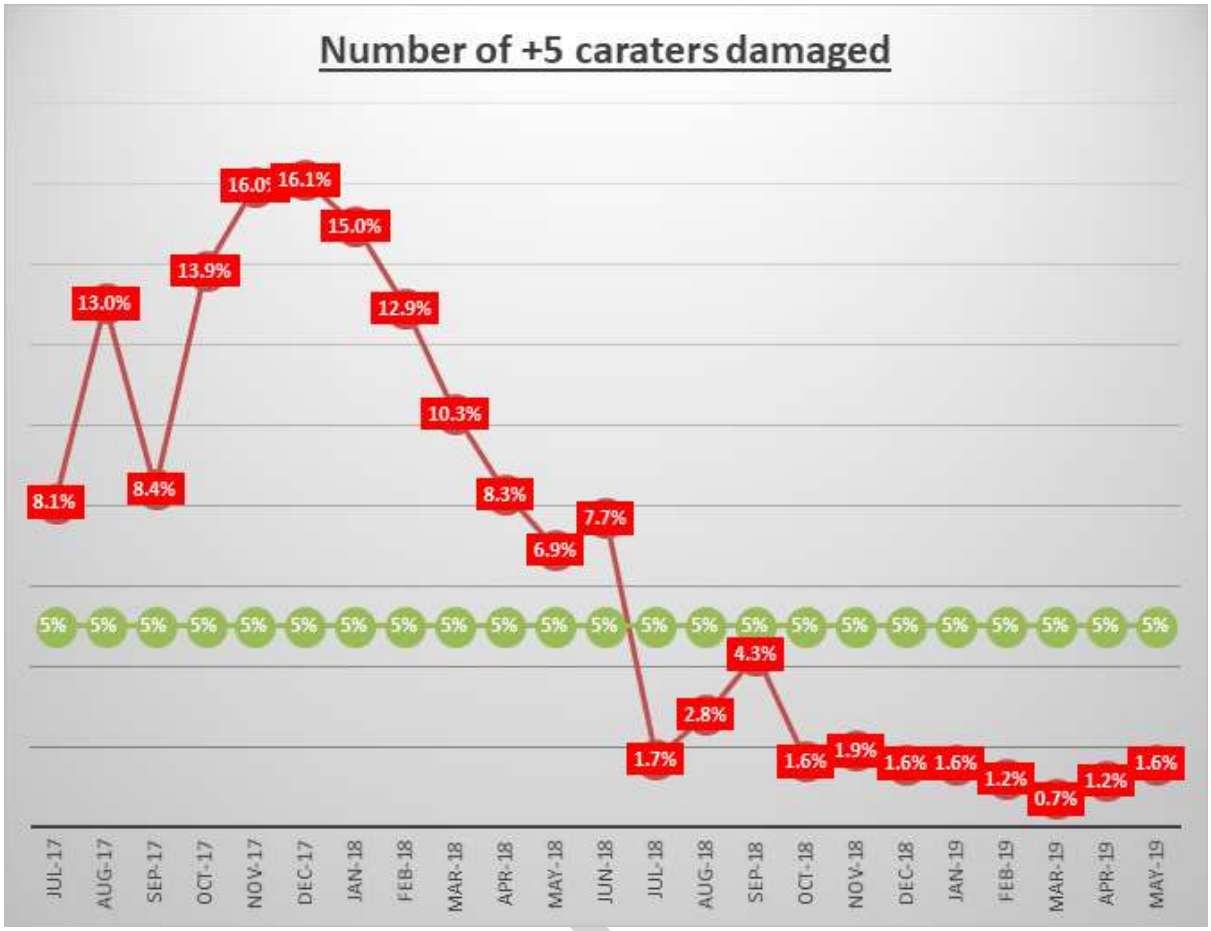

Figure 81: Diamond breakage monitoring graph.

CHAPTER 8

8. CONCLUSIONS AND RECOMMENDATIONS

This section of the thesis focuses on the key observations of the work undertaken. The conclusions are outlined with suggested recommendations for future work.

8.1 Diamond breakage within processing plant determined by using ceramic diamond simulants

The ceramic diamond simulants were used to identify the areas in the process flowsheet that are prone to damage. All the simulants that were used showed some level of breakage. As discussed in chapter 4, diamond damage may be expected to be synonymous with crushing, when designed and operated correctly, It has been indicated that transport systems such as centrifugal pumps can be more prone to diamond breakage. The probability of diamond breakage within correctly operated primary jaw crushers can be regarded as relatively low, while properly designed secondary cone and high-pressure roll crushers should also incur minimal diamond damage (Daniel & Morley.,2010). High pressure grinding roll crushers are preferred to cone crushers in tertiary crushing applications due to the inter-particle breakage mechanisms of the roll crushers resulting in less diamond damage and are preferred to cone crushers in secondary applications due to a combination of increased diamond liberation and reduced diamond damage.

The two most important factors to take note are:

- The minimum set of the crusher must be maintained so that it is always larger than the size of the largest diamond expected in that process stream.
- Recirculating load in a closed-circuit application must be minimised. This reduces the probability of a liberated diamond being returned to the crusher where it may be in contact with the crusher liners.

In a conventional diamond processing plant, a crushing circuit incorporating an impact crusher is not recommended due to its high potential of damage. Diamond damage can be estimated using ceramic diamond simulants, either in liberated or encapsulated form. However, it must be emphasized that once significant diamond damage has been detected with simulants, tests with actual diamonds and simulants need to be done to establish the true revenue implications of the diamond damage. It is recommended that the work could further be investigated to establish the diamond damage probability function.

8.2 Effect of varying close side setting

The test work undertaken on both the secondary cone crushers and tertiary cone crushers has demonstrated that, the more CSS is lowered the higher the probability of breakage however it is imperative not to compromise the efficiency of crushing hence mineral liberation. It was also noted that interparticle crushing (choke feeding) on the crusher could release the mineral without breakage.

The current available production of the ceramic diamond simulants are produced in cylindrical form, which then necessitate future investigation of breakage behaviour of particles considering their orientation and particle shape.

8.3 Effect of energy input in material characterisation tests

The tested energy levels showed that an increase in specific input energy results in a finer particle product size distribution hence higher degree of breakage of the material tested (Kimberlite ore, Concrete and Ceramic diamond simulants), as also observed by Chikochi (2017) in UG2 ore. This observation holds when the input energy is increased, the stressing intensity in the particles also increases. This intensifies the propagation of cracks in the parent particles resulting in fracturing into finer progeny.

The maximum energy threshold tested was 2.5kWh/t and it proved to be enough for the breakage of the above-mentioned material tested particularly in the DWT which had been simulated in operation of the current comminution units in the process that was studied.

The breakage characterisation tests showed that the simulants are very hard, while the concrete at 77Mpa of medium hardness and both Kimberlite, 34 Mpa concrete and 55 Mpa are classified as ‘soft’. The A value of 108 for the Kimberlite indicates a low degree of fragmentation, which has a large impact on the plant throughput and circulating load.

The t_{10} breakage model and size dependent model were fitted to the breakage data of the Kimberlite ore, Ceramic diamond simulants and embedded simulants in concrete of different strengths. From the model fittings, ore hardness parameters were determined. As expected, the breakage models confirmed the exponential relationship between the degree of breakage and the input energy. This reflects that increasing energy inputs results in higher degrees of breakage until no further breakage takes place. Furthermore, the following conclusions were also drawn from the hardness parameters.

The parameters, A and b, were extracted from the t_{10} breakage model fittings and used to determine the ore hardness indicator. The maximum degree of breakage, A, obtained from a

single impact of ceramic diamond simulants particles were found to be lower than both of concrete and kimberlite ore samples indicating the hardness of the diamond mimicked by the simulants.

8.4 Optimum operational parameters of the circuit under review

During a process of establishing optimum operational parameters a full circuit survey to assess the mass splits around the circuit and quantifying the size reduction occurring in various comminution equipment was performed. From the survey data it was observed that there is negligible size reduction in the scrubbers (Drum) and that most of the size reduction occurred in the secondary and tertiary crushers. Further work was done on the secondary and tertiary crushers where the closed side settings (CSS) were changed to assess the influence of this variable on size reduction. The profiles obtained from this study showed that as you increase the CSS the product became coarser. It can be concluded that operating at larger CSS would lead to minimal size reduction but high circulating loads. In addition to evaluating size reduction, simulants were seeded for selected CSS to identify conditions that were susceptible to diamond breakage. The optimal production set point would be the “sweet spot” between diamond breakage (minimal) and crusher product yield (maximal).

It is recommended to operate the tertiary crushers at the closed side setting region of 11 – 13 mm and the secondary crushers at around 35 - 37 mm. The breakage probability for a given diamond size is directly related to the crusher CSS. Therefore, in this type of application it is of importance to have a precise knowledge of the current operation CSS (with respect to wear) and a well-functioning control system.

Another recommendation is maintaining a direct central feeding arrangement of the secondary crushers. Segregation of the feed in the crusher also affects the performance in the product size distribution that is being discharged. To obtain a consistent product, even feeding is the key requirement.

Last recommendation in this section is to develop an optimisation strategy for the tertiary crushers from Discrete Element Method simulations of crusher chamber profiles. This will allow the suitable chamber profile to minimise diamond breakage and enhance the preferred set under ratio as well as increase throughput.

9. REFERENCES

Robinson D. N, (1979). Surface texture and other features of diamonds. PhD Thesis, University of Cape town. Part2.

Bearman, R. A., Briggs, C. A., & Kojovic, T. (1997). The application of rock mechanics parameters to the prediction of comminution behaviour. Minerals Engineering, 10(3), 255–264. https://doi.org/10.1016/S0892-6875(97)00002-2

Herbst. J, Potapov. A, Hambidge.G & Rademan.J, (2008).Modelling of diamond liberation and damage for Debswana kimberlitic ores. Minerals Engineering. 21:766-769.

Hogg. R, (1999). Breakage mechanisms and mill performance in ultrafine grinding, Powder Technology,105 (1-3),135-140.

Weedson.D.M & Wilson. F. (2000). Modelling iron ore degradation using a twin pendulum breakage device. International Journal of Mineral Processing 59(3):195-213.DOI: 10.1016/S0301-7516(99)00066-6

Kolsky, H. (1949) An Investigation of the Mechanical Properties of Materials at Very High Rates of Loading. Proceedings of the Physical Society. Section B, 62, 676-700. http://dx.doi.org/10.1088/0370-1301/62/11/302

De Magalhães, F. N., & Tavares, L. M. (2014). Rapid ore breakage parameter estimation from a laboratory crushing test. International Journal of Mineral Processing, 126, 49–54. https://doi.org/10.1016/j.minpro.2013.11.007

Genç, Ö., Ergün, L., & Benzer, H. (2004). Single particle impact breakage characterization of materials by drop weight testing. Physicochem. Prob. Miner. Process., 38, 241–255. Retrieved from http://www.minproc.pwr.wroc.pl/journal/pdf/2004/241-255.pdf

Dube.T. T, (2017). Measuring the fracture energy of bed breakage using a short impact load cell. MSc Thesis.University of Cape Town.

Chikochi. C, (2017). Ore breakage characterisation of UG2 deposit using the JKRBT. MSc Thesis. University of Cape Town.

Quist.J, (2012). Cone crusher modelling and simulation. Master of Science Thesis. Chalmers University of Technology.

Herbst, J. A., & Potapov, A. V. (2004). Making a discrete grain breakage model practical for comminution equipment performance simulation. Powder Technology, 143–144, 144–150. https://doi.org/10.1016/j.powtec.2004.04.036

Hulthén, E. (2010). Real time Optimization of cone crushers. PhD Thesis. Chalmers University of Technology

Johansson, M., Bengtsson, M., Evertsson, M., & Hulthén, E. (2017). A fundamental model of an industrial-scale jaw crusher. Minerals Engineering, 105, 69–78. https://doi.org/10.1016/j.mineng.2017.01.012

Lee, E., & Evertsson, C. M. (2011). A comparative study between cone crushers and theoretically optimal crushing sequences. Minerals Engineering, 24(3–4), 188–194. https://doi.org/10.1016/j.mineng.2010.07.013

Lee, E., & Evertsson, M. (2013). Implementation of optimized compressive crushing in full scale experiments. Minerals Engineering,43–44,135–147. https://doi.org/10.1016/j.mineng.2012.10.008

Masuret, C., Stellenbosch, E. & Town, E.C. 2015. Developing an abrasion characterisation test for measuring superficial breakage in comminution.

Napier-Munn, T.J., Morrell, S., Morrison, R.D., and Kojovic, T. (1999). Mineral Communition Circuits: Their Operation and Optimisation. JKMRC Monograph Series in Mining and Mineral Processing, 2nd edition, 154–191.

Djordjevic, N., Shi, F.and Morrison, R.,(2004). Determination of lifter design, speed and filling effects in AG Mill by 3D DEM. Minerals Engineering17, 1135-1142.

Quist, J. C. E. (2017). DEM Modelling and Simulation of Cone Crushers and High-Pressure Grinding Rolls.

Quist, J., & Evertsson, C. M. (2015). Cone crusher modelling and simulation using DEM. Minerals Engineering, 85(1652).

Resabal, V. J. (2016). Investigation of the Breakage Mechanism in High Speed Disk-type Impeller Stirred Mill and its Influence on the Mineral Liberation.

Shi, F. (2016). A review of the applications of the JK size-dependent breakage model Part 2: Assessment of material strength and energy requirement in size reduction. International Journal of Mineral Processing, 157, 36–45. https://doi.org/10.1016/j.minpro.2016.09.009

Shi, F., & Kojovic, T. (2007). Validation of a model for impact breakage incorporating particle size effect. International Journal of Mineral Processing, 82(3), 156–163. https://doi.org/10.1016/j.minpro.2006.09.006

Tavares, L. M. (2007). Chapter 1 Breakage of Single Particles: Quasi-Static. Handbook of Powder Technology, 12(April), 3–68. https://doi.org/10.1016/S0167-3785(07)12004-2

Zuo, W., & Shi, F. (2016). Ore impact breakage characterisation using mixed particles in wide size range. Minerals Engineering, 86, 96–103.

Zuo, W., & Shi, F. (2015). A t10-based method for evaluation of ore pre-weakening and energy reduction. Minerals Engineering,79,212–219. https://doi.org/10.1016/j.mineng.2015.06.005

Evertsson, C.M. (2000). Ph.D. Cone crusher performance. Department of Machine and Vehicle Design. Chalmers University of Technology.

DAVIS, S.B. and DAWSON, M.F., 1989, A laboratory study of attrition grinding, J. S. Atr. Inst. Min. Metal/., vol. 89, no. 8, pp. 231-241.

Weedon, D.M & Wilson, F. (2000). Modelling iron ore degradation using twin pendulum breakage device. International journal of mineral processing, volume 59, issue 3, page 195-213.

Shi, F., Kojovic, T., Larbi-Bram, S. & Manlapig, E. 2009. Development of a rapid particle breakage characterisation device - The JKRBT. Minerals Engineering. 22(7–8):602–612. DOI: 10.1016/j.mineng.2009.05.001.

Stamboliadis, E.T. 2002. A contribution to the relationship of energy and particle size in the comminution of brittle particulate materials. Minerals Engineering. 15(10):707–713. DOI: 10.1016/S0892-6875(02)00185-1.

Tavares, L.M. 2007. Chapter 1 Breakage of Single Particles: Quasi-Static. Handbook of Powder Technology. 12(December 2007):3–68. DOI: 10.1016/S0167-3785(07)12004-2.

Tavares, L.. & King, R. 2002. Single-particle fracture under impact loading. International Journal of Mineral Processing. 54(1):1–28. DOI: 10.1016/s0301-7516(98)00005-2.

Lee, E. & Evertsson, M. 2013. Implementation of optimized compressive crushing in full scale experiments. Minerals Engineering. 43–44:135–147. DOI: 10.1016/j.mineng.2012.10.008.

Shi, F. & Kojovic, T. 2007. Validation of a model for impact breakage incorporating particle size effect. International Journal of Mineral Processing. 82(3):156–163. DOI: 10.1016/j.minpro.2006.09.006.

Gupta, A., Yan, D.S., 2006.Mineral processing design and operations: An introduction. Amsterdam: Amsterdam, Boston: Elsevier.p.129 – 141.

Itävuo, P., 2009.Dynamic modelling of rock crushing process. MSc Thesis in a Degree Programme in Automation. Finland: University of Technology.p.102.

Evertsson, C.M. (1999). Modelling of flow in cone crushers. Minerals Engineering, 12, 1479–1499.

Khosrow, N., 2001. Role of simulation software in design and operation of metallurgical pants: A case study. Vancouver, British Columbia, Canada: AMEC Simons Mining and Metals.p.2 - 9.

King, R.P., 2001. Modelling and simulations of mineral processing systems. Oxford, Great Britain: Butterworth-Heinemann.p.353 – 357.

Sbarbaro, D., 2010. Dynamic simulation and model-based control system design for comminution circuits. In Sbarbaro, D. (ed): Advanced Control and Supervision of Mineral Processing plants. London: Springer. p. 213 – 245

Truscott, S., 1923. A Textbook of Ore Dressing. Macmillan & Co, London.p.44.

Whiten, W.J., 1972.The simulation of crushing plants with models developed using multiple spline regression. Journal of the South African Institute of Mining and Metallurgy. p. 257 – 264.

Karra, V.K., 1982. A Process Performance Model for a Cone Crusher. Proc. 14th Intern. Miner Process Congr. Toronto. p. 6.1-6.14.

Banini, G.A., Morrell, S., Bourgeois, F.S., 2000. Quantitative measurement of surface breakage of industrial ores,in preparation.

Napier-Munn, T.J., Morrell, S., Morrison, R.D., Kojovic, T., 1996. Mineral Comminution Circuits—Their Operation and Optimisation. Julius Kruttschnitt Mineral Research Centre, The University of Queensland, Brisbane, Australia.

Wills, B.A. and Napier-Munn, T. (2006) Wills' Mineral Processing Technology. 7th Edition, Butterworth-Heinemann, Oxford.

Appendix A – Plant survey data

Table 23:Secondary cone crusher #1 Feed and Product size distribution at normal plant operating conditions

	Feed				Product		
	Sieve sizes(mm)	**mass retained (kg)**	**retained mass fraction (%)**	**Cumulative passing (%)**	**mass retained (kg)**	**retained mass fraction (%)**	**Cumulative passing (%)**
Sec.Crusher #1	125	42.5	20.49	79.51	0	0.00	100.00
	106	36.22	17.46	62.05	0	0.00	100.00
	75	36.16	17.43	44.62	0	0.00	100.00
	63	20.205	9.74	34.88	0	0.00	100.00
	45	47.785	23.03	11.85	1.333	6.70	93.30
	31.5	20.955	10.10	1.75	5.78	29.04	64.27
	25	0.881	0.42	1.32	2.653	13.33	50.94
	19	0.532	0.26	1.07	2.053	10.31	40.62
	16	0.204	0.10	0.97	1.048	5.27	35.36
	13.2	0.181	0.09	0.88	0.861	4.33	31.03
	11.2	0.165	0.08	0.80	0.751	3.77	27.26
	8	0.228	0.11	0.69	0.981	4.93	22.33
	5.6	0.179	0.09	0.61	0.907	4.56	17.77
	4	0.154	0.07	0.53	0.631	3.17	14.60
	2.8	0.135	0.07	0.47	0.525	2.64	11.97
	2	0.114	0.05	0.41	0.446	2.24	9.73
	1.4	0.114	0.05	0.36	0.384	1.93	7.80
	1.25	0.038	0.02	0.34	0.1	0.50	7.29
	0	0.702	0.34	0.00	1.452	7.29	0.00
		207.452	**100**		**19.905**	**100**	

Table 24:Secondary crusher #1 product size distribution at varied close side settings

CSS1			CSS2			CSS3			CSS4			CSS5		
Mass retained (kg)	Retained mass fraction (%)	Cumulative passing (%)	Mass retained (kg)	Retained mass fraction (%)	Cumulative passing (%)	Mass retained (kg)	Retained mass fraction (%)	Cumulative passing (%)	Mass retained (kg)	Retained mass fraction (%)	Cumulative passing (%)	Mass retained (kg)	Retained mass fraction (%)	Cumulative passing (%)
0	0	100	0	0	100	0	0	100	0	0	100	0	0	100
0	0	100	0	0	100	0	0	100	0	0	100	0	0	100
0	0	100	0	0	100	0	0	100	0.622	1.27	98.73	0	0	100
0	0	100	0	0	100	0	0	100	0.928	1.9	96.83	0.785	1.89	98.11
1.397	4.86	95.14	5.345	14.78	85.22	5.227	13.98	86.02	17.43	35.66	61.17	11.8	28.35	69.76
9.23	32.13	63.01	10.33	28.57	56.65	11.66	31.18	54.84	12.94	26.47	34.7	11.168	26.83	42.93
3.921	13.65	49.36	4.619	12.78	43.87	3.929	10.51	44.33	2.482	5.08	29.63	2.798	6.72	36.2
2.813	9.79	39.57	2.778	7.68	36.19	2.596	6.94	37.39	2.427	4.96	24.66	2.459	5.91	30.3
1.373	4.78	34.79	1.677	4.64	31.55	1.522	4.07	33.32	1.471	3.01	21.65	1.633	3.92	26.37
1.383	4.81	29.98	1.372	3.79	27.75	1.4	3.74	29.58	1.302	2.66	18.99	1.261	3.03	23.34
0.868	3.02	26.96	1.08	2.99	24.77	1.085	2.9	26.68	0.887	1.81	17.18	0.975	2.34	21
1.415	4.93	22.03	1.577	4.36	20.4	1.9	5.08	21.6	1.48	3.03	14.15	1.575	3.78	17.22
1.313	4.57	17.46	1.447	4	16.4	1.595	4.27	17.33	1.423	2.91	11.24	1.438	3.46	13.76
0.872	3.04	14.43	1.005	2.78	13.62	1.172	3.13	14.2	0.895	1.83	9.41	1.027	2.47	11.29
0.761	2.65	11.78	0.837	2.32	11.31	0.952	2.55	11.65	0.813	1.66	7.74	0.888	2.13	9.16
0.598	2.08	9.7	0.715	1.98	9.33	0.787	2.1	9.55	0.642	1.31	6.43	0.691	1.66	7.5
0.531	1.85	7.85	0.65	1.8	7.53	0.694	1.86	7.69	0.62	1.27	5.16	0.655	1.57	5.93
0.144	0.5	7.35	0.167	0.46	7.07	0.233	0.62	7.07	0.158	0.32	4.84	0.192	0.46	5.46
2.111	7.35	0	2.556	7.07	0	2.643	7.07	0	2.365	4.84	0	2.274	5.46	0
28.73	**100**		**36.16**	**100**		**37.40**	**100**		**48.89**	**100**		**41.62**	**100**	

Table 25:Secondary crusher#2 Feed and Product size distribution at normal plant operating conditions

	Feed				Product		
	Sieve sizes(mm)	**mass retained (kg)**	**retained mass fraction (%)**	**Cumulative passing (%)**	**mass retained (kg)**	**retained mass fraction (%)**	**Cumulative passing (%)**
Sec. Crusher #2	125	73.535	36.58	63.42	0	0.00	100.00
	106	34.18	17.00	46.41	0	0.00	100.00
	75	32.9	16.37	30.05	0	0.00	100.00
	63	14.005	6.97	23.08	0.326	1.16	98.84
	45	31.12	15.48	7.60	1.58	5.64	93.19
	31.5	12.67	6.30	1.29	8.05	28.76	64.43
	25	0.554	0.28	1.02	3.8	13.58	50.85
	19	0.404	0.20	0.82	2.698	9.64	41.21
	16	0.246	0.12	0.70	1.48	5.29	35.93
	13.2	0.164	0.08	0.61	1.342	4.79	31.13
	11.2	0.109	0.05	0.56	0.885	3.16	27.97
	8	0.199	0.10	0.46	1.408	5.03	22.94
	5.6	0.139	0.07	0.39	1.249	4.46	18.48
	4	0.113	0.06	0.34	0.857	3.06	15.42
	2.8	0.084	0.04	0.29	0.784	2.80	12.62
	2	0.08	0.04	0.25	0.626	2.24	10.38
	1.4	0.067	0.03	0.22	0.564	2.02	8.36
	1.25	0.025	0.01	0.21	0.138	0.49	7.87
	0	0.418	0.21	0.00	2.203	7.87	0.00
		201.012	**100**		**27.99**	**100**	

Table 26: Secondary crusher#2 product size distribution at varied close side settings

CSS1			CSS2			CSS3			CSS4			CSS5		
Mass retained (kg)	Retained mass fraction (%)	Cumulative passing (%)	Mass retained (kg)	Retained mass fraction (%)	Cumulative passing (%)	Mass retained (kg)	Retained mass fraction (%)	Cumulative passing (%)	Mass retained (kg)	Retained mass fraction (%)	Cumulative passing (%)	Mass retained (kg)	Retained mass fraction (%)	Cumulative passing (%)
0	0	100	0	0	100	0	0	100	0	0	100	0	0	100
0	0	100	0	0	100	0	0	100	0	0	100	0	0	100
0	0	100	0	0	100	0	0	100	0	0	100	1.562	3.35	96.65
0	0	100	0	0	100	0	0	100	1.114	2.79	97.21	1.54	3.3	93.34
1.899	5.69	94.31	1.111	2.85	97.15	6.052	16.06	83.94	5.472	13.68	83.53	8.19	17.57	75.77
4.911	14.71	79.6	8.12	20.82	76.33	9.41	24.98	58.96	9.62	24.05	59.48	12.858	27.59	48.18
3.756	11.25	68.35	4.925	12.63	63.7	3.65	9.69	49.27	4.478	11.2	48.28	3.491	7.49	40.69
3.154	9.45	58.91	3.156	8.09	55.61	2.694	7.15	42.12	2.733	6.83	41.45	2.542	5.45	35.24
1.58	4.73	54.18	1.784	4.57	51.03	1.535	4.07	38.05	1.69	4.23	37.22	1.63	3.5	31.74
1.919	5.75	48.43	1.753	4.5	46.54	1.22	3.24	34.81	1.421	3.55	33.67	1.759	3.77	27.97
1.389	4.16	44.27	1.531	3.93	42.61	0.71	1.88	32.93	1.172	2.93	30.74	1.244	2.67	25.3
2.149	6.44	37.83	2.462	6.31	36.3	1.655	4.39	28.53	2.02	5.05	25.69	1.819	3.9	21.4
2.203	6.6	31.23	2.458	6.3	29.99	1.783	4.73	23.8	1.932	4.83	20.86	1.839	3.95	17.45
1.669	5	26.24	1.723	4.42	25.57	1.514	4.02	19.78	1.376	3.44	17.42	1.289	2.77	14.69
1.462	4.38	21.86	1.677	4.3	21.27	1.206	3.2	16.58	1.145	2.86	14.55	1.159	2.49	12.2
1.335	4	17.86	1.483	3.8	17.47	1.069	2.84	13.74	0.98	2.45	12.1	0.985	2.11	10.09
1.205	3.61	14.25	1.344	3.45	14.02	0.966	2.56	11.18	0.888	2.22	9.88	0.88	1.89	8.2
0.313	0.94	13.31	0.349	0.89	13.13	0.651	1.73	9.45	0.257	0.64	9.24	0.249	0.53	7.66
4.445	13.31	0	5.12	13.13	0	3.561	9.45	0	3.696	9.24	0	3.572	7.66	0
33.39	**100.00**		**39.00**	**100.00**		**37.68**	**100.00**		**39.99**	**100.00**		**46.61**	**100.00**	

Table 27: Tertiary cone crusher #1 Feed and Product size distribution at normal operating conditions

	Feed				Product		
	Sieve sizes(mm)	Mass retained (kg)	Retained mass fraction (%)	Cumulative passing (%)	Mass retained (kg)	Retained mass fraction (%)	Cumulative passing (%)
Tertiary crusher #1	125	0	0.00	100.00	0	0.00	100.00
	106	0	0.00	100.00	0	0.00	100.00
	75	0	0.00	100.00	0	0.00	100.00
	63	0	0.00	100.00	0	0.00	100.00
	45	0.319	1.08	98.92	0	0.00	100.00
	31.5	7.88	26.78	72.13	0	0.00	100.00
	25	5.58	18.96	53.17	0.334	1.37	98.63
	19	5.27	17.91	35.26	1.709	7.00	91.63
	16	3.45	11.73	23.54	3.09	12.66	78.97
	13.2	3.78	12.85	10.69	3.69	15.12	63.85
	11.2	1.709	5.81	4.88	2.601	10.66	53.19
	8	1.154	3.92	0.96	3.31	13.56	39.62
	5.6	0.101	0.34	0.62	2.458	10.07	29.55
	4	0.024	0.08	0.53	1.677	6.87	22.68
	2.8	0.018	0.06	0.47	1.441	5.90	16.78
	2	0.016	0.05	0.42	1.235	5.06	11.72
	1.4	0.013	0.04	0.37	1.053	4.31	7.40
	1.25	0.005	0.02	0.36	0.285	1.17	6.23
	0	0.105	0.36	0.00	1.521	6.23	0.00
		29.424	**100**		**24.404**	**100**	

Table 28: Tertiary crusher#1 product size distribution at varied close side settings

CSS1			CSS2			CSS3			CSS4			CSS5		
Mass retained (kg)	Retained mass fraction (%)	Cumulative passing (%)	Mass retained (kg)	Retained mass fraction (%)	Cumulative passing (%)	Mass retained (kg)	Retained mass fraction (%)	Cumulative passing (%)	Mass retained (kg)	Retained mass fraction (%)	Cumulative passing (%)	Mass retained (kg)	Retained mass fraction (%)	Cumulative passing (%)
0	0.00	100.00	0	0.00	100.00	0	0.00	100.00	0	0.00	100.00	0	0.00	100.00
0	0.00	100.00	0	0.00	100.00	0	0.00	100.00	0	0.00	100.00	0	0.00	100.00
0	0.00	100.00	0	0.00	100.00	0	0.00	100.00	0	0.00	100.00	0	0.00	100.00
0	0.00	100.00	0	0.00	100.00	0	0.00	100.00	0	0.00	100.00	0	0.00	100.00
0	0.00	100.00	0	0.00	100.00	0	0.00	100.00	0	0.00	100.00	0	0.00	100.00
0.173	0.50	99.50	1.225	3.54	96.46	1.923	4.85	95.15	2.755	6.82	93.18	4.034	9.48	90.52
1.255	3.62	95.88	4.057	11.72	84.74	5.884	14.84	80.31	7.058	17.47	75.72	8.997	21.15	69.37
5.319	15.36	80.52	7.85	22.69	62.05	10.754	27.13	53.18	11.224	27.77	47.94	11.966	28.13	41.24
6.004	17.33	63.19	5.901	17.05	45.00	6.84	17.25	35.93	7.012	17.35	30.59	8.148	19.15	22.09
5.769	16.65	46.53	5.397	15.60	29.40	5.596	14.12	21.81	6.15	15.22	15.37	6.466	15.20	6.89
3.52	10.16	36.37	2.885	8.34	21.06	2.896	7.30	14.51	2.699	6.68	8.70	2.433	5.72	1.17
3.853	11.12	25.25	2.72	7.86	13.20	2.259	5.70	8.81	1.592	3.94	4.76	0.368	0.87	0.31
2.79	8.05	17.19	1.711	4.94	8.26	1.411	3.56	5.25	0.833	2.06	2.69	0.058	0.14	0.17
1.714	4.95	12.25	0.974	2.81	5.44	0.782	1.97	3.28	0.453	1.12	1.57	0.03	0.07	0.10
1.386	4.00	8.25	0.707	2.04	3.40	0.559	1.41	1.87	0.311	0.77	0.80	0.016	0.04	0.06
1.054	3.04	5.20	0.531	1.53	1.86	0.365	0.92	0.95	0.179	0.44	0.36	0.005	0.01	0.05
0.809	2.34	2.87	0.361	1.04	0.82	0.214	0.54	0.41	0.077	0.19	0.17	0.002	0.00	0.04
0.167	0.48	2.38	0.058	0.17	0.65	0.031	0.08	0.33	0.011	0.03	0.14	0.001	0.00	0.04
0.826	2.38	0.00	0.226	0.65	0.00	0.131	0.33	0.00	0.058	0.14	0.00	0.018	0.04	0.00
34.639	**100**		**34.603**	**100**		**39.645**	**100**		**40.412**	**100**		**42.542**	**100**	

Table 29: Tertiary cone crusher #2 Feed and Product size distribution at normal plant operating conditions

	Feed				Product		
	Sieve sizes(mm)	Mass retained (kg)	Retained mass fraction (%)	Cumulative passing (%)	Mass retained (kg)	Retained mass fraction (%)	Cumulative passing (%)
Tertiary crusher #2	125	0	0.00	100.00	0	0.00	100.00
	106	0	0.00	100.00	0	0.00	100.00
	75	0	0.00	100.00	0	0.00	100.00
	63	0	0.00	100.00	0	0.00	100.00
	45	0	0.00	100.00	0	0.00	100.00
	31.5	4.66	14.66	85.34	0	0.00	100.00
	25	3.05	9.60	75.74	0.233	1.02	98.98
	19	4.4	13.85	61.89	1.704	7.44	91.55
	16	5.65	17.78	44.12	2.693	11.75	79.79
	13.2	6.7	21.08	23.03	4.18	18.24	61.55
	11.2	4.41	13.88	9.16	2.992	13.06	48.49
	8	2.577	8.11	1.05	3.56	15.54	32.96
	5.6	0.142	0.45	0.60	2.164	9.44	23.51
	4	0.029	0.09	0.51	1.356	5.92	17.60
	2.8	0.02	0.06	0.45	1.151	5.02	12.57
	2	0.017	0.05	0.39	0.967	4.22	8.35
	1.4	0.013	0.04	0.35	0.826	3.60	4.75
	1.25	0.005	0.02	0.34	0.209	0.91	3.84
	0	0.107	0.34	0.00	0.879	3.84	0.00
		31.78	**100**		**22.914**	**100**	

Table 30: Tertiary cone crusher #2 product size distribution at varied close side settings

CSS1			CSS2			CSS3			CSS4			CSS5		
Mass retained (kg)	Retained mass fraction (%)	Cumulative passing (%)	Mass retained (kg)	Retained mass fraction (%)	Cumulative passing (%)	Mass retained (kg)	Retained mass fraction (%)	Cumulative passing (%)	Mass retained (kg)	Retained mass fraction (%)	Cumulative passing (%)	Mass retained (kg)	Retained mass fraction (%)	Cumulative passing (%)
0	0.00	100.00	0	0.00	100.00	0	0.00	100.00	0	0.00	100.00	0	0.00	100.00
0	0.00	100.00	0	0.00	100.00	0	0.00	100.00	0	0.00	100.00	0	0.00	100.00
0	0.00	100.00	0	0.00	100.00	0	0.00	100.00	0	0.00	100.00	0	0.00	100.00
0	0.00	100.00	0	0.00	100.00	0	0.00	100.00	0	0.00	100.00	0	0.00	100.00
0	0.00	100.00	0	0.00	100.00	0	0.00	100.00	0	0.00	100.00	0	0.00	100.00
0	0.00	100.00	0	0.00	100.00	1.151	3.34	96.66	2.267	6.31	93.69	2.626	7.73	92.27
0.187	0.68	99.32	0.721	2.39	97.61	3.518	10.20	86.46	3.991	11.11	82.58	5.075	14.93	77.34
2.086	7.56	91.76	3.427	11.35	86.26	6.47	18.76	67.70	8.83	24.59	57.99	8.36	24.60	52.74
3.59	13.02	78.74	4.571	15.14	71.12	6.622	19.20	48.49	7.7	21.44	36.55	6.9	20.30	32.44
4.933	17.88	60.86	5.558	18.41	52.70	7.62	22.10	26.40	7.28	20.27	16.28	6.77	19.92	12.52
3.599	13.05	47.81	3.825	12.67	40.03	4.19	12.15	14.25	3.533	9.84	6.44	3.218	9.47	3.05
3.458	12.54	35.27	3.625	12.01	28.03	2.301	6.67	7.57	1.416	3.94	2.50	0.831	2.45	0.61
2.469	8.95	26.32	2.477	8.21	19.82	1.046	3.03	4.54	0.419	1.17	1.33	0.099	0.29	0.32
1.718	6.23	20.09	1.518	5.03	14.79	0.565	1.64	2.90	0.213	0.59	0.74	0.045	0.13	0.19
1.445	5.24	14.85	1.294	4.29	10.50	0.382	1.11	1.80	0.125	0.35	0.39	0.023	0.07	0.12
1.23	4.46	10.39	0.993	3.29	7.22	0.252	0.73	1.06	0.061	0.17	0.22	0.008	0.02	0.09
1.027	3.72	6.67	0.799	2.65	4.57	0.164	0.48	0.59	0.029	0.08	0.14	0.004	0.01	0.08
0.259	0.94	5.73	0.198	0.66	3.91	0.034	0.10	0.49	0.005	0.01	0.13	0.001	0.00	0.08
1.581	5.73	0.00	1.181	3.91	0.00	0.169	0.49	0.00	0.046	0.13	0.00	0.027	0.08	0.00
27.582	**100**		**30.187**	**100**		**34.484**	**100**		**35.915**	**100**		**33.987**	**100**	

Appendix B – Raw data for breakage tests

Kimberlite crushed particles															
Size (mm)	63.0 x 53.0			45 x 37.5			31.5x26.5			22.4 x 19.0			16,0 x 13.2		
Ecs (kWh/t)	0.1	0.25	0.4	0.1	0.25	1	0.25	1	2.5	0.25	1	2.5	0.25	1	2.5
No. of particles	30														
Initial Mass (g)	9160	9630	9670	3610	3780	3550	1123	1058	1299	412	514	440	151	181	149
After breakage (g)	9150	9570	9610	3600	3770	3540	1122	1051	1290	409	510	439	149	180	147
45	1933	416	0	0	0	0	0	0	0	0	0	0	0	0	0
37.5	1739	690	417	74	183	0	0	0	0	0	0	0	0	0	0
26.5	2449	2347	1429	887	723	394	34	0	0	0	0	0	0	0	0
19	1022	1942	1858	1009	955	598	278	22	33	0	0	0	0	0	0
13.2	690	1423	1819	670	683	643	371	215	200	26	96	21	0	0	0
9.5	300	702	918	282	364	463	135	214	197	51	107	70	3	35	7
5.6	365	678	1060	224	292	494	103	232	272	113	152	127	43	55	50
4.75	62	169	208	47	56	97	26	42	69	28	20	25	17	15	15
2.8	193	376	587	132	158	233	54	104	142	63	47	69	33	29	26
2.36	36	94	119	28	45	62	15	26	38	12	10	17	8	8	6
1.7	74	157	242	51	49	111	21	39	69	24	18	23	11	9	10
1.25	50	110	180	38	67	90	16	26	50	15	12	17	8	7	6
1	31	67	99	20	27	44	9	15	27	9	8	10	4	4	3
-1	180	396	657	135	164	304	55	101	189	53	38	58	21	18	21
sum (g)	9124	9567	9593	3597	3766	3533	1117	1036	1286	394	508	437	148	180	144
Breakage Loss (g)	10.0	60.0	60.0	10.0	10.0	10.0	1.0	7.0	9.0	3.0	4.0	1.0	2.0	1.0	2.0
Loss Breakage (%)	0.109	0.623	0.621	0.277	0.265	0.282	0.089	0.662	0.693	0.728	0.778	0.227	1.325	0.553	1.342
Sieving loss (g)	26.0	3.0	17.0	3.0	4.0	7.0	5.0	15.0	4.0	15.0	2.0	2.0	1.0	0.0	3.0
Loss Sieving (%)	0.284	0.031	0.177	0.083	0.106	0.198	0.446	1.427	0.310	3.668	0.392	0.456	0.671	0.000	2.041

Ceramic diamond simulants crusherd particles								
Size (mm)	25x25		20x20		12x12		8x8	
Ecs (kWh/t)	1	2.5	1	2.5	1	2.5	1	2.5
No. of particles	10		10		10		10	
Initial Mass (g)	429.0	436.0	232.0	231.0	49.0	50.0	14.0	15.0
After breakage (g)	429	429	230	230	48	50	14	14
53	0	0	0	0	0	0	0	0
45	0	0	0	0	0	0	0	0
37.5	0	0	0	0	0	0	0	0
26.5	0	0	0	0	0	0	0	0
19	92	0	0	0	0	0	0	0
13.2	94	0	18	13	0	0	0	0
9.5	48	15	41	11	0	0	0	0
5.6	72	101	66	53	8	7	9	1
4.75	11	24	15	13	2	5	0.3	0.3
2.8	36	98	36	51	14	13	2.3	2.4
2.36	9	26	7	13	3	4	0.3	0.9
1.7	14	41	13	19	5	6	1.3	2.4
1.25	11	30	9	13	4	4	0	1.9
1	6	14	5	8	2	2	0.2	1
-1	33	80	20	36	9	9	0.6	3.7
sum (g)	**426**	**429**	**230**	**230**	**47**	**50**	**14**	**13.6**
Breakage Loss (g)	-	7.00	2.00	1.00	1.00	-	-	1.00
Loss Breakage (%)	-	1.61	0.86	0.43	2.04	-	-	6.67
Sieving loss (g)	3.00	-	-	-	1.00	-	-	0.40
Loss Sieving (%)	0.70	-	-	-	2.08	-	-	2.86

34MPa concrete blocks crushed particles						
Size (mm)	60x60			30x30		
Ecs (kWh/t)	0.1	0.25	0.35	0.1	1.0	2.0
No. of particles	10			10		
Initial Mass (g)	5190.0	5100.0	5100.0	751.0	727.0	717.0
After breakage (g)	5170	5080	5050	734	721	708
53	3140	0	0	0	0	0
45	139	309	163	0	0	0
37.5	0	83	285	0	0	0
26.5	407	991	502	278	0	0
19	428	1137	941	47	0	0
13.2	291	505	717	68	29	17
9.5	154	424	505	88	69	75
5.6	201	489	521	93	147	145
4.75	30	71	113	8	34	29
2.8	95	260	306	38	83	83
2.36	27	72	75	10	31	21
1.7	44	134	158	20	48	48
1.25	35	91	113	13	43	32
1	26	59	91	9	19	28
-1	153	447	560	61	212	230
sum (g)	**5170**	**5072**	**5050**	**733**	**715**	**708**
Breakage Loss (g)	20.00	20.00	50.00	17.00	6.00	9.00
Loss Breakage (%)	0.39	0.39	0.98	2.26	0.83	1.26
Sieving loss (g)	-	8.00	-	1.00	6.00	-
Loss Sieving (%)	-	0.16	-	0.14	0.83	-

55MPa concrete blocks crushed particles						
Size (mm)	60x60			30x30		
Ecs (kWh/t)	0.1	0.25	0.35	0.1	1.0	2.0
No. of particles	10					
Initial Mass (g)	5100.0	5040.0	5030.0	744.0	763.0	749.0
After breakage (g)	5070	5027	4990	734	757	742
53	3270	1652	0	0	0	0
45	152	109	96	0	0	0
37.5	103	450	359	0	0	0
26.5	315	285	730	307	34	0
19	311	542	897	63	8	0
13.2	249	423	641	109	28	67
9.5	148	270	384	56	55	94
5.6	137	375	550	64	143	157
4.75	25	76	87	6	33	23
2.8	78	209	303	29	94	89
2.36	24	61	75	9	22	23
1.7	44	111	165	17	56	42
1.25	36	69	95	12	34	32
1	20	51	73	6	21	26
-1	158	334	534	55	222	188
sum (g)	**5070**	**5017**	**4989**	**733**	**750**	**741**
Breakage Loss (g)	30.00	13.00	40.00	10.00	6.00	7.00
Loss Breakage (%)	0.59	0.26	0.80	1.34	0.79	0.93
Sieving loss (g)	-	10.00	1.00	1.00	7.00	1.00
Loss Sieving (%)	-	0.20	0.02	0.14	0.92	0.13

Appendix C – Mass balance and experimental data

Table 31: Mass balance and experimental data for the scrubbers

STREAM	TPH - Solids		P80		% Sub 16 [mm]		% Sub 4 [mm]		% Sub 1.25 [mm]	
	Exp	Bal	Exp	Bal	Exp	Bal	Exp	Bal	Exp	Bal
Scrubber Feed - Prod	500	500	214	199	19.0	19.0	4.02	3.75	0	0
Scrubber Feed split - Top Prod	250	250	198	199	19.0	19.0	3.50	3.50	0	0
Scrubber 1 - Prod	250	250	126	128	19.9	19.4	5.48	5.28	2.58	2.50
Screen 1 top deck - U/S	68.0	73.4	42.2	41.8	47.3	47.5	13.2	13.2	6.30	6.32
Screen 1 top deck - O/S	175	177	156	162	7.34	7.73	1.97	1.99	0.93	0.92
Screen 1 bottom deck - U/S	7.00	6.97	3.79	3.79	100	99.9	82.4	82.5	46.1	45.2
Screen 1 bottom deck - O/S	57.0	66.4	43.3	44.1	42.3	42.0	5.94	5.93	2.26	2.25
Scrubber Feed split - Bot Prod	250	250	198	199	19.0	19.1	4.02	4.01	0	0
Scrubber 2 - Prod	250	250	170	168	20.0	20.4	3.62	3.67	0.87	0.88
Screen 2 top deck - U/S	61.7	61.7	30.1	30.1	54.9	55.0	10.6	10.6	3.55	3.58
Screen 2 top deck - O/S	190	188	197	195	8.57	9.07	1.35	1.39	0.00	0.00
Screen 2 bottom deck - U/S	4.69	4.69	3.75	3.76	99.9	99.9	84.8	84.6	31.8	31.7
Screen 2 bottom deck - O/S	57.5	57.0	31.0	31.1	51.4	51.3	4.56	4.54	1.27	1.26

Table 32:Secondary crushers mass balance data

Stream	TPH - Solids		P80		% Sub 32 [mm]		% Sub 10 [mm]		% Sub 1.25 [mm]	
	Exp	Bal	Exp	Bal	Exp	Bal	Exp	Bal	Exp	Bal
Crusher Feed Bin - Prod	910	911	111	103	13.43	13.17	5.16	5.10	1.42	1.40
Bin Split - Bot Prod	486	486	107	103	12.80	12.57	5.03	4.99	1.33	1.33
Bin Split - Top Prod	425	425	114	103	14.04	13.87	5.27	5.24	1.48	1.48
Secondary Crusher 1 - Prod	485	486	67.1	67.7	39.06	41.25	16.25	17.21	6.86	7.08
Secondary Crusher 2 - Prod	425	425	68.6	69.1	37.91	40.10	15.33	16.09	6.17	6.33
Screen top deck - U/S	365	365	30.6	30.7	82.40	82.10	33.50	33.68	13.76	13.74
Screen top deck - O/S	545	546	74.7	74.7	13.37	13.13	5.42	5.39	2.03	2.04
Screen bottom deck - U/S	41.6	47.9	3.36	3.32	100	100	99.02	99.02	68.43	68.88
Screen bottom deck - O/S	308	317	31.8	32.6	80.42	79.39	23.88	23.73	5.30	5.40

Table 33: Tertiary crushing circuit mass balance and experimental data

STREAM	TPH - Solids		P80		% Sub 32 [mm]		% Sub 10 [mm]		% Sub 1.25 [mm]	
	Exp	Bal	Exp	Bal	Exp	Bal	Exp	Bal	Exp	Bal
Feed	420	420	36.59	34.33	76.26	78.10	0.88	0.87	0.00	0.00
Vibratory Feeder 1	312	314	25.39	25.78	90.02	89.68	1.50	1.50	0.00	0.00
Vibratory Feeder 2	313	315	25.39	25.78	90.02	89.68	1.50	1.50	0.00	0.00
Vibratory Feeder 3	312	314	25.39	25.78	90.02	89.68	1.50	1.50	0.00	0.00
Crusher 1 Product	312	314	19.36	19.48	99.95	99.19	36.21	36.17	0.00	0.00
Crusher 2 Product	313	315	19.07	19.18	99.96	99.39	29.71	29.73	0.00	0.00
Crusher 3 Product	312	314	16.59	16.59	99.99	99.82	43.81	43.62	0.00	0.00
Screen Top deck - O/S	518	523	21.54	21.50	99.38	99.96	2.00	1.99	0.00	0.00
Screen Top deck - U/S	420	420	10.24	10.01	99.64	99.60	79.57	80.90	0.00	0.00
Screen Bottom deck - O/S	354	355	10.16	10.60	100.0	99.53	80.02	77.36	0.00	0.00
Screen Bottom deck - U/S	65.9	64.3	1.400	1.400	100.0	100.0	100.0	100.0	0.00	0.00

Appendix D

I. Calculations – t_{10} vs Specific input energy

The relationship between the parameter t_{10} and specific input energy (E_{cs} or E_{is}) as described by Tavares (2007). The value of parameter A corresponds to the maximum degree of breakage (t_{10}) obtainable for an ore or material. It indicates that at higher energies little additional size reduction occurs as the specific input energy is increased. Parameter b is the linear gradient of the curve at energies lower than 1 kWh/t and can be related to material stiffness (Napier-Munn et al., 1996).

$$t_{10} = A(1 - e^{-bEcs}) \quad (20)$$

where t_{10} is a size distribution 'fineness' index, E_{cs} is the specific input energy (kWh/t), and A and b are the ore impact breakage parameters.

This equation is also implemented in JKSimMet (Mineral Processing Simulator – an industry standard software package) to analyse and predict AG/SAG mill performance (Schwarz & Richardson, 2013; Morrison & Richardson, 2002). The impact breakage parameters, A and b, characterize the material's fragmentation behaviour and can be determined through interpretation of typical t_{10}-E_{cs} curve (Taveres.,2007).

It is also important to note that the value of slope of the curve at 'zero' input energy derived from equation above results in a differentiating equation below in respect to E_{cs} gives,

$$\frac{dt10}{dEcs} = (-Ae^{-bEcs}).(-b) \quad (21)$$

Then by letting Ecs to approach zero, it results in the following equation:

$$\lim_{Ecs \to 0} \left(\frac{dt10}{dEcs}\right) = Axb \quad (22)$$

Axb is the slope of the curve at 'zero' input energy. It represents material's amenability to fragmentation via impact (ore hardness indicator) (Shi & Kojovic, 2007). A lower Axb value

shows that the ore has a high resistance to impact breakage whilst a higher Axb indicates a readiness to fracture of the ore type (Hahne et al., 2003).

II. Calculations – Progeny particles size distribution

The calculations below demonstrate the procedure undertaken for particles size analysis on the results of impact breakage tests.

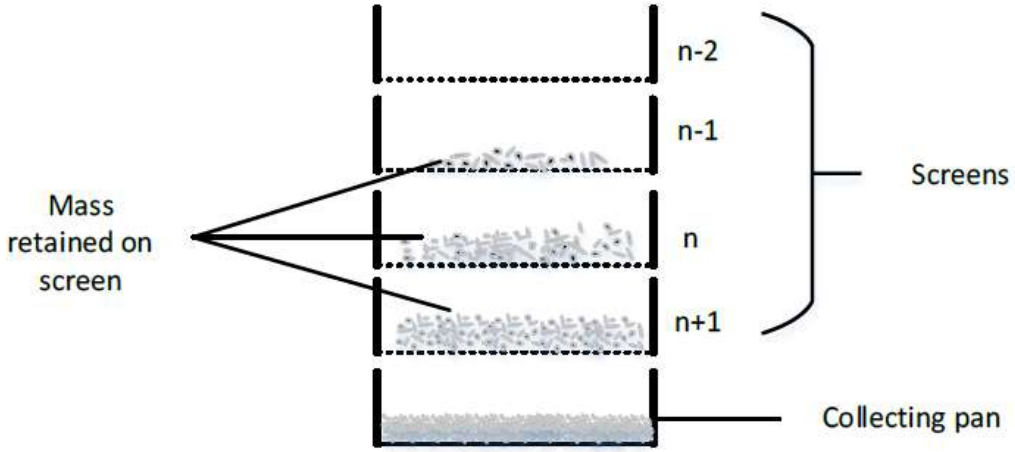

Figure 82:Schematic diagram showing the mass retained on each screen(Adapted from Chikochi,2017)

The following calculations are going to be used for the analysis of the progeny particles from the impact breakage in the drop weight device. The mass retained on screen (sieve) will be determined by weighing the particles collected on each screen.

$$Mass\ retained\ (g) = Weigh\ particles\ collected\ on\ each\ screen$$

The total mass retained is the sum of the masses retained at each screen. This should be equal to the original mass before screening.

$$Total\ mass\ retained\ (g) = \sum mass\ retained\ on\ each\ screen$$

The percentage retained is given by:

$$Percentage\ retained\ (\%) = \frac{Mass\ retained\ (g)}{Total\ mass\ retained\ (g)} \times 100$$

Cumulative percentage retained is obtained by adding up the percentages of the mass retained on each screen. This should total up to 100%.

$$Cumulative\ percentage\ retained\ (\%) = \sum Percentage\ retained\ on\ each\ screen$$

The percentage of material passing the nth sieve is calculated by the following equation:

$$\begin{Bmatrix} Percentage\ passing \\ n^{th}\ screen \end{Bmatrix} = \begin{Bmatrix} Percentage\ passing \\ n-1^{th}\ screen \end{Bmatrix} - \begin{Bmatrix} Percentage\ retained \\ on\ the\ n^{th}\ screen \end{Bmatrix}$$

If no mass is retained on a screen, the percentage passing is 100%. Usually, no mass is retained on the top screen, thus the percentage passing is 100%.

The original particle feed size is obtained by taking a geometric mean of the two screens sizes as given by the following equation:

$$Geometric\ mean = \sqrt{X_{top} \times X_{bottom}}$$

The t_{10} size is 1/10th of the original particle feed size

$$t_{10,\ size} = \frac{Geometric\ mean}{10}$$

The percentage material passing 1/10th of the original feed size(t_{10}) is determined by interpolation

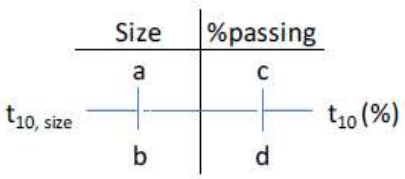

If a>b and c>d, then t_{10} is determined by the following equation:

$$t_{10}\ (\%) = \left[\left(\frac{t_{10,\ size} - b}{b - a}\right) \times (c - d)\right] + d$$